ISTITUZIONI DI ASTROFISICA E COSMOLOGIA:
COSMOLOGIA OSSERVATIVA

A.A. 2024/2025 | Matteo Costanzi - University of Trieste / INAF

GENERAL FRAMEWORK: UNIVERSE TIMELINE
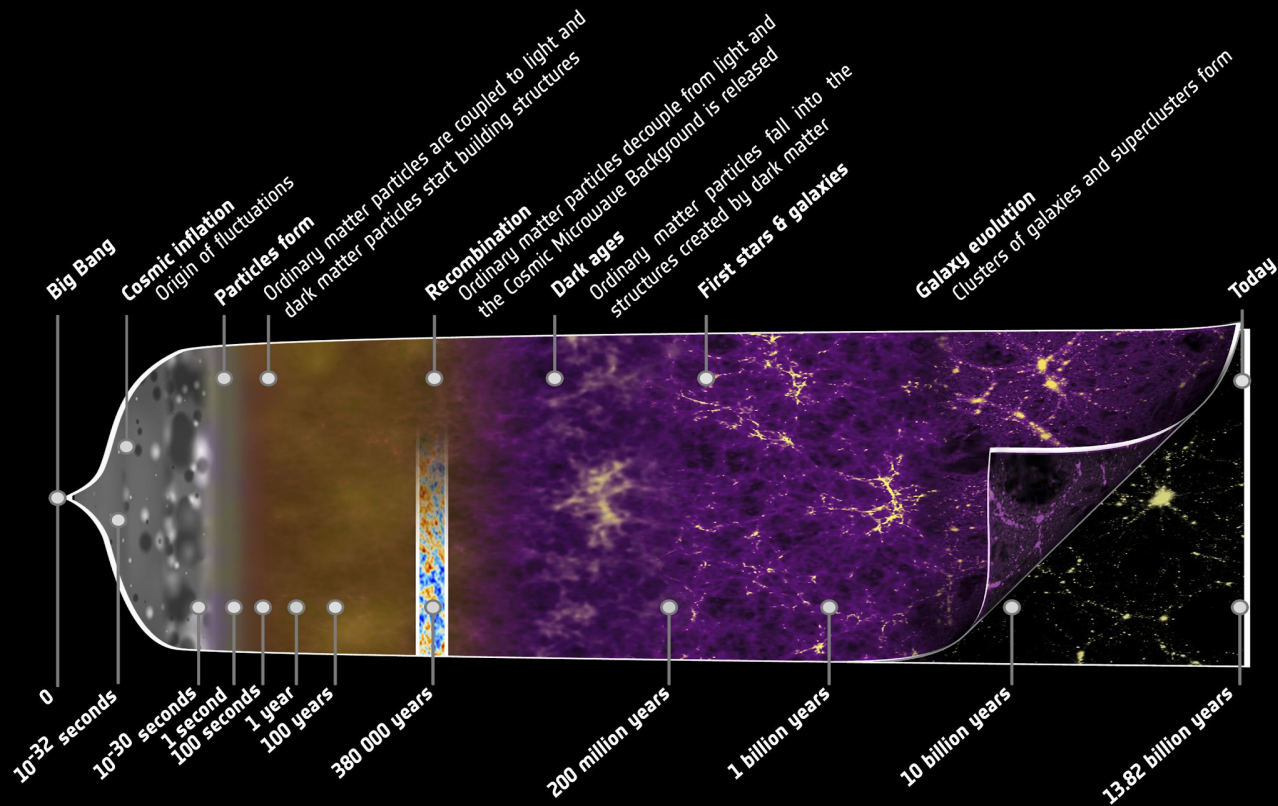
$t_{BBN} \simeq 100$ s

$t_{eq} \simeq 56.000$ yr
$z_{eq} \simeq 3800$

$t_{rec} \simeq 380.000$ yr
$z_{rec} \simeq 1100$

$t_{rei} \simeq 0.2 - 1$ Gyr
$z_{rei} \simeq 6 < z < 20$

$t_{\Lambda} \simeq 9$ Gyr
$z_{\Lambda} \simeq 0.33$

GENERAL FRAMEWORK: ΛCDM MODEL

ASSUMPTION OF ΛCDM:

- **Gravity is described by GR**

- **Particles and forces are described by QFT**

- **The cosmological principle is valid**

- **The Universe underwent accelerated expansion at early times (Inflation)**

- **Most matter is made up by a collisionless particle (Dark Matter)**

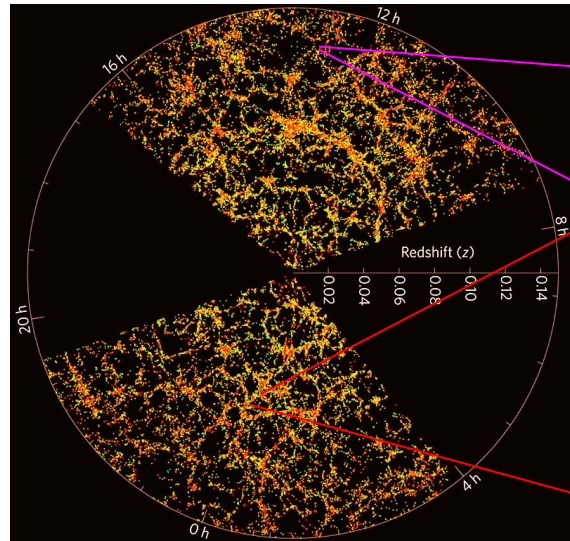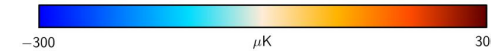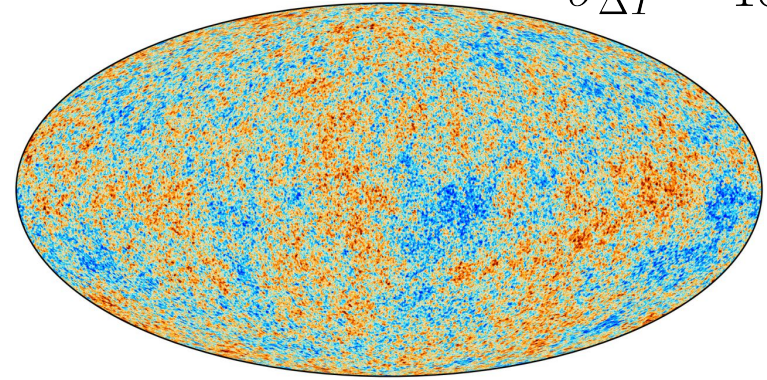- **The Universe is undergoing an accelerated expansion (Λ)**

$$\sigma_{\Delta T} = 18 \mu K$$

Cosmological principle: the Universe is isotropic* and homogeneous** on large scale (~100 Mpc/h)

* from observation (LSS and CMB)

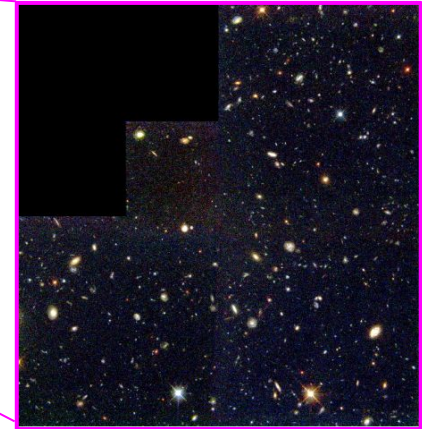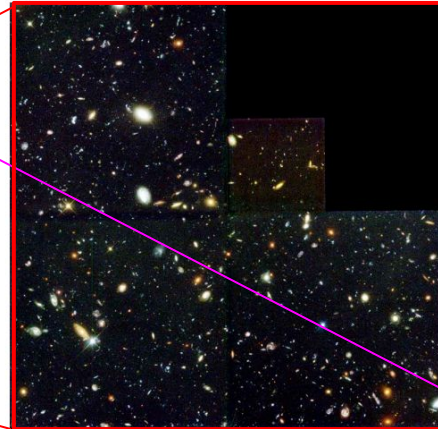**** Copernican principle**

−300 μK 300

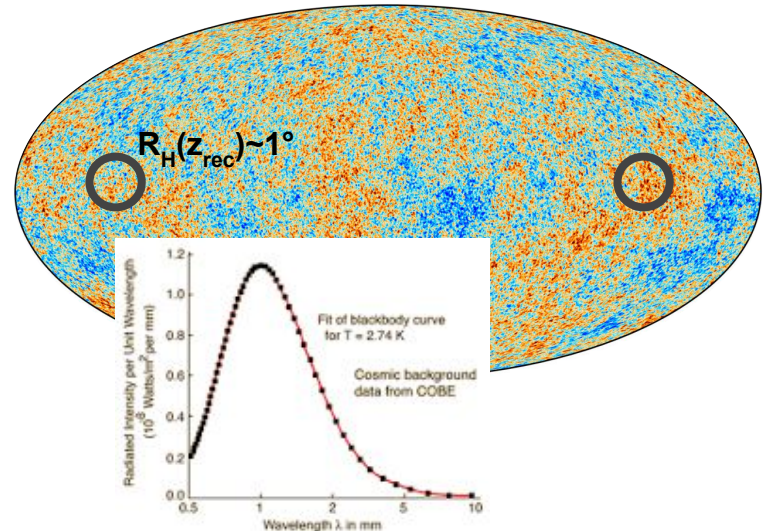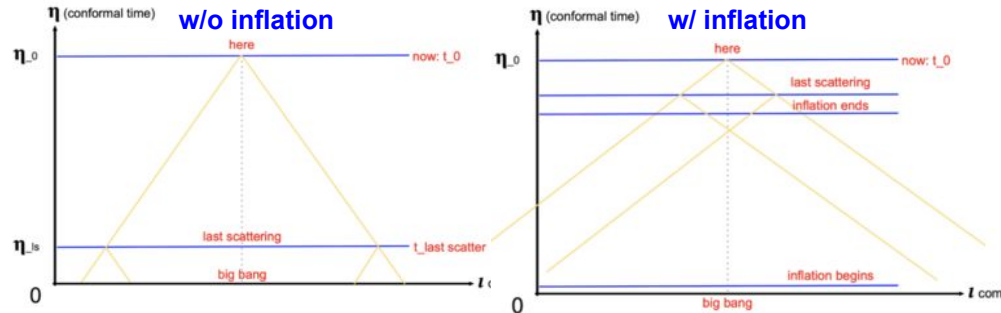HDF-North   HDF-South

Inflation: exponential expansion (e-fold~60) happened in the early stages of the Universe ($t \simeq 10^{-37} - 10^{-35}$ s).

Horizon problem

Flatness problem (today $\Omega_k \simeq 0$)

$R_H(z_{rec}) \sim 1°$
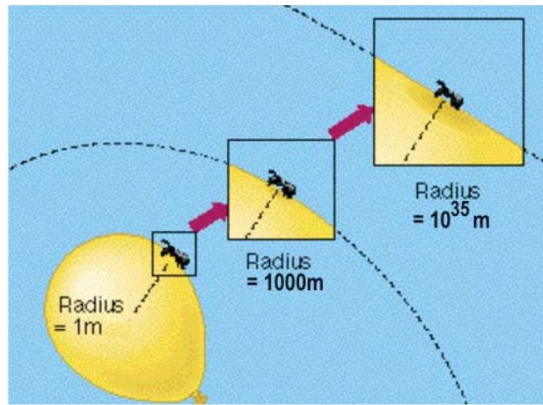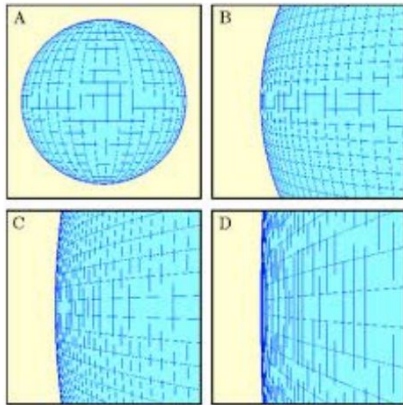
+ **Magnetic monopole problem: Inflation dilutes the Universe by a factor e^{3N} , with N~60**

Dark Matter: massive particles which interacts only via gravitational forces

$$\langle M/L \rangle \sim 100 - 400\, h\; M_\odot/L_\odot$$

Galaxy velocity dispersion in Coma cluster (Zwicky 1933)
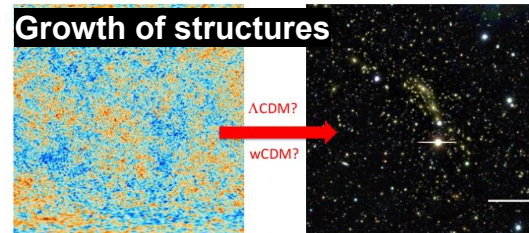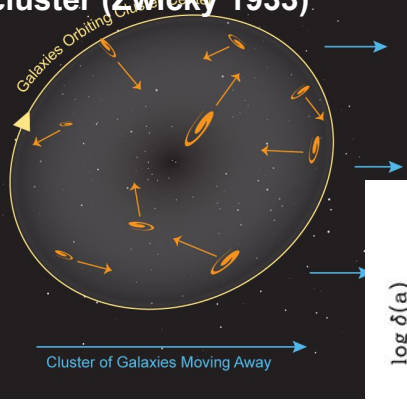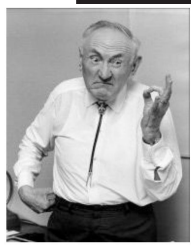
Galaxies Orbiting Cluster Center

Cluster of Galaxies Moving Away

Growth of structures

Structure at 380,000 years – 10^{-5} of CMB

ΛCDM?

wCDM?

Structure at 13.8 billion years – density contrasts > 10^3

a) k=0.1 hMpc^{-1}

$\log \delta(a)$

δ_{CDM}

δ_B

δ_γ

Galaxy rotation curve

Observations from starlight

Observations from 21 cm hydrogen

Velocity (km s^{-1})

100

50

Expected from the visible disk

10,000   20,000   30,000   40,000

Distance (light years)
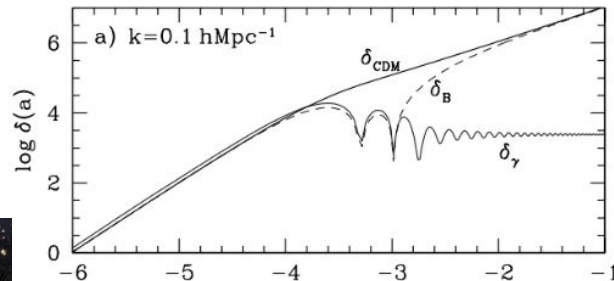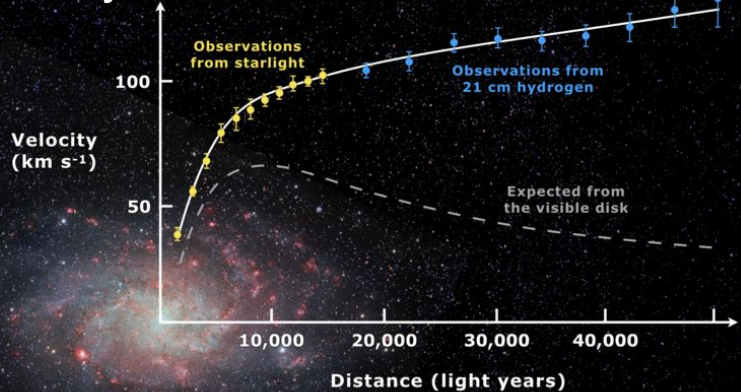
$$\langle M/L \rangle \sim 30\, h\; M_\odot/L_\odot$$

Mass Distribution from Lensing

Gas

DM

DM
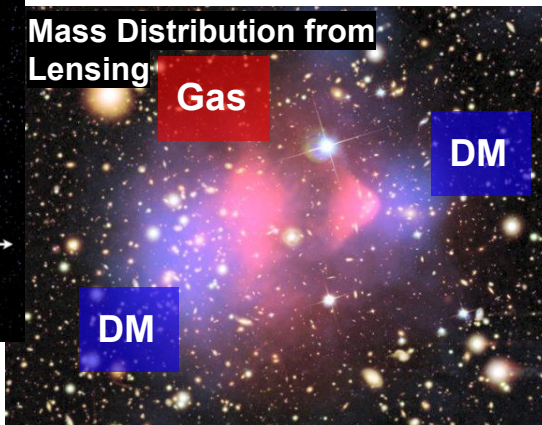
Accelerated expansion: the Universe is undergoing a phase of accelerated expansion driven by a dark energy component, Λ
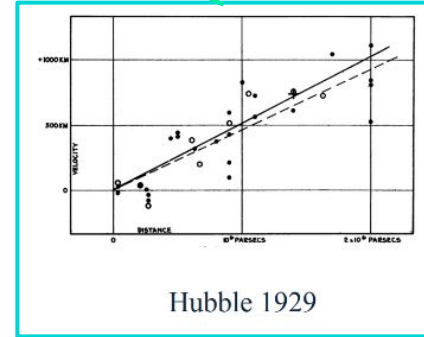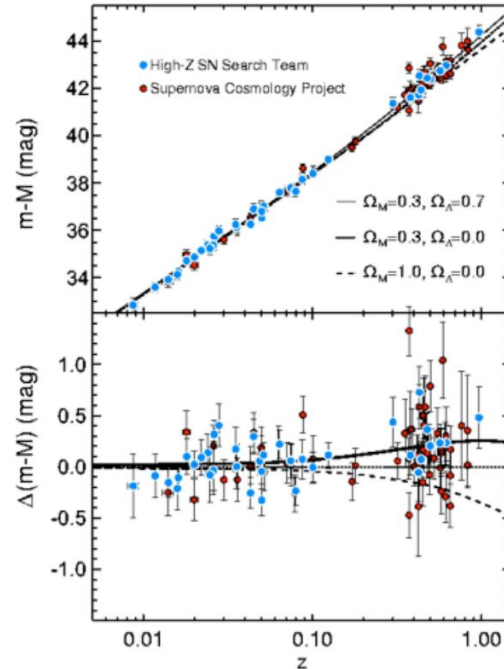
M51 "The Whirlpool galaxy"

SN 2005cs

High-Z SN Search Team
Supernova Cosmology Project

$\Omega_M=0.3, \Omega_\Lambda=0.7$
$\Omega_M=0.3, \Omega_\Lambda=0.0$
$\Omega_M=1.0, \Omega_\Lambda=0.0$

Hubble 1929

1998/99 High-Z Supernova Search Team and Supernova Cosmology Project found evidence for accelerated expansion of the Universe (2011 Nobel Prize)

The CMB TT power spectrum (Planck coll. 18)
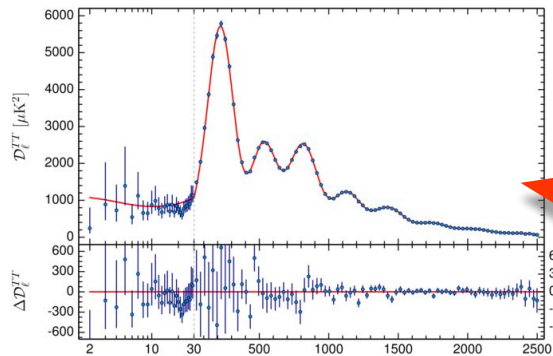
~380.000 yr after the Big Bang

BAO galaxy (DES Coll. 22)

BAO template best fit
BAO template Planck
DES Y3 Data (0.6<z<1.1)

~10^10 yr after the Big Bang

Several cosmological probes point towards a consistent model of
flat ΛCDM
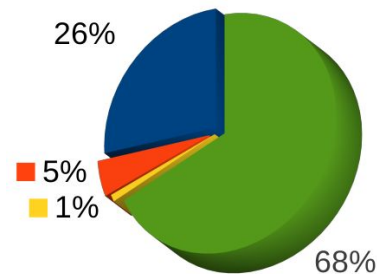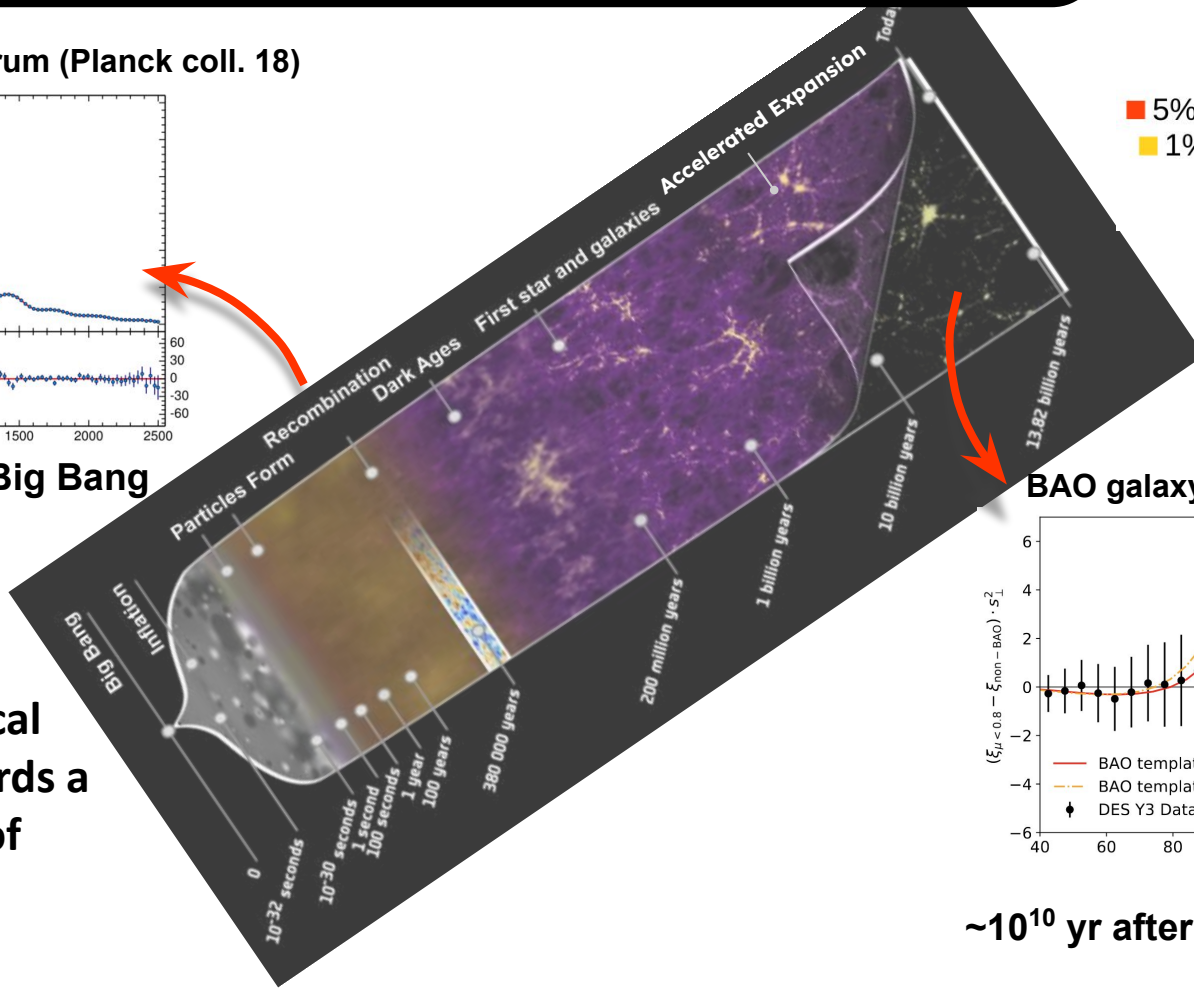
The ΛCDM universe

Several cosmological probes point towards a consistent model of flat ΛCDM

26%

- CDM
- Baryons
- Neutrinos
- Lambda

5%

1%

68%

Energy density parameters (total mass, baryons, neutrinos) w.r.t. the critical density of the universe

Hubble constant

ΛCDM+ν parameters: $\Omega_{\mathrm{m}}, \; \Omega_{\mathrm{b}}, \; \Omega_{\nu}, \; \sigma_8, \; H_0, \; \tau, \; n_s$

Amplitude of the matter fluctuations on a 8 Mpc/h scale

Optical depth

Spectral index of primordial fluctuations

For a flat Universe:

$$\Omega_k = 1 - \sum_i \Omega_i = 0$$
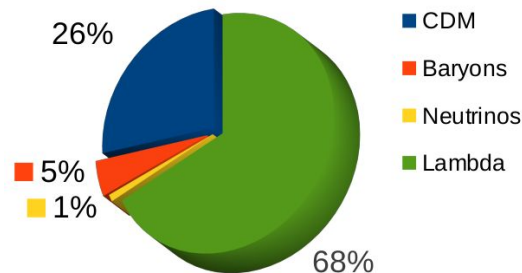
But the two dominants components of this model lack a fundamental theory to connect them with the rest of physics:

- **What is the nature of Dark Matter?**

- **What is the cause of observed cosmic acceleration?**

    - **Is it Dark Energy or a modification of general relativity?**

    - **If it is Dark Energy, is it constant (ΛCDM) or evolving (wCDM)**

    - **If we interpret DE as vacuum energy, how we reconcile its value with QFT predictions?**

$$\frac{\rho_{\Lambda\ \text{QFT}}}{\rho_{\Lambda\ \text{observed}}} \approx 10^{120}$$

- **What is the driver of cosmic inflation?**

26%

■ CDM
■ Baryons
■ Neutrinos
■ Lambda

5%
1%

68%

See also: https://arxiv.org/pdf/2405.18307
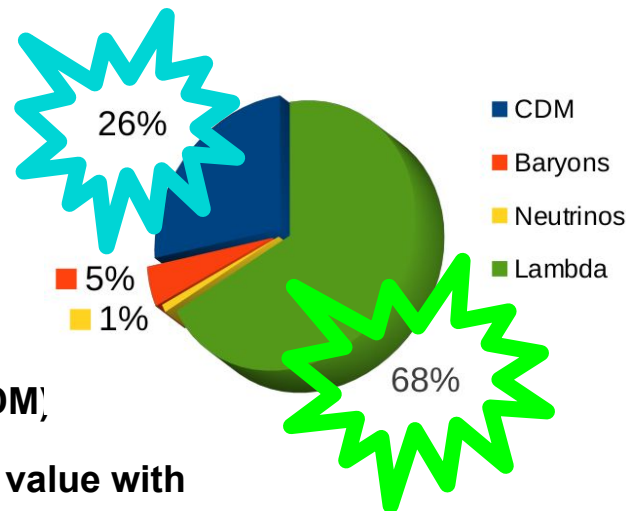
Moreover, there are tensions between parameters derived from early Universe probes (e.g. CMB) and low-redshift probes (e.g. SN, cosmic shear, galaxy clustering, cluster of galaxies)

Tension on the Hubble's constant:
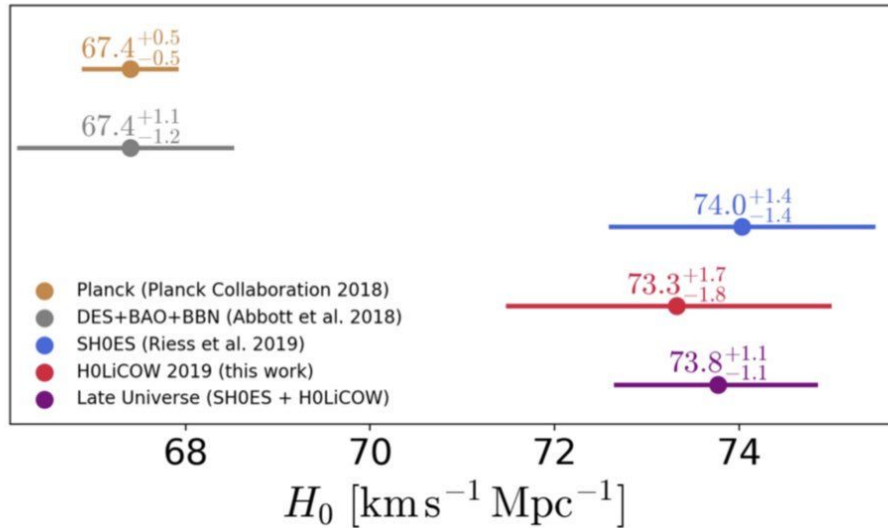
Tension on S_8 (growth of structures)

See also: https://arxiv.org/pdf/2406.12106
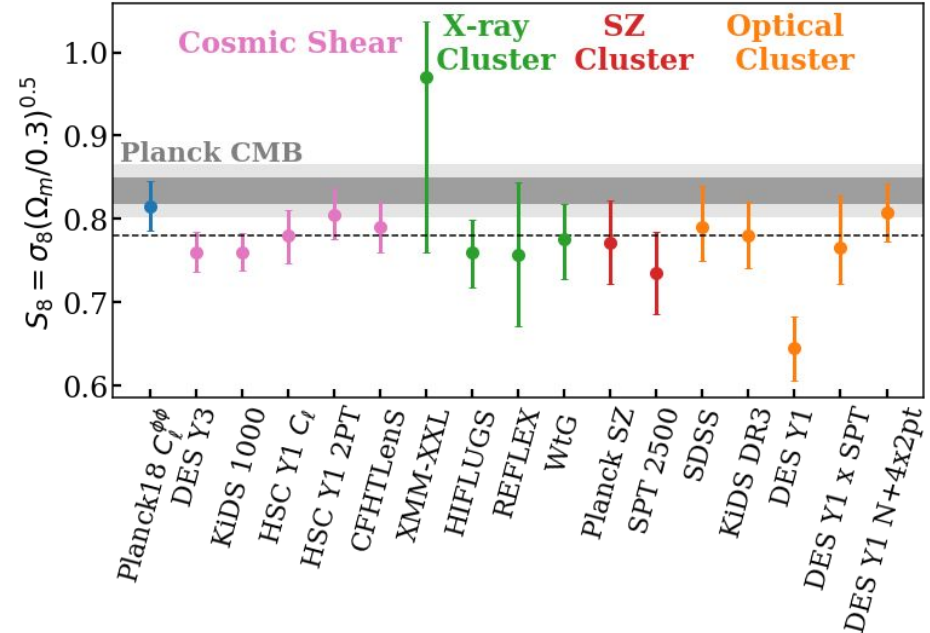
Latest results from the spectroscopic survey DESI, in combination with other probes, suggest a dark energy with a time-evolving equation of state parameters ($w_0 w_a$CDM) to solve the ΛCDM tension

See : https://arxiv.org/pdf/2503.14738
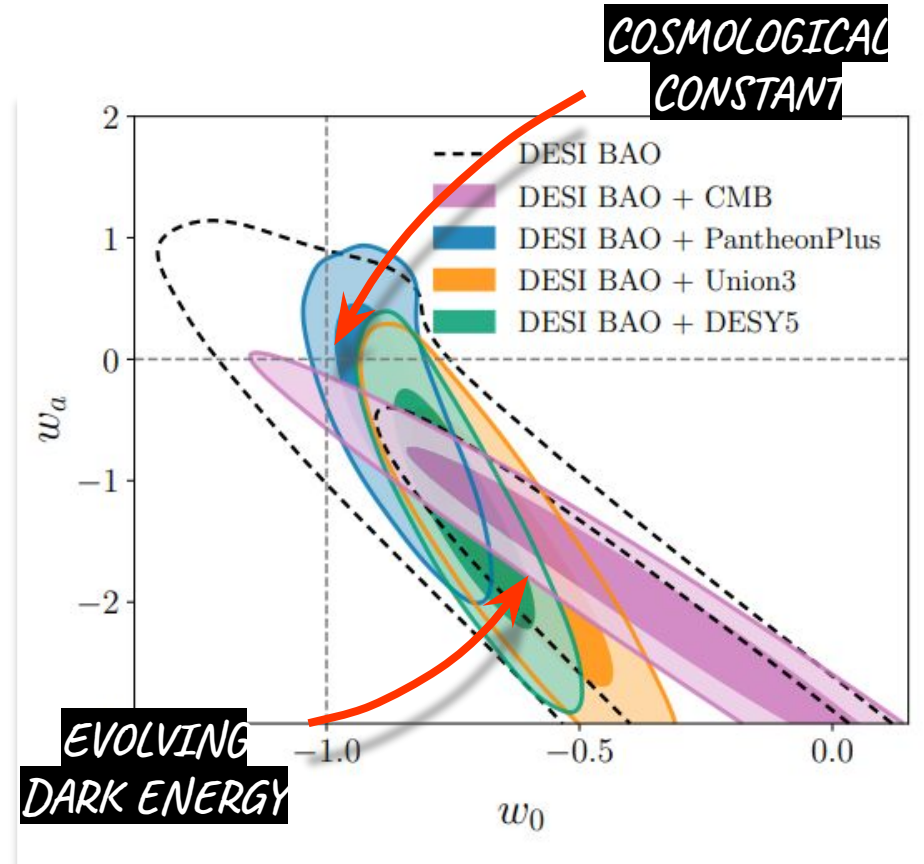
- **What can we measure with cosmological probes:**

Growth of density perturbation
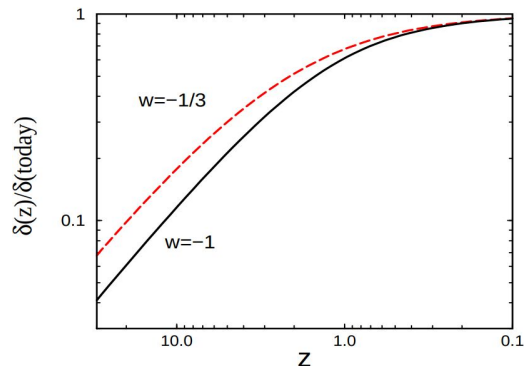
Expansion history
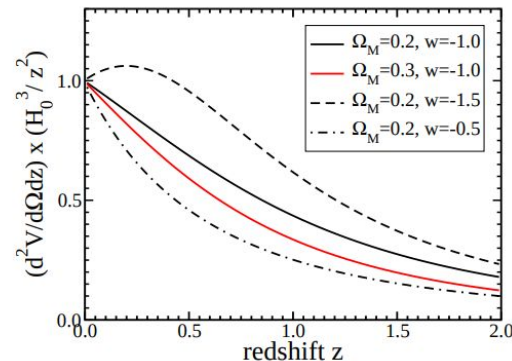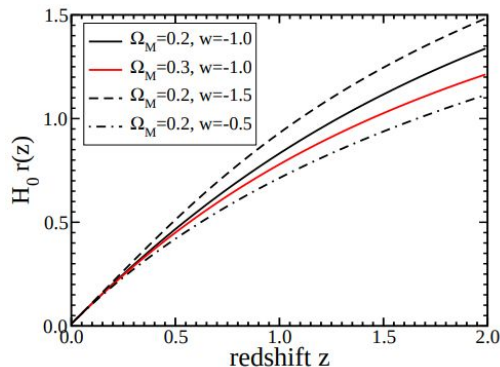
Freiman+08

A good strategy to disentangle different models is to combine early and late time Universe probes to maximize the redshift leverage
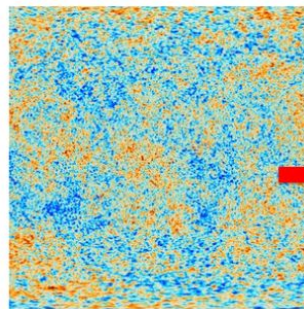
Structure at 380,000 years –
10^{-5} of CMB
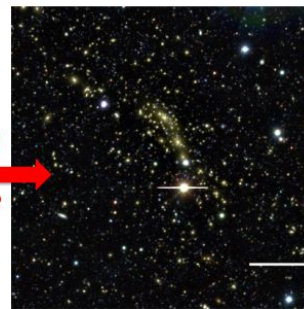
Structure at 13.8 billion years –
density contrasts > 10^3

GENERAL FRAMEWORK: COSMOLOGICAL PROBES

Galaxy Clusters

Gravitational waves

Quasars and Ly-α forest

21cm intensity maps

ΛCDM VS DARK ENERGY
GR VS Mod. Gravity
Neutrino mass
...

Galaxy distribution

Cosmic Microwave Background Anisotropies

Weak lensing mass map

Supernovae Ia

Big Bang Nucleosynthesis
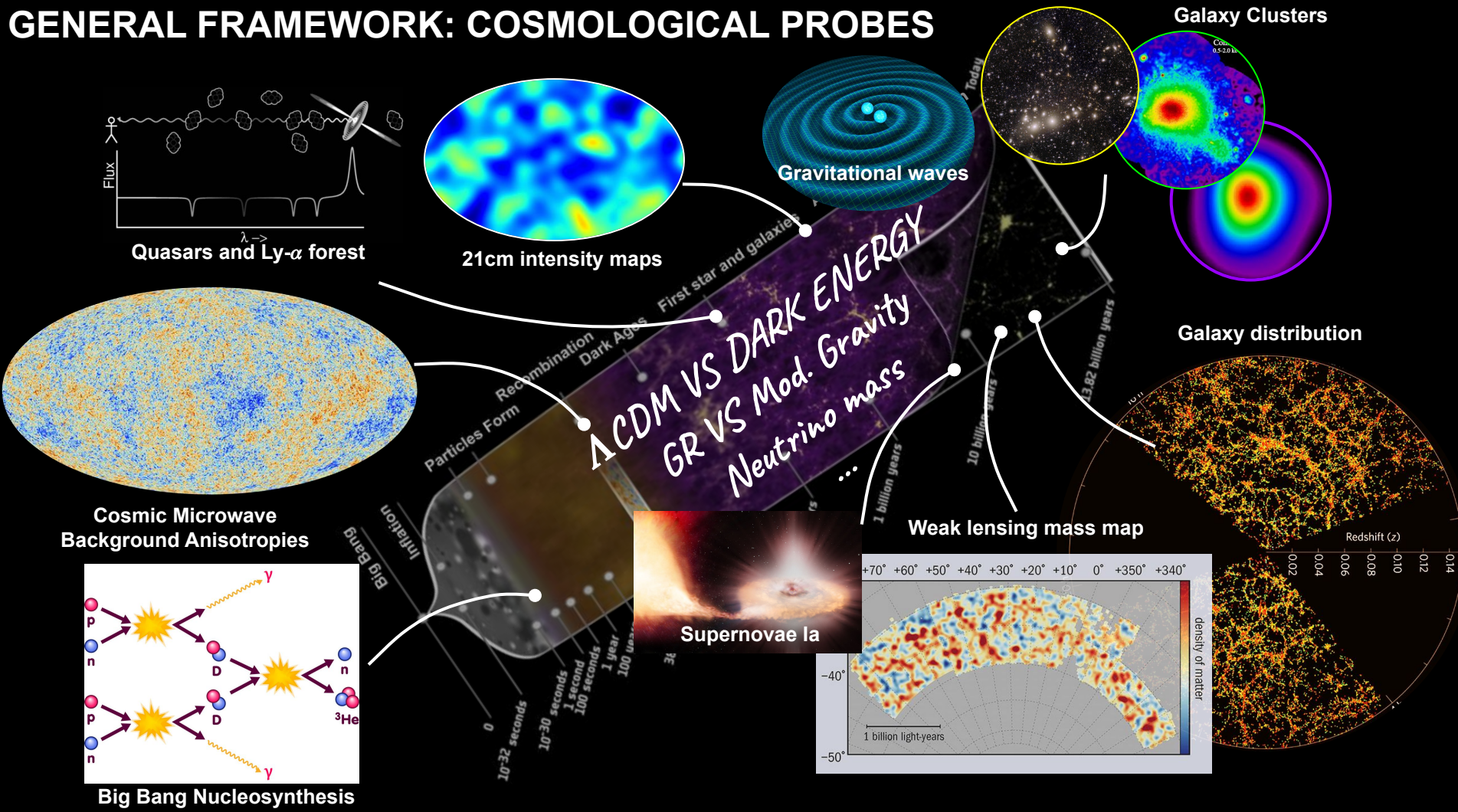
BIG BANG NUCLEOSYNTHESIS

For a review: https://arxiv.org/pdf/astro-ph/0511534.pdf or https://arxiv.org/pdf/astro-ph/0601514.pdf

$t = 13.73\,\mathrm{Gyr}$	$T = 2.726\,\mathrm{K}$	present
$t = 9\,\mathrm{Gyr}$	$T = 5\,\mathrm{K}$	Solar system forms
matter era		structure formation
$t = 10^6\,\mathrm{yr}$	$T = 3000\,\mathrm{K}$	recombination --> CMB
$t = 10^5\,\mathrm{yr}$	$T = 10^4\,\mathrm{K}$	matter-radiation equality
radiation era		
$t = 300\,\mathrm{s}$		
BBN	$T = 10^9\,\mathrm{K}$	BBN = Big-Bang Nucleosynthesis
$t = 10\,\mathrm{s}$		
Lepton era		
$t = 10^{-4}\,\mathrm{s}$	$T = 10^{12}\,\mathrm{K}$	
Hadron era		
$t = 10^{-6}\,\mathrm{s}$	$T = 10^{13}\,\mathrm{K}$	quark-hadron phase transition
Quark Soup		
$t = 10^{-33}\,\mathrm{s}$	$T = 10^{27}\,\mathrm{K}$	
inflation		
$t = 10^{-35}\,\mathrm{s}$	$T = 10^{28}\,\mathrm{K}$	
$t = 10^{-43}\,\mathrm{s}$	$T = 10^{32}\,\mathrm{K}$	
???? ????		Big Bang

PRIMORDIAL NUCLEOSYNTHESIS

Primordial nucleosynthesis takes place in the first 3 minutes of life of the Universe, and it is a crucial piece of evidence in favor of standard hot big bang model:

At a temperature of kT>1MeV the rate of weak interactions, $\Gamma_{n\leftrightarrow p,}$ is higher than the expansion rate of the universe, H; p, n, e are in equilibrium vai the reactions:

$$e^+ + n \longleftrightarrow p + \bar{\nu}_e$$
$$\nu_e + n \longleftrightarrow p + e^-$$

At temperatures below 1 MeV (t~1 s), neutrinos decouple and the weak interactions are frozen out, $\Gamma_{n\leftrightarrow p}$ < H; neutrons and protons cease to interconvert. The equilibrium abundance of neutrons at this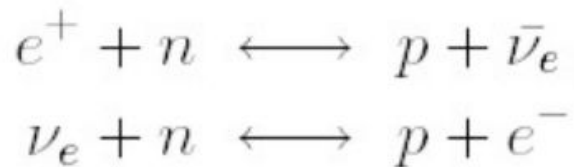 temperature is about 1/6 the abundance of protons (due to the slightly larger neutron mass). The neutrons have a finite lifetime (τ = 890 s) that is somewhat larger than the age of the universe at this epoch, t(1 MeV) ≈ 1 s, but they begin to gradually decay into protons and leptons (β-decay) until the neutron-to-proton ratio has dropped to ~1/7.

Protons and neutrons can combine to form ^{4}He through the chain of reactions:

$$p+n \leftrightarrow {}^2H+\gamma \qquad {}^2H+n \rightarrow {}^3H+\gamma \qquad {}^3H+p \rightarrow {}^4He+\gamma$$

$$\phantom{p+n \leftrightarrow {}^2H+\gamma \qquad} {}^2H+p \rightarrow {}^3He+\gamma \qquad {}^3He+n \rightarrow {}^4He+\gamma$$
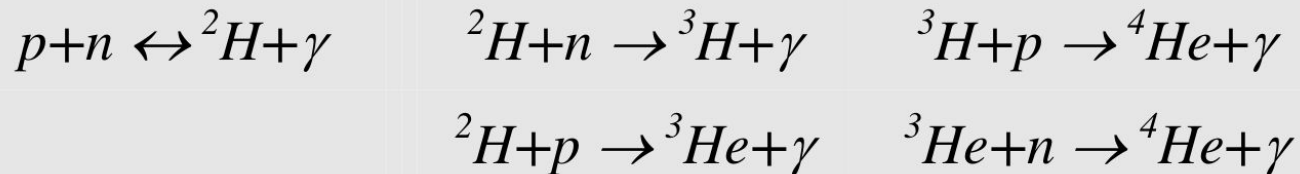
The bottleneck of these reactions is the formation of Deuterium, which is destroyed by energetic photons, until their number, n_γ^{diss} , becomes comparable with the number of baryons, n_b, at kT~0.1 MeV (T~10^9 K). At this epoch, t_{BBN}~150s, D is not destroyed and basically all the neutrons which are not decayed forms ^{4}He nuclei. The (mass) abundance of ^{4}He is determined mainly by:

- **The temperature at which neutrino decouples and the n-to-p ratio at frozen, $\Gamma_{n\leftrightarrow p}$ ~ H, which in turns depends on the total number of neutrino species.**
- **The mean neutron lifetime (~889 s)**
- **The baryon-to-photon ratio , $\eta = n_b / n_\gamma = 2.7 \times 10^{-8} \, \Omega_b h^2$, which determines t_{BBN}**

Further reactions lead to the formation of ^{7}Li:

$$^4He + {}^3H \leftrightarrow {}^7Li + \gamma \qquad {}^4He + {}^3He \leftrightarrow {}^7Be + \gamma \qquad {}^7Be + \gamma \leftrightarrow {}^7Li + p$$

with a relative abundance compared to the hydrogen of ~10^{-9} - 10^{-10}. Heavier elements cannot be synthesized because:

- There are no stable isotopes with mass numbers 5 or 8, in particular ^{8}Be is unstable.

- The density and temperature is too low for the triple-alpha process that could form ^{12}C to occur.

**All the other heavier elements (C, N, O, Fe) are formed by thermonuclear processes inside stars**

Deuterium is the baryometer of choice since its post-BBN evolution is simple (and monotonic!):

There are no astrophysical process that produce D and, as the most weakly bound of the light nuclides, any deuterium cycled through stars is burned to ^{3}He. Thus, deuterium observed anywhere, anytime, should provide a lower bound to the primordial D abundance.

For "young" systems at high redshift and/or with very low metallicity, which have experienced very limited stellar evolution, the observed D abundance should be close to the primordial value.

Thus, although there are observations of deuterium in the solar system and the interstellar medium (ISM) of the Galaxy which provide interesting lower bounds to the primordial abundance, it is the observations of relic D in a few, high redshift, low metallicity, quasars absorption line systems which are of most value in enabling estimates of its primordial abundance
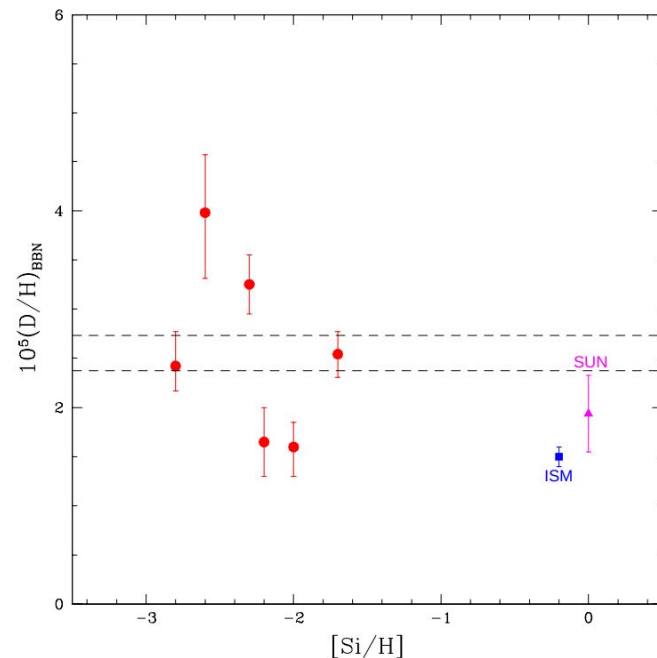
Deuterium abundance in intergalactic neutral hydrogen clouds at high redshift (observed as absorption lines in quasar spectra). Dashes lines indicate what is expected from WMAP CMB analysis.

PRIMORDIAL NUCLEOSYNTHESIS

- Observations of ^{3}He, are restricted to the solar system and HII region of our Galaxy. The post-BBN **evolution of ^{3}He**, involving competition among stellar production, destruction, and survival, is considerably more **complex and model dependent** than that of D.

- The post-BBN evolution of ^{4}He is quite simple. As gas cycles through generations of stars, hydrogen is burned to helium-4 (and beyond), increasing the ^{4}He abundance above its primordial value. The key data for inferring its primordial abundance are provided by observations of helium and hydrogen emission (recombination) lines from low-metallicity, extragalactic H II regions

- In the post-BBN universe ^{7}Li is produced in the Galaxy by cosmic ray spallation and (at least in some) stars. Therefore, in order to probe the BBN yield of ^{7}Li, it is necessary to restrict attention to the oldest, most metal-poor halo stars in the halo of our galaxy
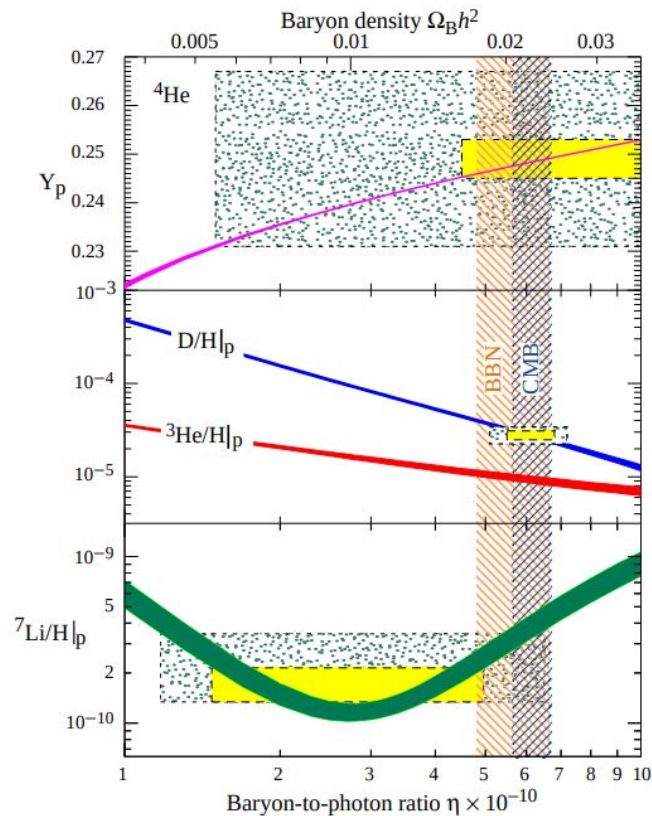

Figure 1.1: The abundances of ^{4}He, D, ^{3}He and ^{7}Li as predicted by the standard model of big-bang nucleosynthesis. Boxes indicate the observed light element abundances (smaller boxes: 2σ statistical errors; larger boxes: $\pm 2\sigma$ statistical and systematic errors). The narrow vertical band indicates the CMB measure of the cosmic baryon density. See full-color version on color pages at end of book.

PRIMORDIAL NUCLEOSYNTHESIS

- **^{7}Li problem: BBN predictions** (based on the standard ΛCDM model and baryon density from the CMB) **overestimate the primordial abundance of ^{7}Li** by a factor of **~3** compared to what we **observe in old, metal-poor (Population II) stars** in the galactic halo:

$$\left(\frac{^7\text{Li}}{\text{H}}\right)_{\text{BBN}} \sim 5 \times 10^{-10} \qquad \left(\frac{^7\text{Li}}{\text{H}}\right)_{\text{obs}} \sim 1.6 \times 10^{-10}$$

Proposed Solutions (none fully successful yet):

- **Astrophysical**: ^{7}Li depletion in stars (e.g. diffusion, mixing, destruction)

  → but no known stellar process explains the uniform low abundance in old stars (Spite plateau).

- **Nuclear physics**: Re-evaluating nuclear reaction rates (e.g., ^{7}Be destruction)

  → but updated measurements haven't fixed the problem.
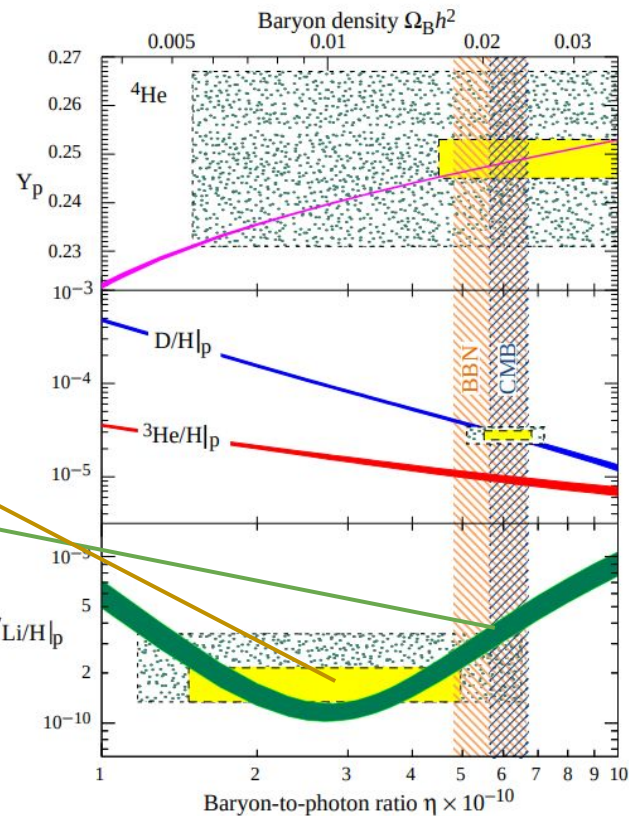
  See e.g.: https://arxiv.org/pdf/1801.08023

Figure 1.1: The abundances of ^{4}He, D, ^{3}He and ^{7}Li as predicted by the standard model of big-bang nucleosynthesis. Boxes indicate the observed light element abundances (smaller boxes: 2σ statistical errors; larger boxes: $\pm 2\sigma$ statistical and systematic errors). The narrow vertical band indicates the CMB measure of the cosmic baryon density. See full-color version on color pages at end of book.

STANDARD CANDLES: SUPERNOVAE IA

For a short review: https://link.springer.com/article/10.1007/s40766-022-00034-1

STANDARD CANDLES

Standard candles: Astronomical objects with known absolute magnitude (i.e. intrinsic luminosity), like variable stars (Cepheid and RR Lyrae), or Type Ia supernovae.

Standard candles are valuable cosmological tools since by measuring their apparent magnitude we can determine their (luminosity) distance; by looking at the relation between distance and redshift (Hubble diagram) it is possible to infer cosmological parameters.

We define the luminosity distance D_L operationally as the distance that relates the intrinsic (bolometric) luminosity L of an object (e.g. a galaxy) at redshift z to its observed flux *f* via:

$$f = \frac{L}{4\pi D_L^2}$$

For a flat LCDM universe, at late time ($z \ll z_{eq}$):

$$D_L(z) = (1+z)D_M = (1+z)\frac{c}{H_0}\int_0^z \frac{dz'}{E(z')}$$

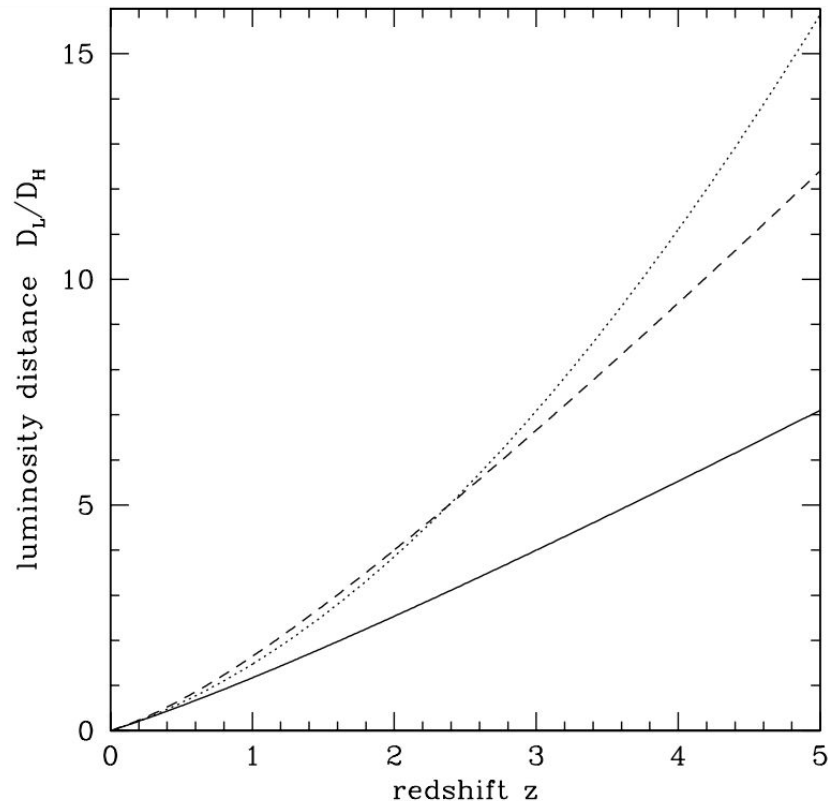$$E(z) = \frac{H(z)}{H_0} = \sqrt{\Omega_m(1+z)^3 + \Omega_\Lambda}$$

Figure 3: The dimensionless luminosity distance D_L/D_H. The three curves are for the three world models, $(\Omega_M, \Omega_\Lambda) = (1,0)$, solid; $(0.05, 0)$, dotted; and $(0.2, 0.8)$, dashed.

Apparent magnitude:

$$m = -2.5 \log_{10}(f) + \text{cost.}$$

Distance modulus:

$$\mu = m - M = 5 \log_{10}(D_L/10pc)$$

Absolute magnitude ≡ Apparent magnitude of an object seen from 10 pc
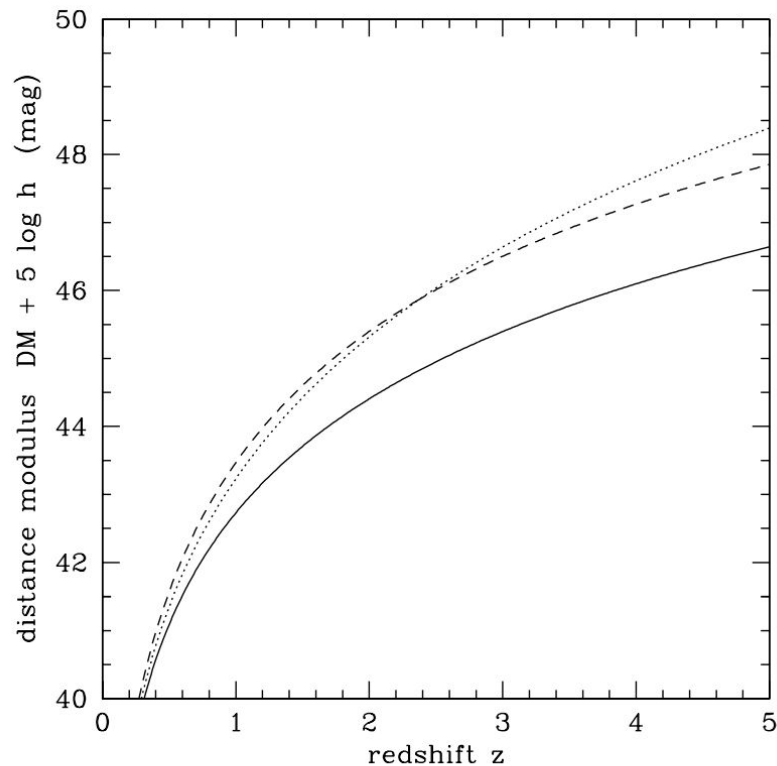
Figure 4: The distance modulus DM. The three curves are for the three world models, $(\Omega_M, \Omega_\Lambda) = (1,0)$, solid; $(0.05, 0)$, dotted; and $(0.2, 0.8)$, dashed.

CEPHEIDS

Pulsating stars with a well-defined relationship between their **pulsation period** and **intrinsic luminosity**

Period–Luminosity Relation (Leavitt Law, 1908) allows us to determine their **absolute magnitude**

→ **First standard candle** used in astronomy.

Role in Cosmology:

- Crucial rungs in the **cosmic distance ladder**

- Used to anchor the calibration of **Type Ia Supernovae**

$$M = -2.78 \, [\log(P) - 1] - 4.00$$
(Storm et al. 2011, A&A 534)
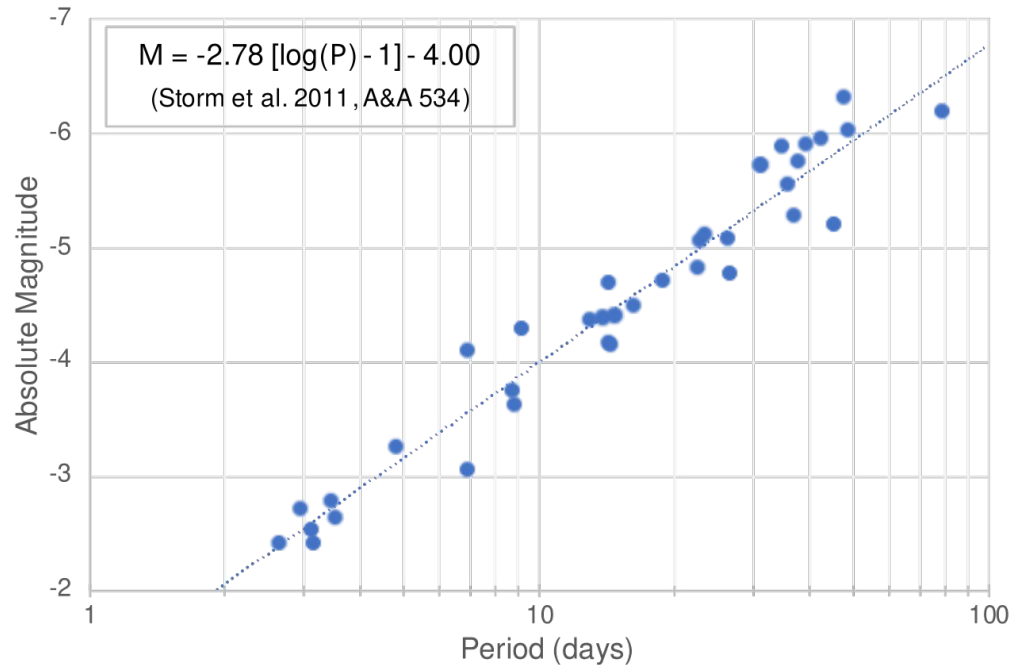
SUPERNOVAE TYPE Ia

The progenitor of a SN Ia is a white dwarf in a close binary system, which accrete matter from its companions until it reaches the Chandrasekhar limit ($M_{Ch} \sim 1.4$ M$_\odot$); after that the start is destroyed by an explosive thermonuclear burning that produces iron-peak elements. Having a similar mass at the time of explosion, the SN Ia have a small luminosity dispersion.

SN 2005cs

M51 "The Whirlpool galaxy"
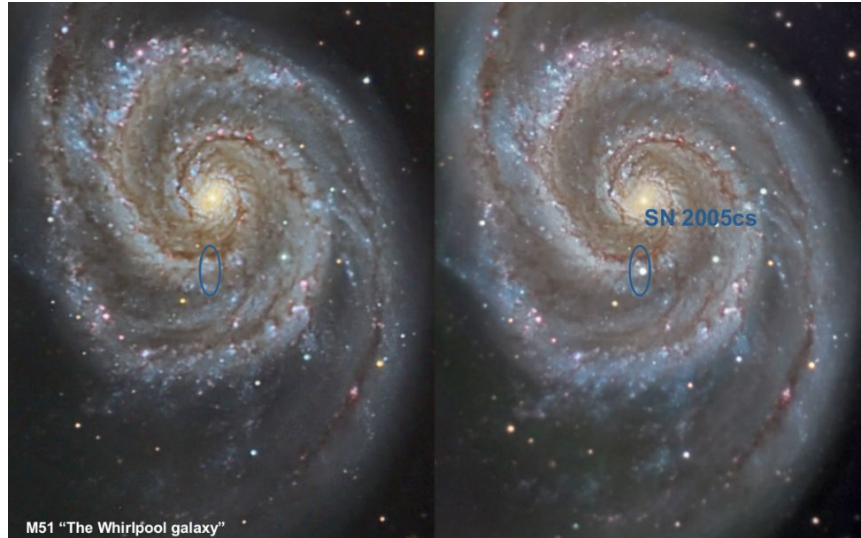
SN Ia explosions are quite rare events, ~1.0e-4 [yr Mpc^3]$^{-1}$ (~1 per century in our galaxy), but their extremely high luminosity – M_V=-19.3, 5×10^9 times brighter than the Sun, typically comparable to the brightness of the entire host galaxy – allows us to detect them at very large distances (z>1)

With regards to the luminosity evolution, SNe Ia show the highest homogeneity among SN types. Actually, it is recognised that, strictly speaking, even SNe Ia are not standard candles since they show significant diversity in their absolute magnitudes at maximum (40% scatter in the peak brightness). Standardisation methods have been developed promoting their use as powerful cosmic distance indicators
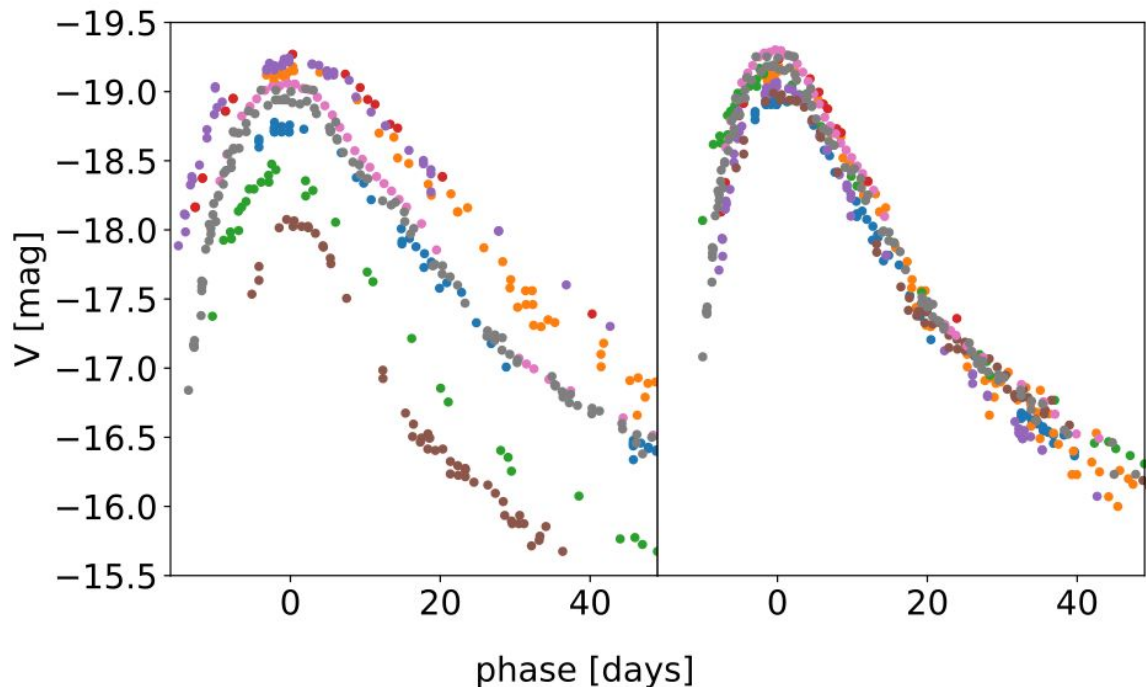

Fig. 6 Illustration of the standardization of SN Ia light curves using the stretch factor. Left panel shows the light curve in absolute V magnitude (corrected for extinction) for a sample on nearby SNe Ia with different decline rates. Right panel: after stretching the time axis to match the luminosity evolution, the luminosity is scaled based on the light curve evolution-luminosity relation. Data from [100]

- **Studying the evolution of the distance modulus with redshift is it possible to measure H_0 and the expansion history of the Universe.**

- **1998/99: High-Z Supernova Search Team and Supernova Cosmology Project found evidence for accelerated expansion of the Universe (Nobel prize 2011)**

- **Precise measurements of the Hubble's constant from SN Ia:**

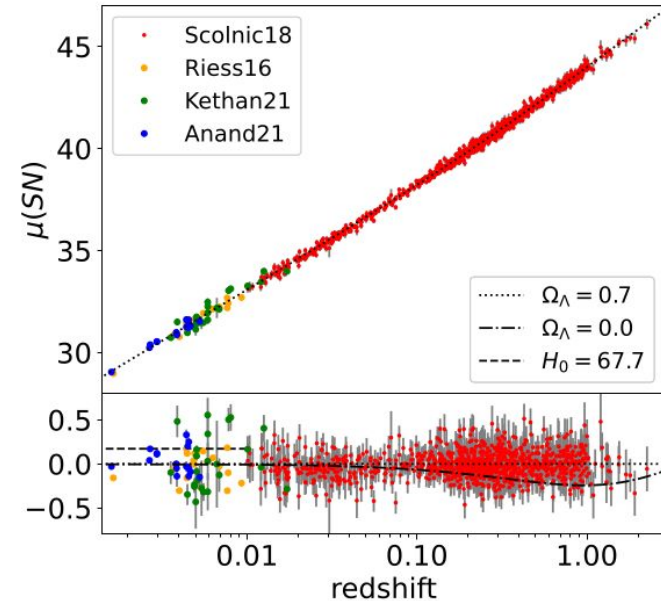   **H_0 = 73.2 ± 1.3 km/s/Mpc (SH0ES Team, Riess et al 2021)**

Fig. 8 Hubble diagram for SNe Ia. SNe Ia in the Hubble flow (red points) are from the Pantheon compilation ([179], https://archive.stsci.edu/prepds/ps1cosmo/) whereas low redshift SNe Ia are retrieved from [74] (Riess16, calibrated with Cepheids), [183] (Khetan21, calibrated with SBF) and [184] (Anand21, calibrated with TRGB). The distance moduli are computed for a flat cosmology with $\Omega_\Lambda = 0.7$ and adopting the [70] calibration of nearby SN Ia ($H_0 = 73.2$). The bottom panel shows the residuals with respect to the adopted cosmology. The dot-dashed line is the expected trend for a null cosmological constant. Instead the dashed line at redshift $z < 0.01$ illustrates the shift of the Planck H_0 calibration with respect to local SN Ia calibration
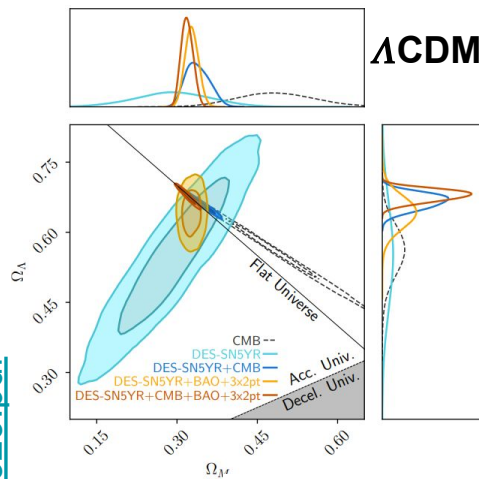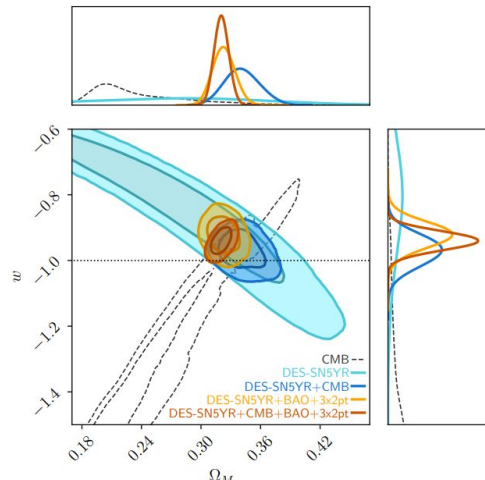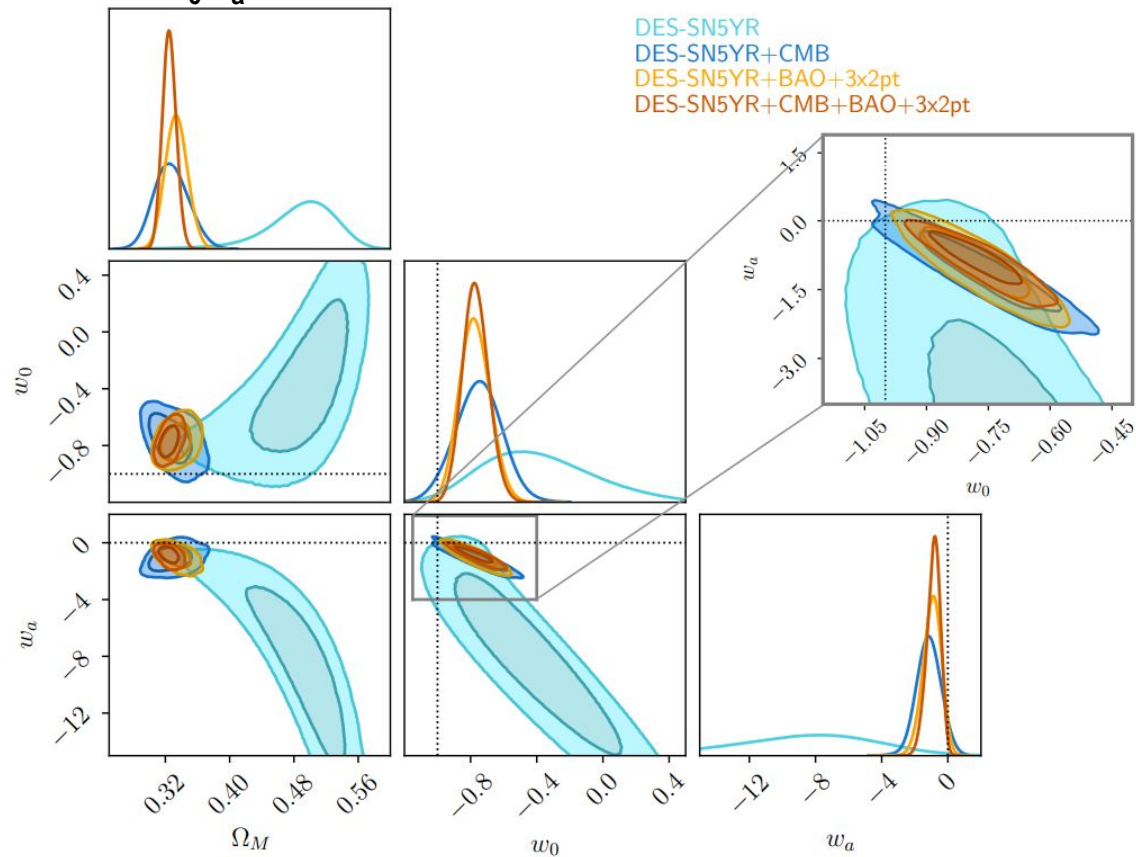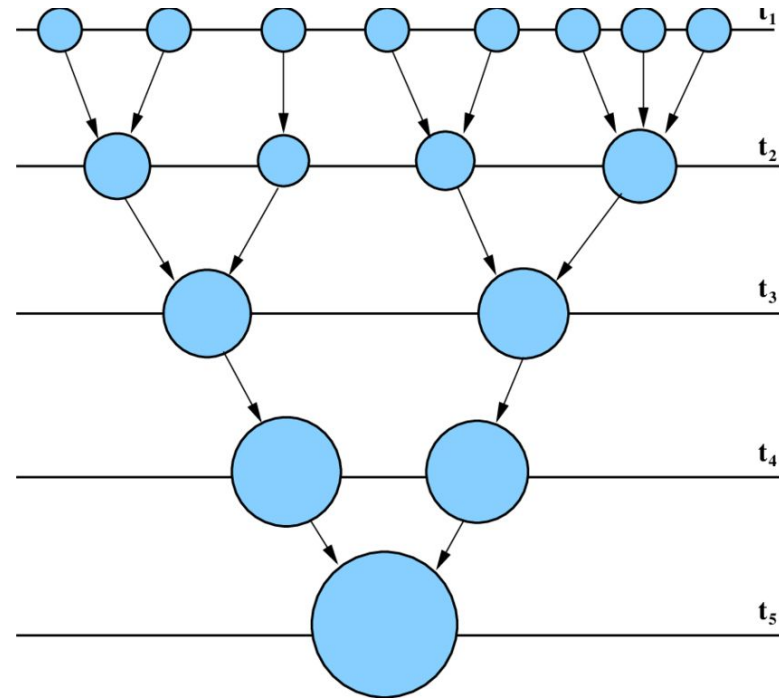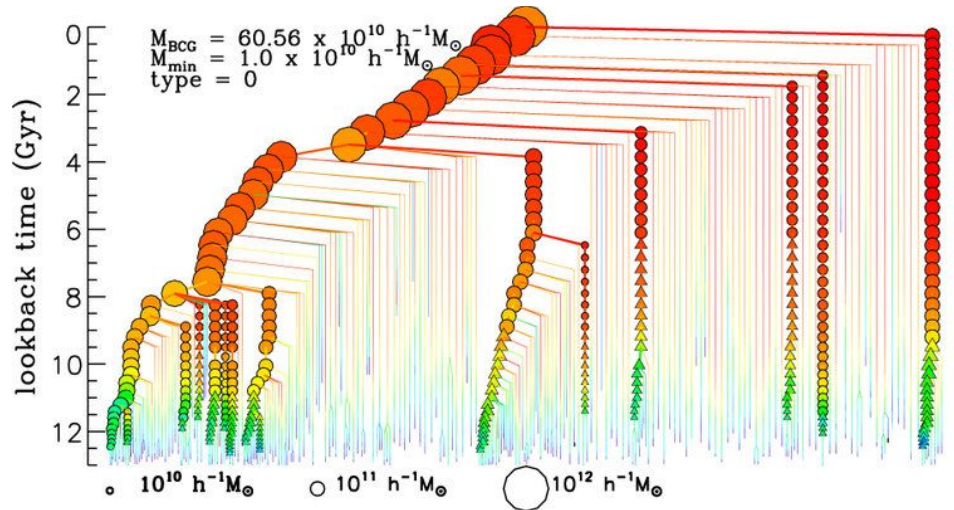
STATISTICAL PROPERTIES OF THE LARGE SCALE STRUCTURES:
CLUSTER NUMBER COUNTS

For a review: **Allen+2011 or Kravtsov+2012**

In the LCDM scenario, structures grow *hierarchically*: Small overdensities are able to overcome the cosmological expansion and collapse first, and the resulting dark matter "halos" merge together to form larger halos which serve as sites of galaxy and galaxy cluster formation

We can follow the collapse of a spherical overdensity in a homogeneous universe. SC model becomes inaccurate (brakes down) shortly after turn-around it is still a useful model to identify important epochs in the linearly evolved density field.

- The linearly extrapolated density field collapses when $\delta_{lin} = \delta_c = 1.686$
- Virialized dark matter haloes have an average overdensity of $\Delta_{vir} = 178$

According to the spherical collapse model, regions with $\delta(x,t) > \delta_c \simeq 1.686$ will have collapsed to produce dark matter haloes by time *t.*

Assuming a Gaussian density field, the fraction of cosmic volume with $\delta(x,t) > \delta_c$ depends only on the variance of the matter density field:

$$\sigma^2 = <\delta^2>$$

GALAXY CLUSTERS

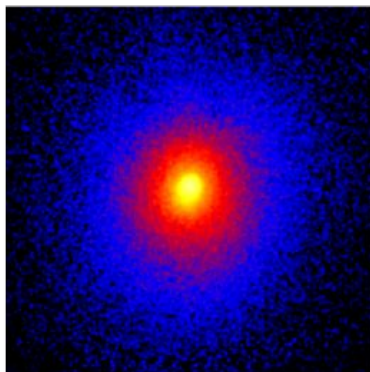- **Most massive bound objects in the Universe:**
  M ≃ 10^{13} - 10^{15} M$_\odot$ and R ≃ 1 - 5 Mpc

- **Multi-component systems:**
  Galaxies and stars (~5%), ICM (~15%), DM (~80%)
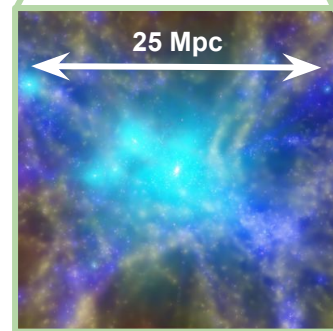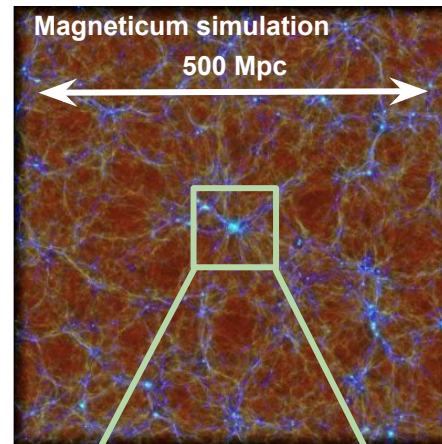
OPTICAL
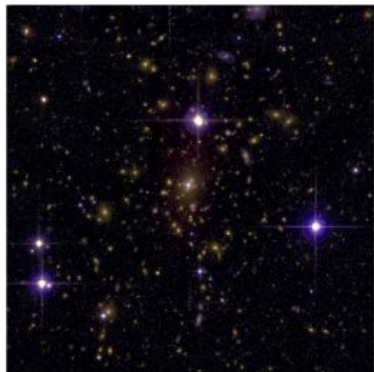
RICHNESS, LENSING
EFFECTS

X-RAYS

LUMINOUS AND EXTENDED
X-RAY SOURCES

MICROWAVES
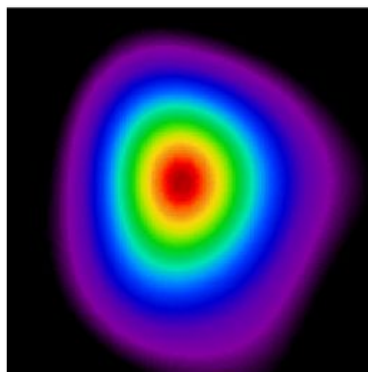
SUNYAEV-ZEL'DOVICH
EFFECT

Magneticum simulation
500 Mpc

25 Mpc

From Hirschmann+2014

GALAXY CLUSTERS AS COSMOLOGICAL PROBE

Evolution of the clusters population in 2 N-body simulations

The abundance and spatial distribution of galaxy clusters are sensitive to the **growth rate** of cosmic structures and **expansion history** of the Universe

σ_8: Amplitude of the matter power spectrum

Ω_m: Present-day total matter density
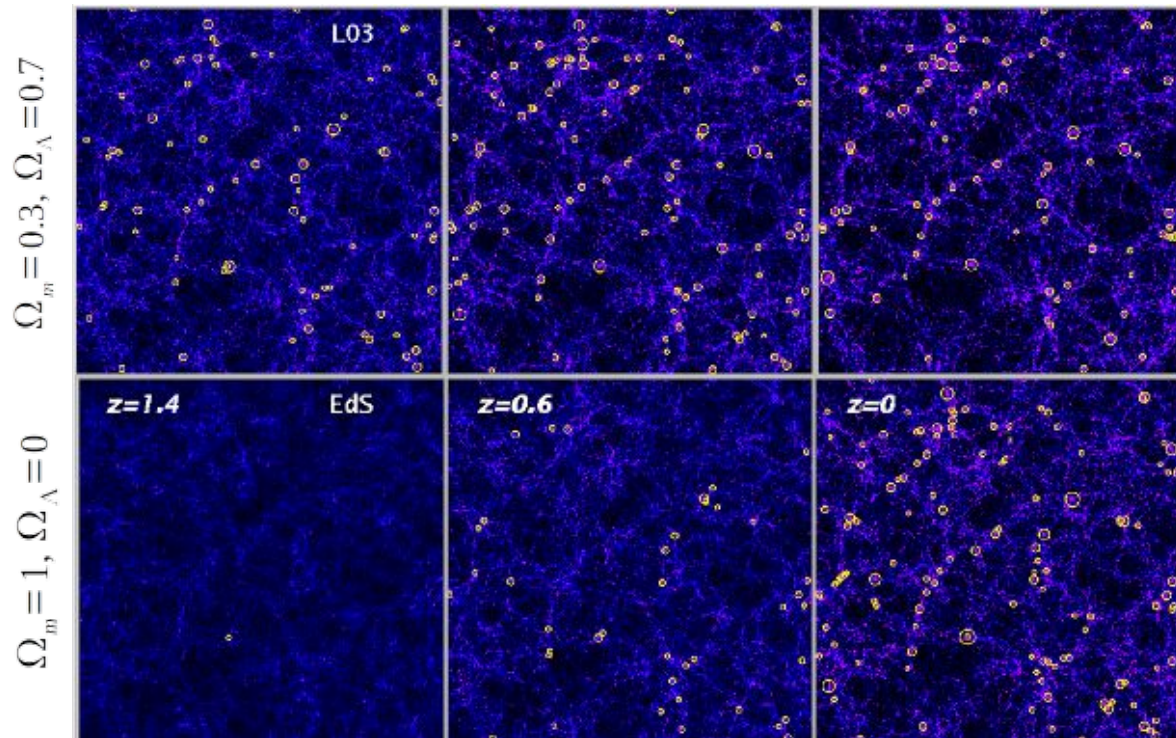
$$S_8 = \sigma_8 \, (\Omega_m / 0.3)^{0.5}$$

Dark energy equation of state parameter w
Total neutrino mass
Deviation from GR

….

$\Omega_m = 0.3, \ \Omega_\Lambda = 0.7$

$\Omega_m = 1, \ \Omega_\Lambda = 0$

L03

z=1.4   EdS   z=0.6   z=0

time

From Borgani, Guzzo 2001

Cluster abundance:

geometry

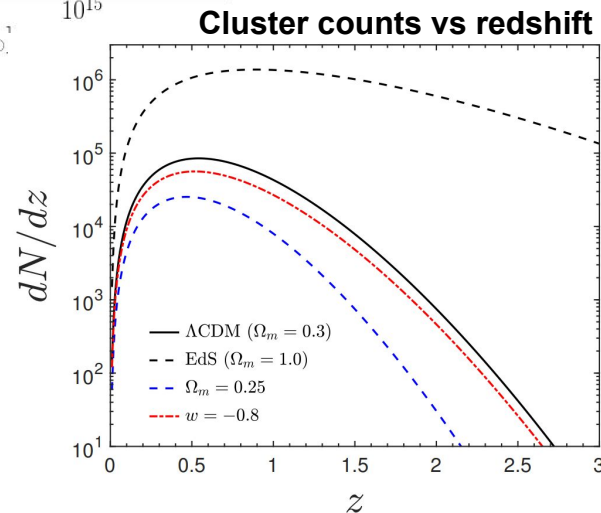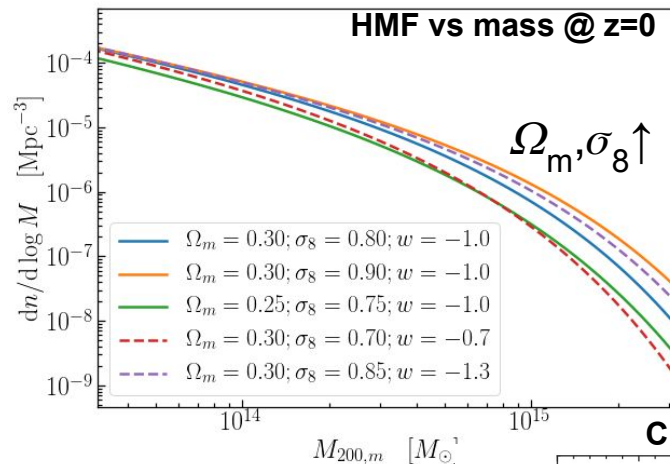$$\frac{dN}{dz d\Omega} = \frac{dV}{dz d\Omega} n(M, z)$$

growth

The halo mass function:

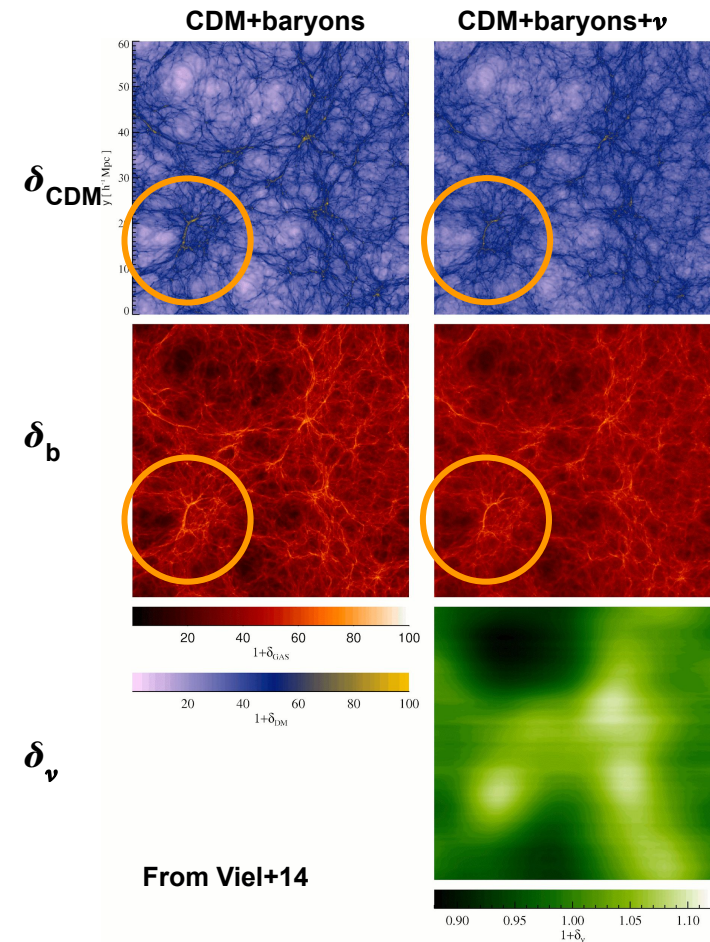$$n(z, M) = \frac{\rho_m}{M} f(\sigma) \frac{d \ln(\sigma^{-1})}{dM}$$

Variance of the density field:

$$\sigma(z, R) = \frac{1}{2\pi^2} \int_0^\infty dk\, k^2 \boxed{P_m(z, k)} |W(kR)|^2$$
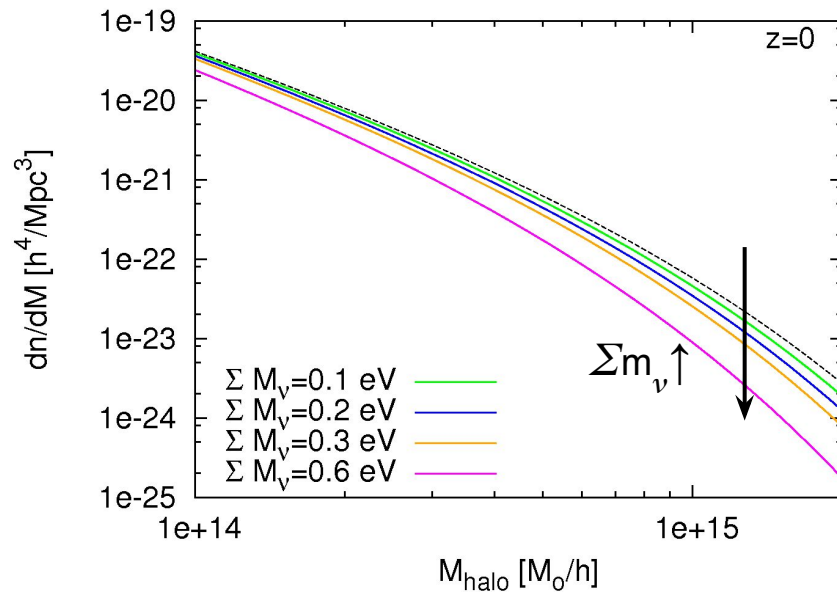
Matter power spectrum

HMF vs mass @ z=0

$\Omega_m, \sigma_8 \uparrow$

$\Omega_m = 0.30; \sigma_8 = 0.80; w = -1.0$
$\Omega_m = 0.30; \sigma_8 = 0.90; w = -1.0$
$\Omega_m = 0.25; \sigma_8 = 0.75; w = -1.0$
$\Omega_m = 0.30; \sigma_8 = 0.70; w = -0.7$
$\Omega_m = 0.30; \sigma_8 = 0.85; w = -1.3$

$M_{200,m}\ [M_\odot]$

Cluster counts vs redshift

$\Lambda\mathrm{CDM}\ (\Omega_m = 0.3)$
EdS $(\Omega_m = 1.0)$
$\Omega_m = 0.25$
$w = -0.8$

CDM+baryons **CDM+baryons+ν**

δ_{CDM}

δ_b

δ_ν

From Viel+14

Massive neutrinos:

- Delay the epoch of matter-radiation equality
- Suppress the growth of density fluctuation on scale smaller than the free-streaming length

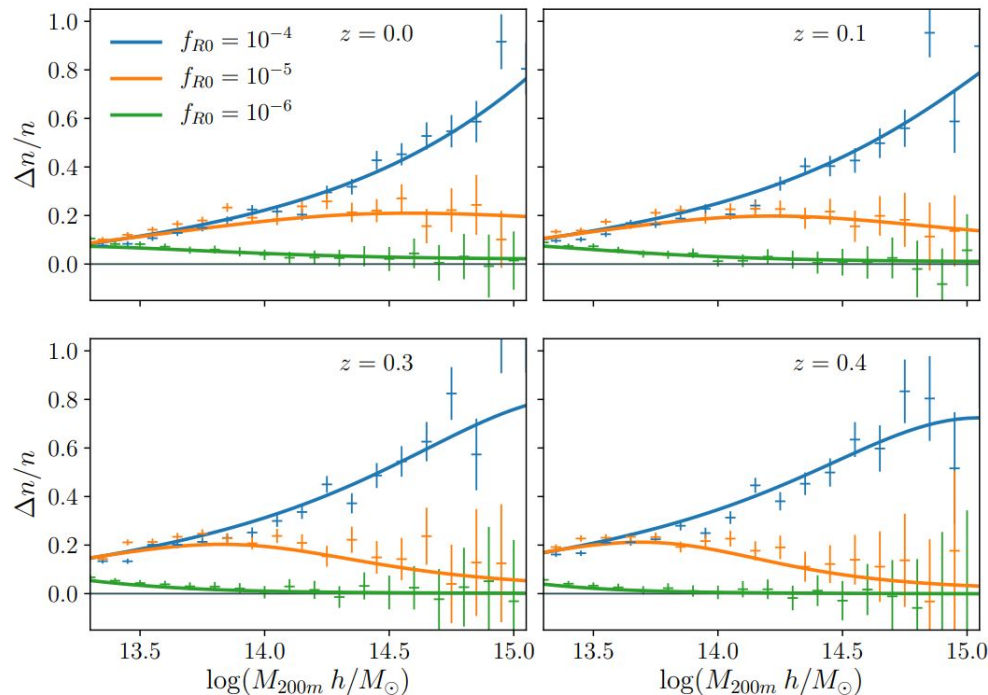**Effects on the number density of halos as a function of mass**

z=0

$\Sigma m_\nu \uparrow$

$\Sigma M_\nu = 0.1$ eV
$\Sigma M_\nu = 0.2$ eV
$\Sigma M_\nu = 0.3$ eV
$\Sigma M_\nu = 0.6$ eV

dn/dM [h^4/Mpc^3]

M_{halo} [M_0/h]

Modified gravity models, e.g. f(R):

$$S = \frac{1}{16\pi G} \int \sqrt{-g}[R + f(R)]d^4x.$$

- Give rise to accelerated expansion and enhance gravity

- Introduce screening mechanism that restores GR in high density environments

Relative effect on the Halo Mass Function compared to ΛCDM


From Hagstotz+18

LIMITATIONS FOR CLUSTER COSMOLOGY STUDIES

DES Collaboration 2020
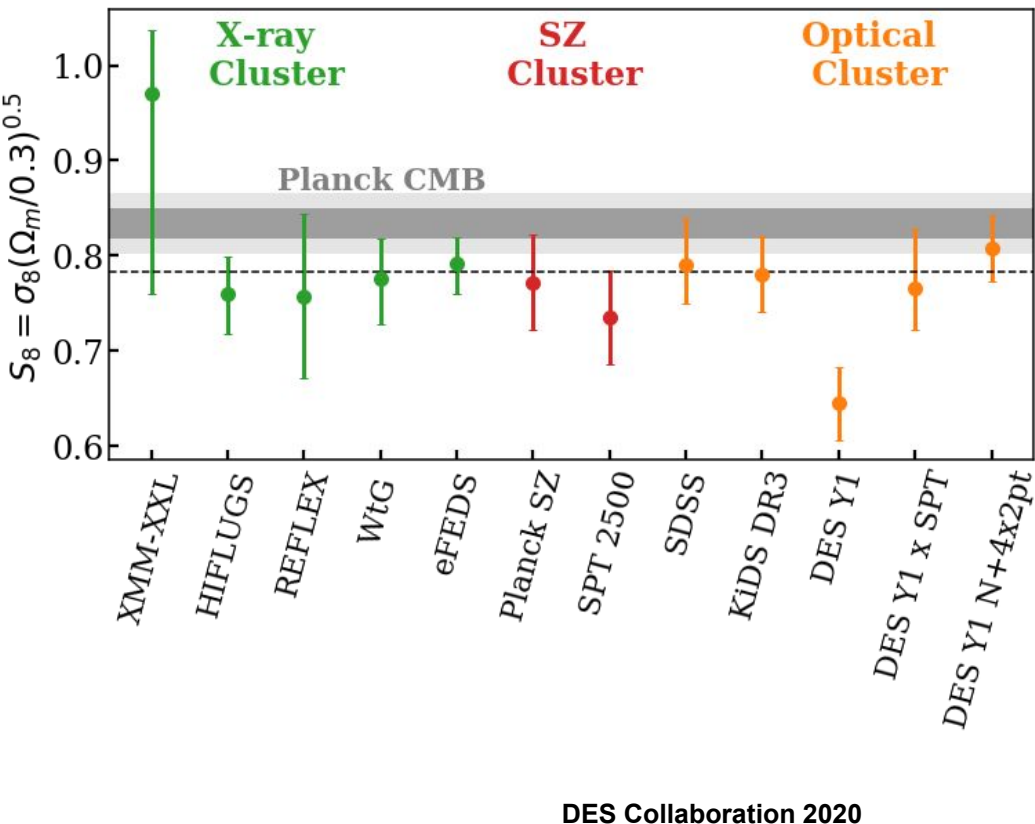
- **Cosmological constraints independent and competitive with other cosmological probes**

- **Slight to moderate tension between different cluster studies**

- **Currently limited by the mass (i.e. scaling relation) calibration**

Planck-SZ results assuming 3 different mass calibrations (Planck Collaboration 2015)
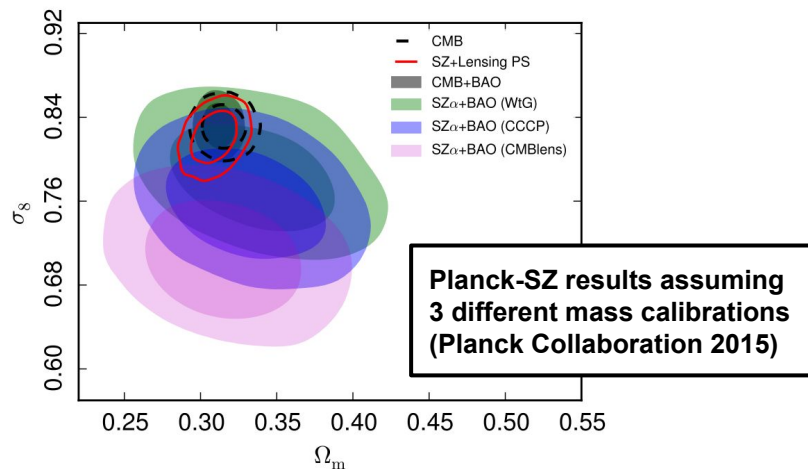
STATISTICAL PROPERTIES OF THE LARGE SCALE STRUCTURES:
CLUSTERING

For a review on structure formation:
https://sites.astro.caltech.edu/~george/ay127/kamionkowski-perturbations-notes.pdf
https://people.ast.cam.ac.uk/~pettini/Intro%20Cosmology/Lecture14.pdf
For a review on BAO: https://arxiv.org/pdf/0910.5224.pdf
For a review on RSD: https://arxiv.org/pdf/astro-ph/9708102.pdf

Inflation generates primordial perturbations through the amplification of quantum fluctuations, which are stretched to astrophysical scales by the rapid expansion.

The simplest models of inflation predict that the initial fluctuations constitute a Gaussian random field, with an almost purely adiabatic primordial perturbations with a near scale-invariant power spectrum. In these models the primordial power spectrum is often described in terms of a spectral index n_s and an amplitude of the perturbations A_s as (k_p = 0.05 Mpc^{-1} = pivot scale):

$$P(k) = A_s \left(\frac{k}{k_p} \right)^{n_s}$$
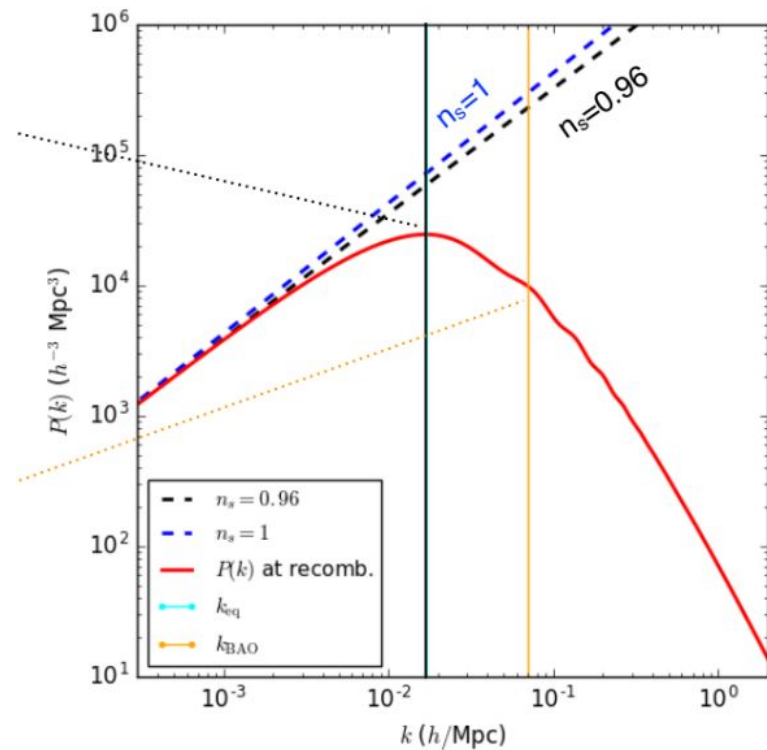
Large scale ⟵ ⟶ Small scale

EVOLUTION OF DENSITY PERTURBATIONS

After the perturbations are created in the early Universe, they undergo a complex evolution which depends on the theory of gravity (GR), and the expansion history of the Universe.
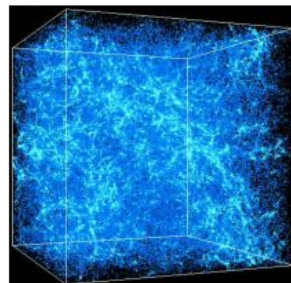
- **Gravity is the dominant force that moves matter on the largest scales.**
- **The dark matter, which constitutes ~ 5/6 of the nonrelativistic matter in the Universe, is composed of "cold dark matter", pressureless matter that interacts with everything else only gravitationally.**
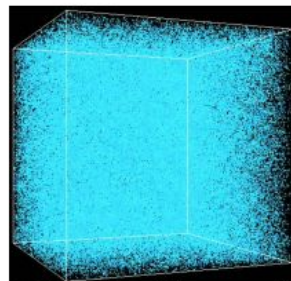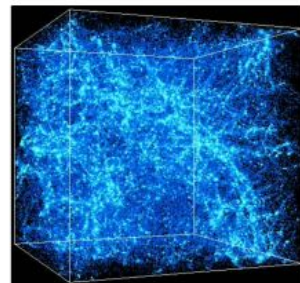

Universe 120 million years old
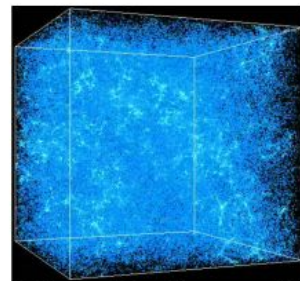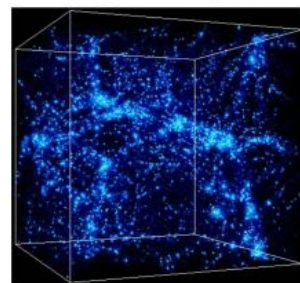
Universe 490 million years old

Universe 1.2 billion years old

Universe 2.2 billion years old
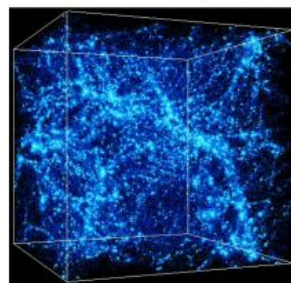
Universe 6.0 billion years old

Universe 13.7 billion years old

- **Overdensity field:**

$$\delta(\mathbf{x}) \equiv \frac{\rho(\mathbf{x}) - \langle\rho\rangle}{\langle\rho\rangle}$$

For CDM model:

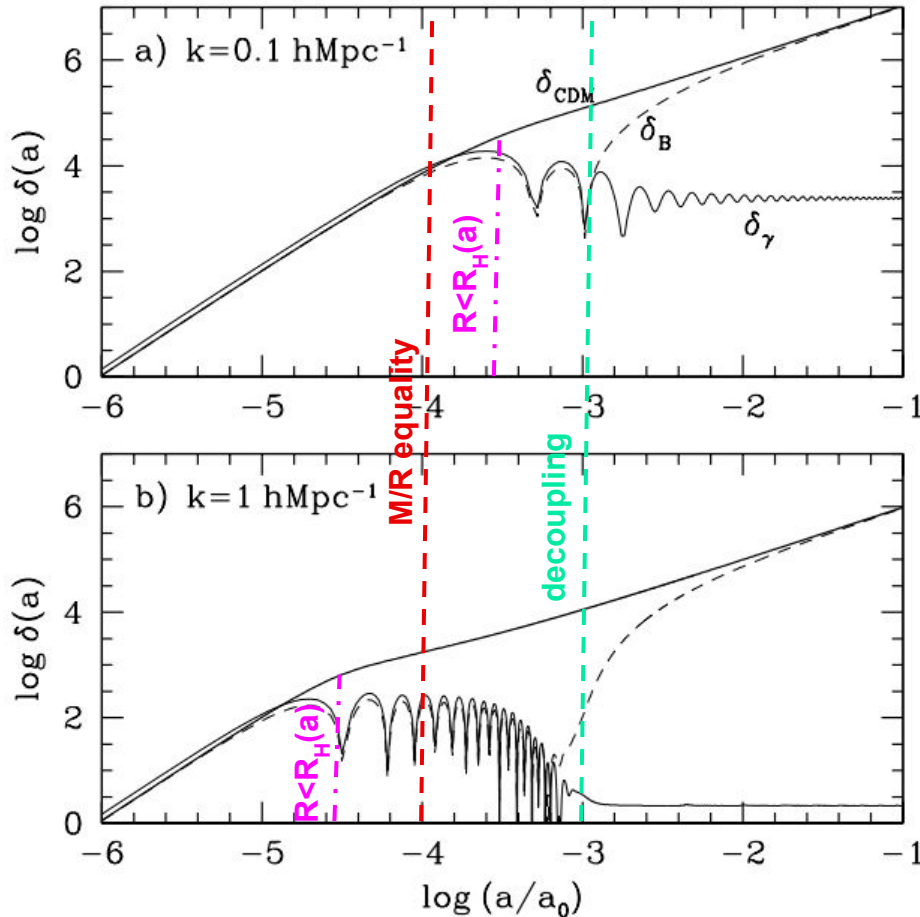|	$z > z_{eq}$	$z < z_{eq}$
$R > R_H$	$\delta_r \propto \delta_m \propto a^2$	$\delta_r \propto \delta_m \propto a$
$R < R_H$	$\delta_{cdm} \sim const$ $\delta_{b+\gamma}$ *oscillations*	$\delta_{cdm} \propto a$ $z < z_{rec}: \delta_b \rightarrow \delta_{cdm}$

Matter-radiation equality

$$\frac{\rho_m(a_{eq})}{\rho_r(a_{eq})} = 1$$

$$1 + z_{eq} = \frac{a_0}{a_{eq}} \simeq 3250$$

Hubble radius

$$R_H(t) = \frac{c}{H(t)} \sim c\,t$$

The evolution of adiabatic perturbations in a CDM universe with $\Omega_{m,0} = 1$, $\Omega_{B,0} = 0.05$, $h = 0.5$.
The scale factor is normalized at the present time.
Decoupling: $a \sim 10^{-3}$
Matter/radiation equality: $a \sim 10^{-4}$

Note: Since these modes enters horizon after (k=0.1) or just before (k=1) matter-radiation equality, there is no Meszaros effect (δ_{cdm} ~ cost)

The primordial power spectrum of density fluctuations gets "processed" by the growth of density perturbations:

$$P(k, z) = P_{\mathrm{primordial}}(k)T^2(k, z)$$

**where the transfer function T(k) takes into account the effects of gravitational amplification of density perturbation mode of wavelength *k***
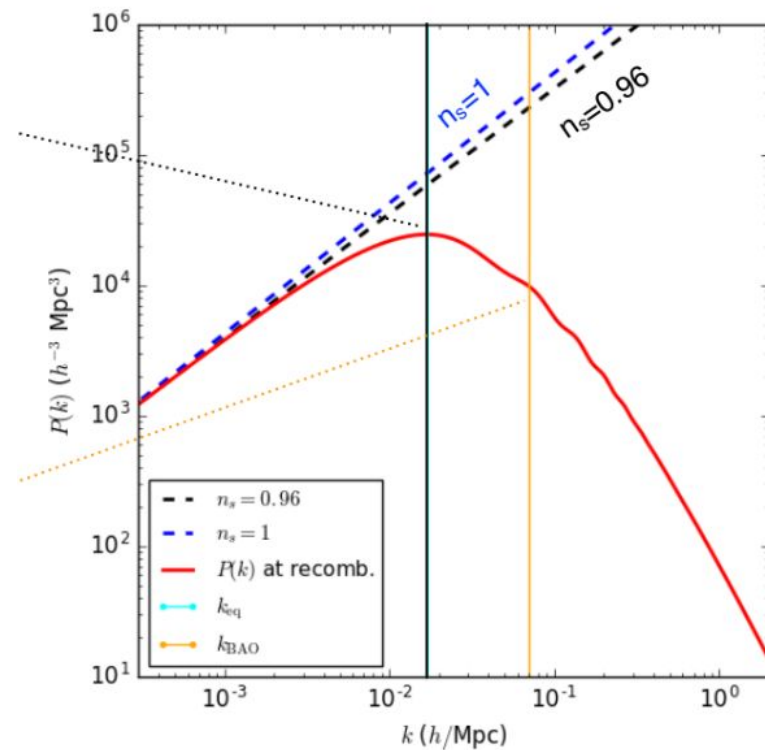
Transfer function (CDM):

$$T(k) \simeq \begin{cases} 1, & k \lesssim k_{eq}, \\ (k/k_{eq})^{-2}, & k \gtrsim k_{eq}, \end{cases}$$

The characteristic length scale is the horizon-size at matter-radiation equality, $k_{eq} = 2\pi(ct_{eq})^{-1} \propto \Omega_{m,0}h^2$; before t_{eq}, below the horizon, dark matter fluctuations cannot growth.

Thus, if $P_{primordial}(k) \propto k^n$, the processed power spectrum is:

- **$P(k) \propto k^n$ for $k \ll k_{eq}$**
- **$P(k) \propto k^{n-4}$ for $k \gg keq$**
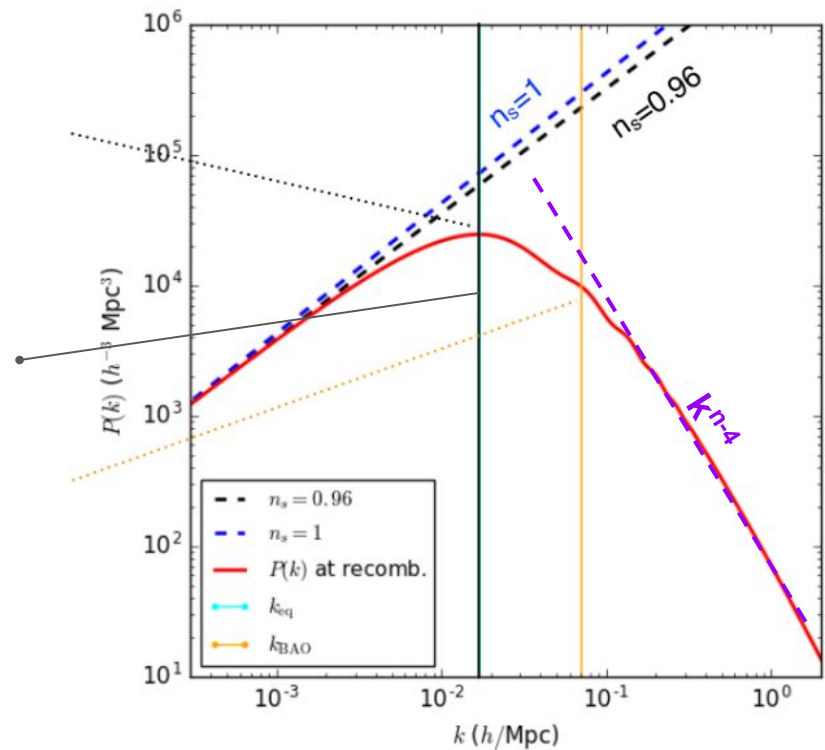
Large scale ⟷ Small scale

EVOLUTION OF DENSITY PERTURBATIONS

Baryonic Acoustic Oscillations:

In the early, high-temperature Universe, baryons and photons were tightly coupled by Compton scattering, in a so-called photon-baryon fluid; the competing forces of radiation pressure and gravity set up oscillations in the photon-baryon fluid. As the Universe expands and cools down, atoms form (Recombination) and the interaction rate between baryons and photons decreases: **photons begin to free-stream, leaving baryons in a shell with a radius approximately equal to the sound horizon at the time of decoupling**. From that moment on, only the gravitational interaction between dark matter and baryonic matter remains. **This characteristic radius is therefore imprinted as an overdensity and the power spectrum have an excess of power on this scale**.
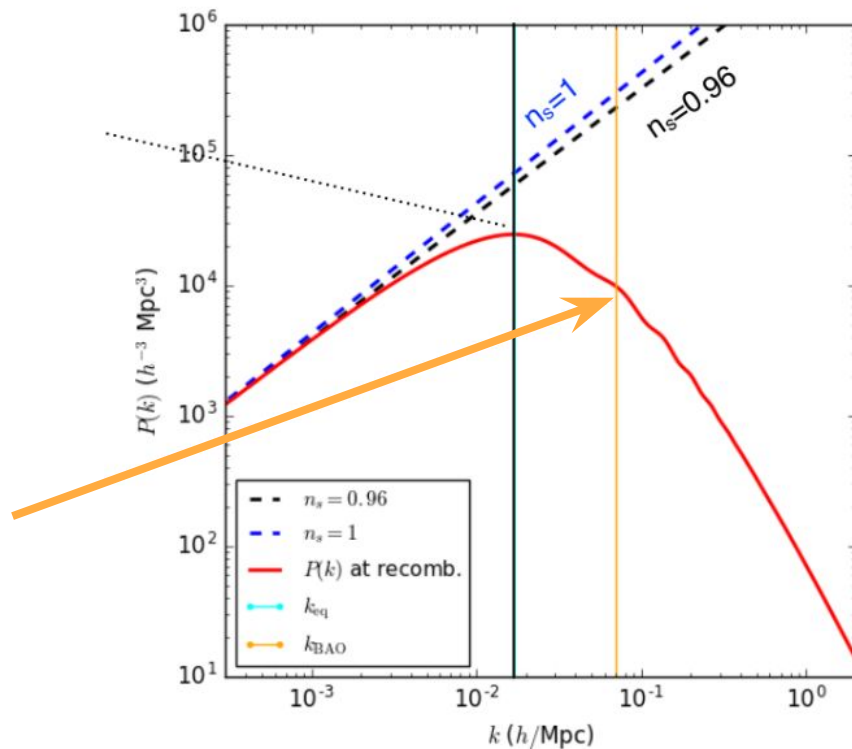
2PT CORRELATION FUNCTION

The most commonly used quantitative measure of large scale structure is the two-point correlation function. The two-point correlation function, **ξ(r), is the excess probability (compared to an unclustered Poisson distribution) of finding two tracers of the matter density field (e.g. galaxies) separated by a distance r from each other**:
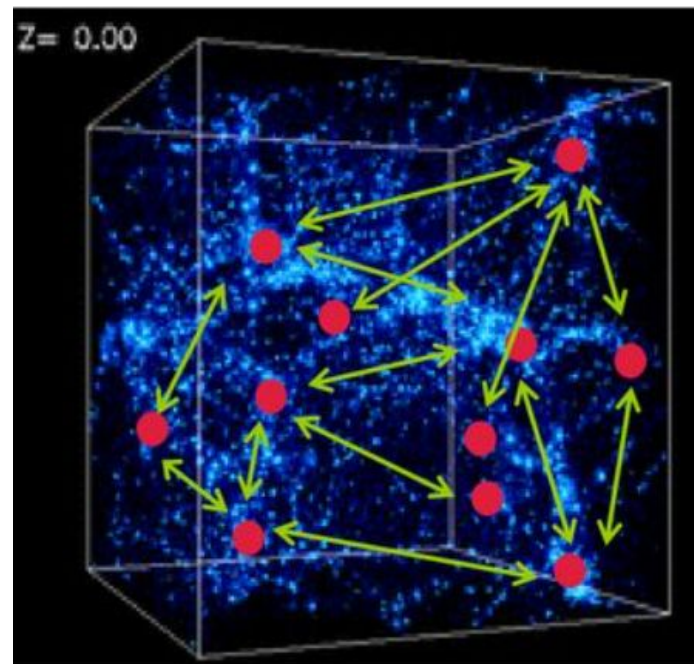
$$dP = n(1 + \xi(r))dV$$

Where **n is the mean number density of the tracer in question.**

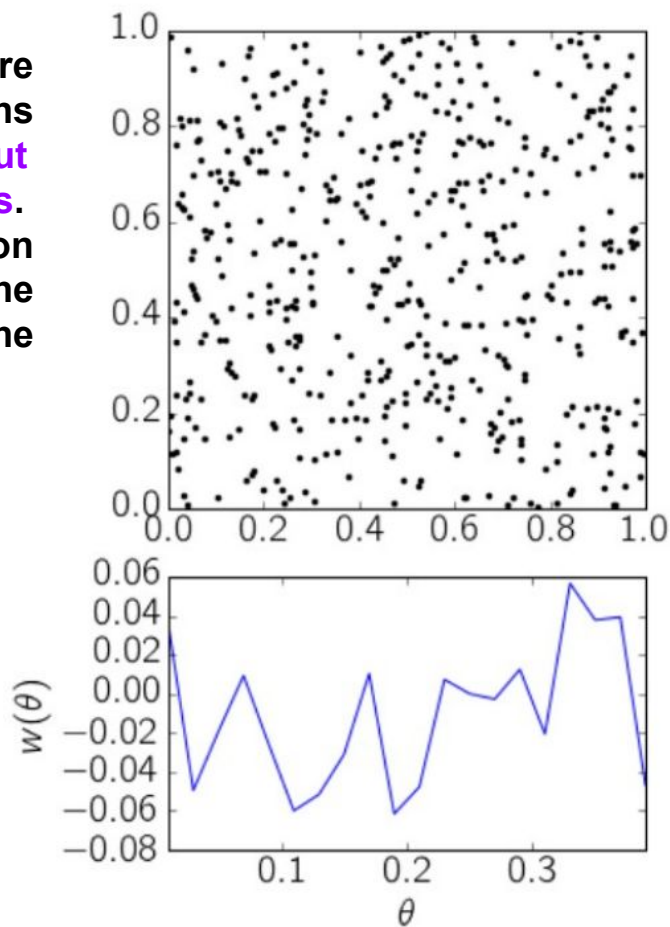2 pt. Correlation Function Estimators:

$$\hat{\xi}(r) = \frac{DD(r) - RR(r)}{RR(r)} \qquad \text{(Peebles \& Hauser, 1974)}$$

$$\hat{\xi}(r) = \frac{DD(r) - 2DR(r) + RR(r)}{RR(r)} \qquad \text{(Landy \& Szalay, 1993)}$$

Z= 0.00

E.g.: the data points in Figure are drawn from distributions with equal densities, but different clustering properties. Using the two-point correlation function we can characterize the difference between the distributions.
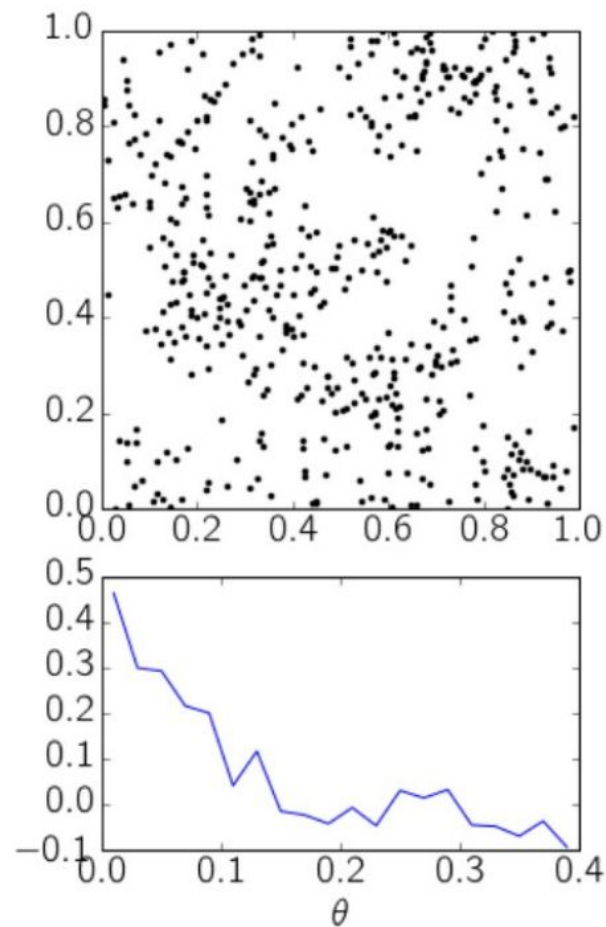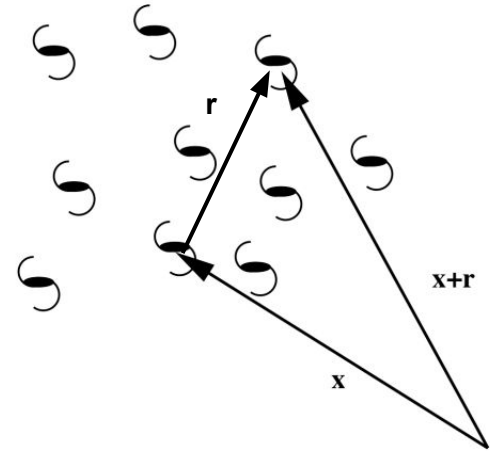
2PT CORRELATION FUNCTION

Assuming the universe is isotropic, the correlation function is a function of a scalar distance. The two-point correlation function can then be written as

$$\xi(\vec{r}) := \langle \delta(\vec{x})\delta(\vec{x}+\vec{r}) \rangle$$

The 2PCF is closely connected to the power spectrum;
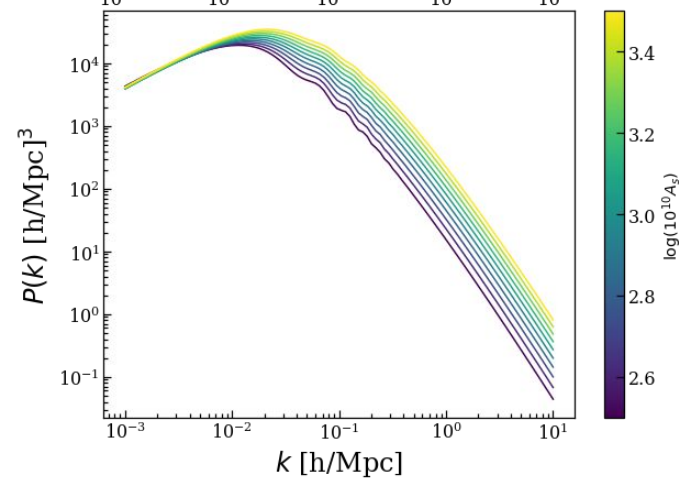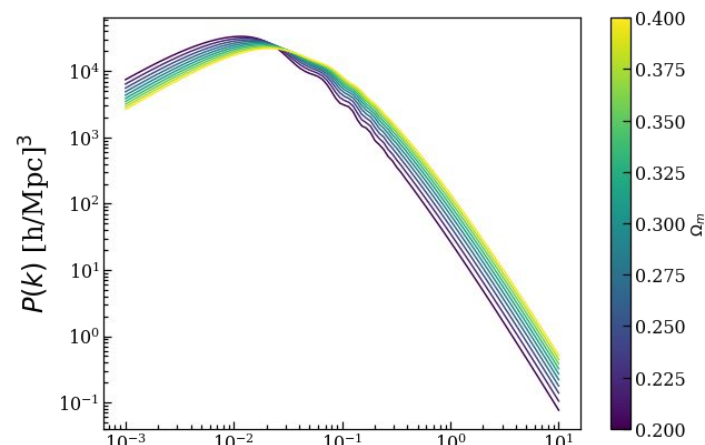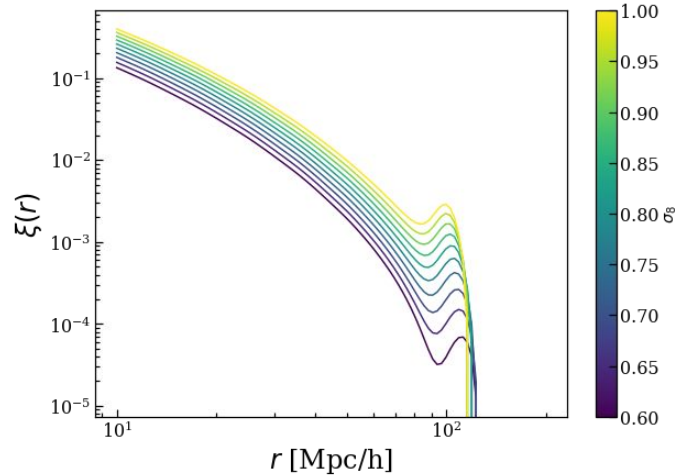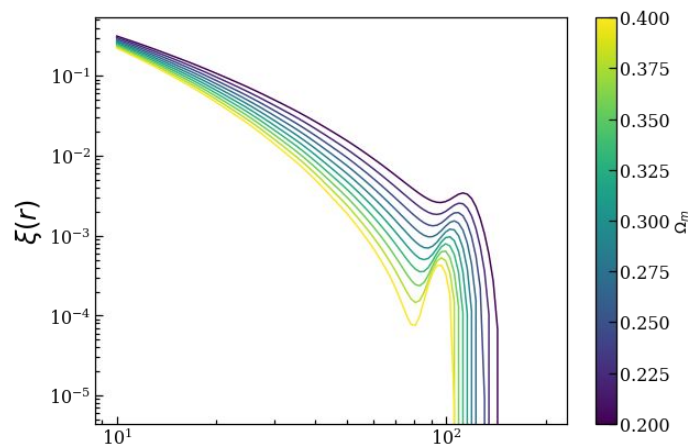They form a Fourier transform pair:

$$\xi(\vec{r}) = \frac{1}{(2\pi)^3} \int d^3 k\, P(\vec{k}) e^{i\vec{k}\cdot\vec{r}},$$

$$P(\vec{k}) = \int d^3 r\, \xi(\vec{r}) e^{-i\vec{k}\cdot\vec{r}},$$

A Gaussian random field is completely specified by either the two-point correlation function , or, equivalently, the power spectrum P(k)!
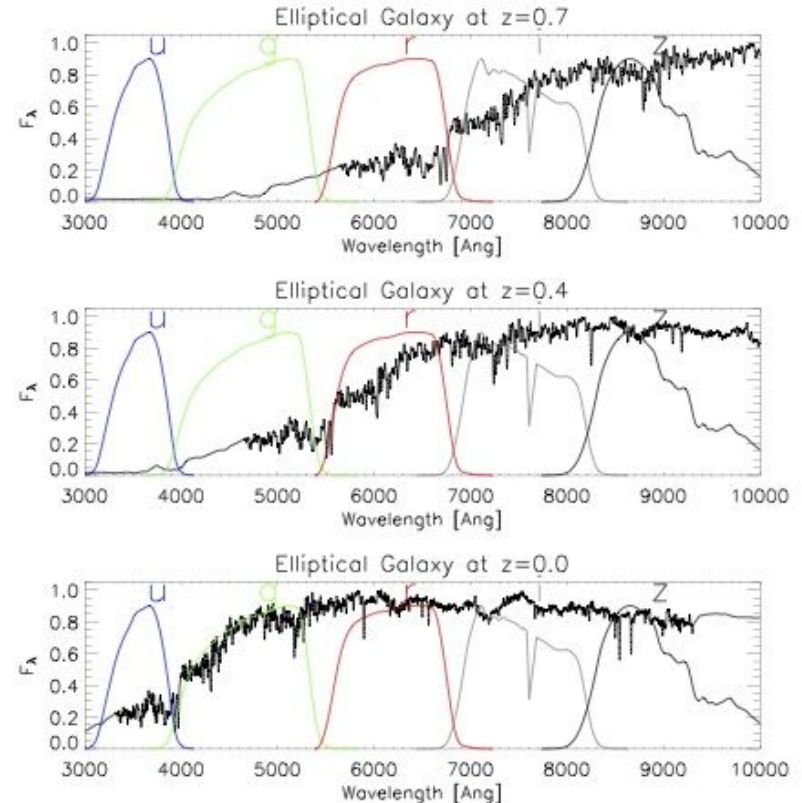
The clustering signal is 3D. However, while angular positions are in general easy to measure, the radial distance can be inferred only from redshift measurements, i.e. the shift to longer wavelengths of the light emitted by distant galaxies due to the recessional velocity ($v = H_0 \cdot d$).

This can be done in two ways:

1) Spectroscopic redshift [$\sigma_z \sim 0.001 \times (1+z)$] : Measuring the spectrum of galaxies, and hence the shift of known emission/absorption lines.

2) Photometric redshift [$\sigma_z \sim 0.01 \times (1+z)$]: Estimate from broadband photometry by fitting template spectra predicted from galaxy Spectral Energy Distribution or from observed galaxies with known spectroscopic redshift.
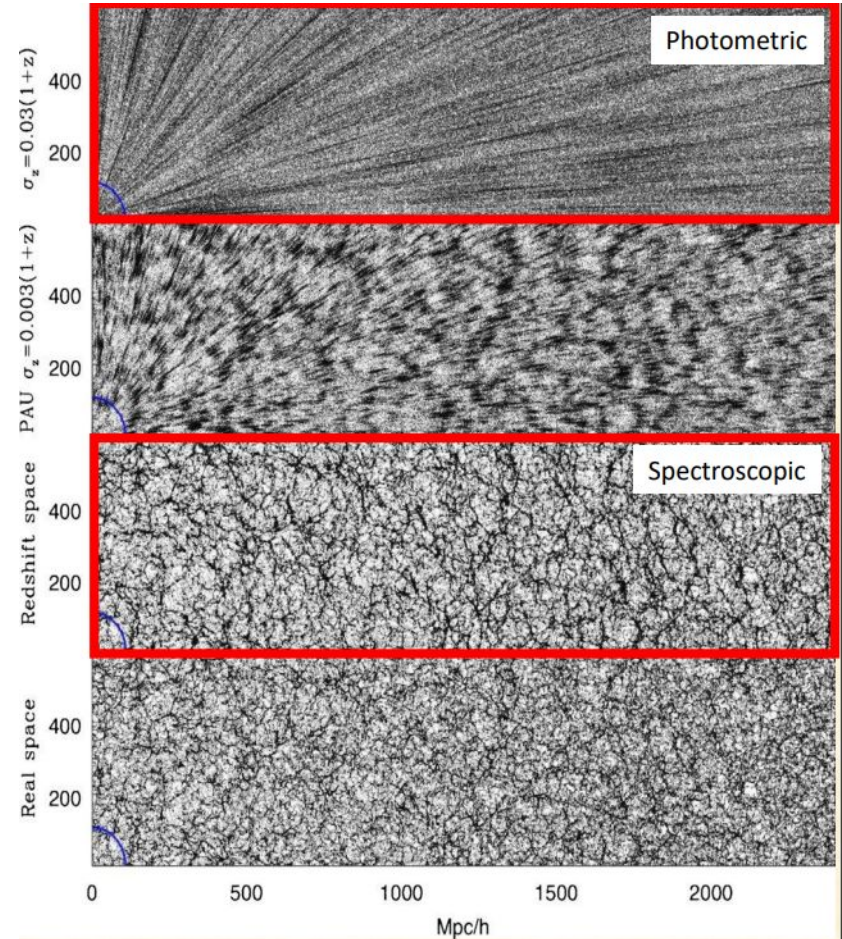

Elliptical Galaxy at z=0.7

Elliptical Galaxy at z=0.4

Elliptical Galaxy at z=0.0

The clustering signal is 3D. However, while angular positions are in general easy to measure, the radial distance can be inferred only from redshift measurements, i.e. the shift to longer wavelengths of the light emitted by distant galaxies due to the recessional velocity (v=H$_0$ · d).

This can be done in two ways:

1) Spectroscopic redshift [$\sigma_z \sim 0.001 \times (1+z)$] : Measuring the spectrum of galaxies, and hence the shift of known emission/absorption lines.

2) Photometric redshift [$\sigma_z \sim 0.01 \times (1+z)$]: Estimate from broadband photometry by fitting template spectra predicted from galaxy Spectral Energy Distribution or from observed galaxies with known spectroscopic redshift.

SPECTROSCOPIC VS PHOTOMETRIC SURVEYS

Photometric redshifts can be measured much faster than their spectroscopic counterparts. In spectroscopy, the light from the galaxy is separated into narrow wavelength bins a few angstroms across. Each bin then receives only a small fraction of the total light from the galaxy. Hence, to achieve a sufficiently high signal-to-noise ratio in each bin, long integration times are required, and only luminous sources can be targeted. For photometry, however, the bins are much larger, and it requires only a short exposure time to reach the same signal-to-noise ratio. Further, imaging detectors usually cover a greater area of the sky than multi-object spectrographs. This means that the redshifts of more objects can be measured simultaneously by using photometry than by spectroscopy. Thus in general:
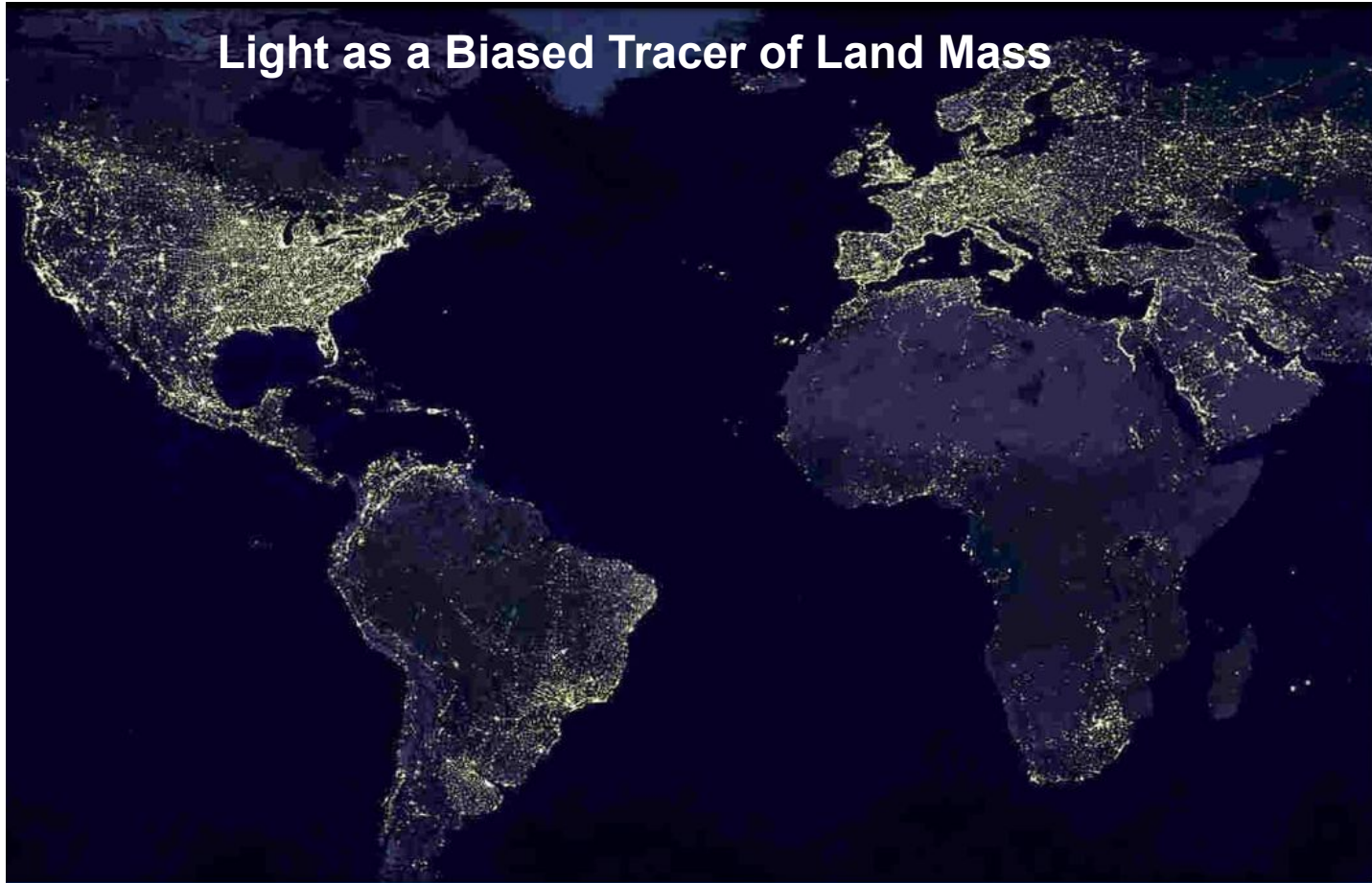
Spectroscopic survey:
- **Accurate 3D reconstruction**
- **Medium depth**
- **Low density**
- **Strong selection effects**

Photometric survey:
- **Low resolution along the line-of-sight**
- **Usually deeper and larger area (i.e. larger volume)**
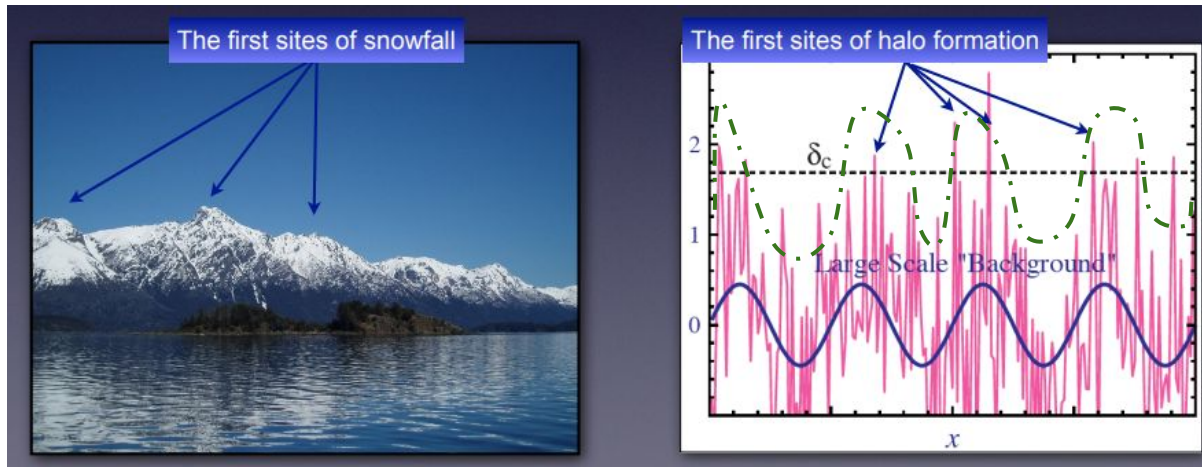- **High density**
- **~ No selection effects**

Light as a Biased Tracer of Land Mass

Halo formation is not a random process; haloes are not a Poisson sampling of the matter field. Rather, they only form where the (smoothed) density field has a sufficiently high value: the critical overdensity for collapse. This `threshold' causes haloes to be biased tracers of the mass distribution. Because of the modulation of the small-scale density field by the long-wavelength modes, overdense regions (on large scales) contain enhanced abundance of dark matter haloes, so that these haloes display enhanced clustering.

$$\delta_h = b_h \delta_m \longrightarrow \xi_{hh}(r) = \langle \delta_h(x)\delta_h(x+r)\rangle = b_h^2 \xi_{mm}$$

The first sites of snowfall

The first sites of halo formation

The clustering of matter encodes a preferred scale, the sound horizon at the baryon drag epoch of the early universe. This feature, which is imprinted on the matter distribution of the early universe by physics around recombination and earlier, is stretched with the expansion of the universe, appearing at a comoving galaxy separation of r_d ~ 150 Mpc. Since galaxies trace the matter content of the universe, the BAO feature is transferred into galaxy clustering, where it manifests as a single localised peak in the galaxy correlation function and an oscillatory signature, or "wiggles", in the galaxy power spectrum. The signature is also visible in other tracers of mass such as fluctuations in the Lyman-α forest — spectral features that indicate the radial distribution of neutral hydrogen clouds between the observer and distant quasars – as well as the CMB. Using BAO we can test for dark energy dynamics and spatial curvature, and in combination with other probes constrain the Hubble constant, the sum of neutrino masses, and the number of light species.
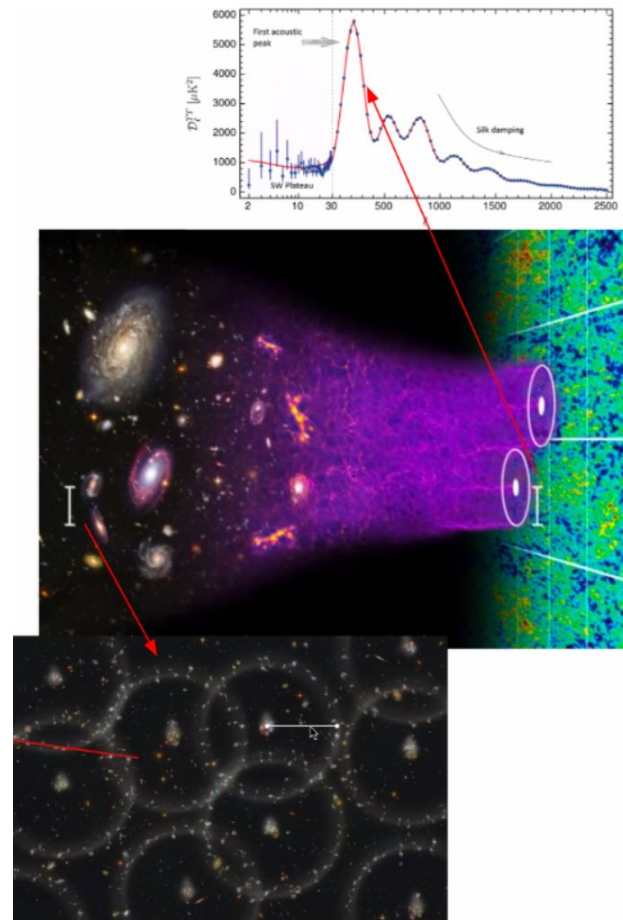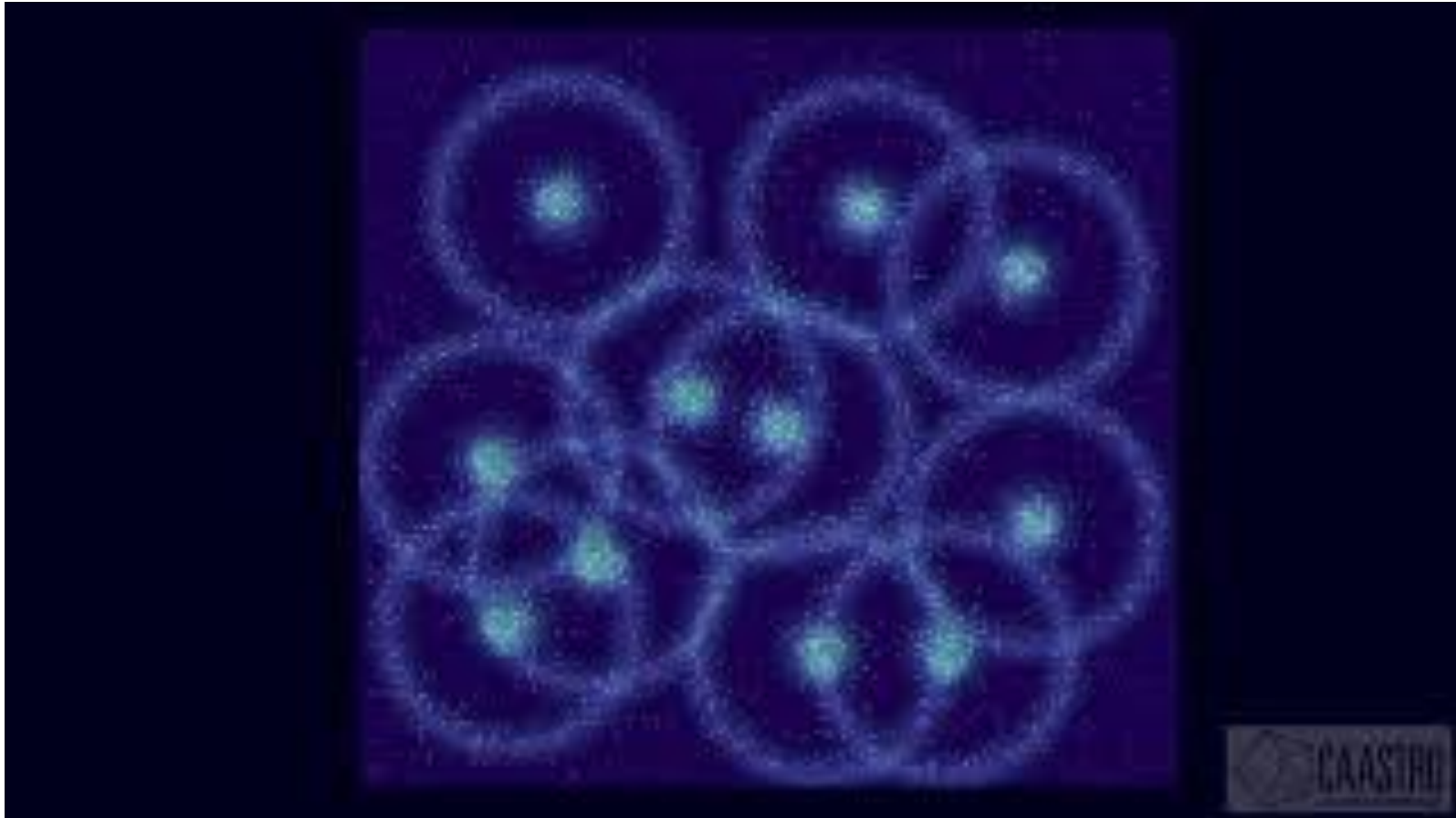
The physics of the propagation of the baryon waves in the early universe is fairly simple, and the sound horizon at drag epoch (~recombination) can be predicted, making r_d is a standard ruler. The (comoving) distance that sound can travel before the drag epoch (which indicates the time when the baryons decoupled (at $z_d \simeq 1060 \simeq z_*$) is given by:

Speed of sound

$$r_d = \int_{z_d}^{\infty} \frac{c_s(z)}{H(z)} dz \qquad c_s(z) = \frac{c}{\sqrt{3\left(1 + \frac{3\rho_B(z)}{4\rho_\gamma(z)}\right)}}$$

$$r_d = \frac{147.05}{\mathrm{Mpc}} \left(\frac{\omega_m}{0.1432}\right)^{-0.23} \left(\frac{N_{\mathrm{eff}}}{3.04}\right)^{-0.1} \left(\frac{\omega_b}{0.02236}\right)^{-0.13}$$
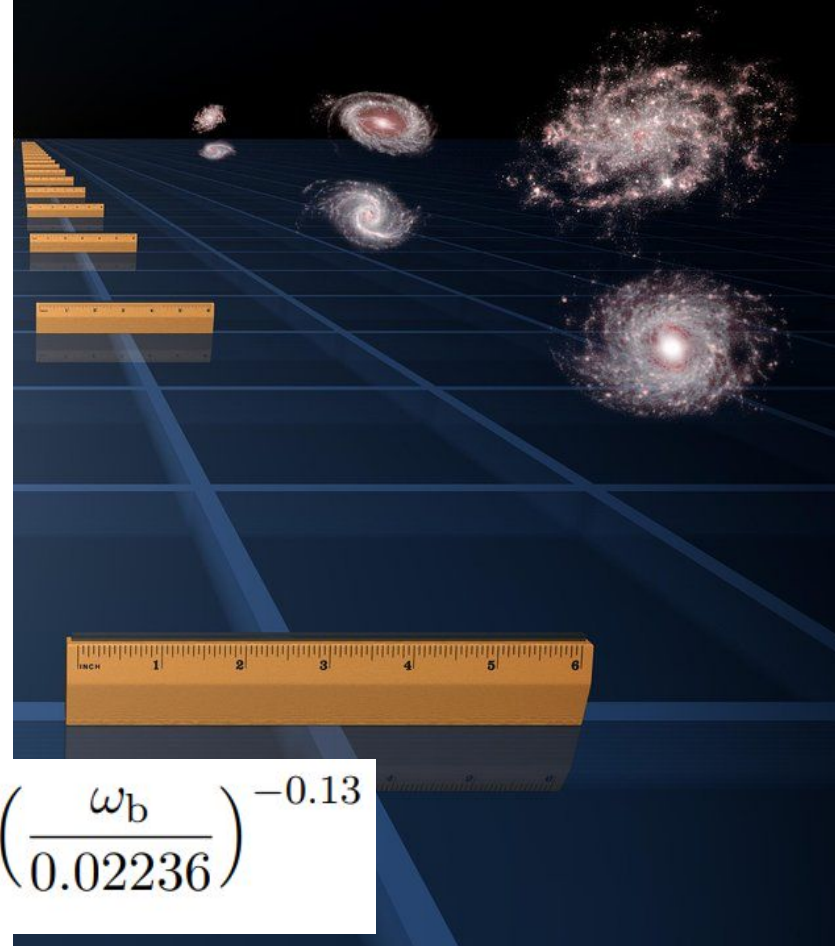
BARYONIC ACOUSTIC OSCILLATIONS

- **Perpendicular** to the observer's line-of-sight, a preferred angular separation of galaxies θ can be observed:

$$\theta = \frac{r_d(z)}{(1+z)d_A(z)}$$

- **Parallel** to the observer's line-of-sight, a preferred redshift separation **Δz** can be observed:
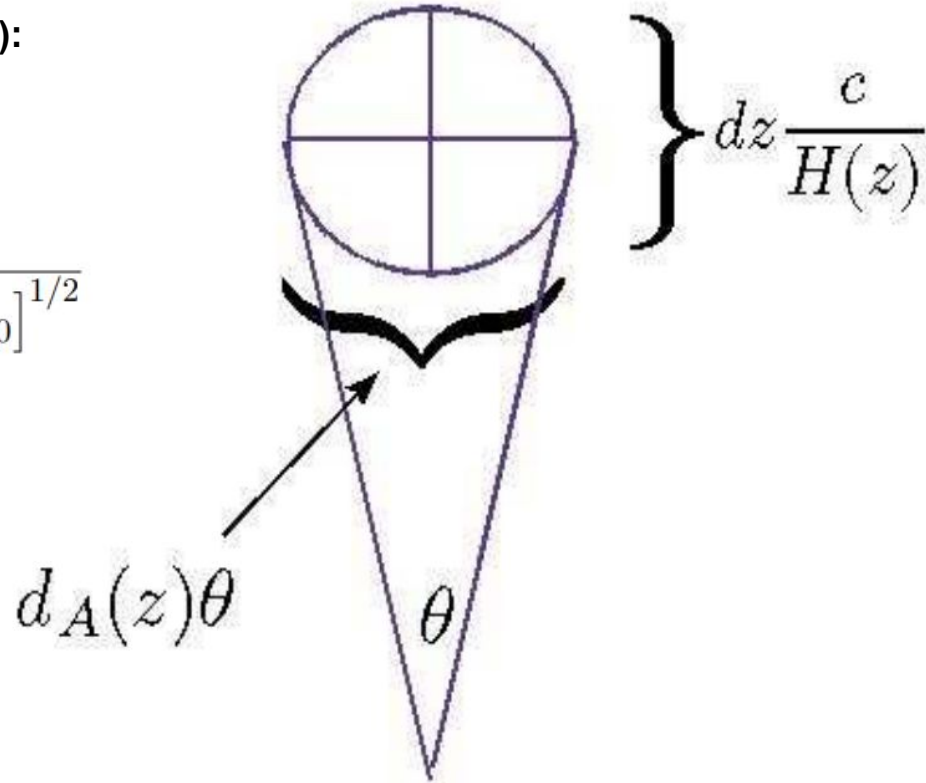
$$\Delta z = \frac{H(z)r_d}{c}$$

$$\Big\} dz \frac{c}{H(z)}$$

$$d_A(z)\theta$$

$$\theta$$
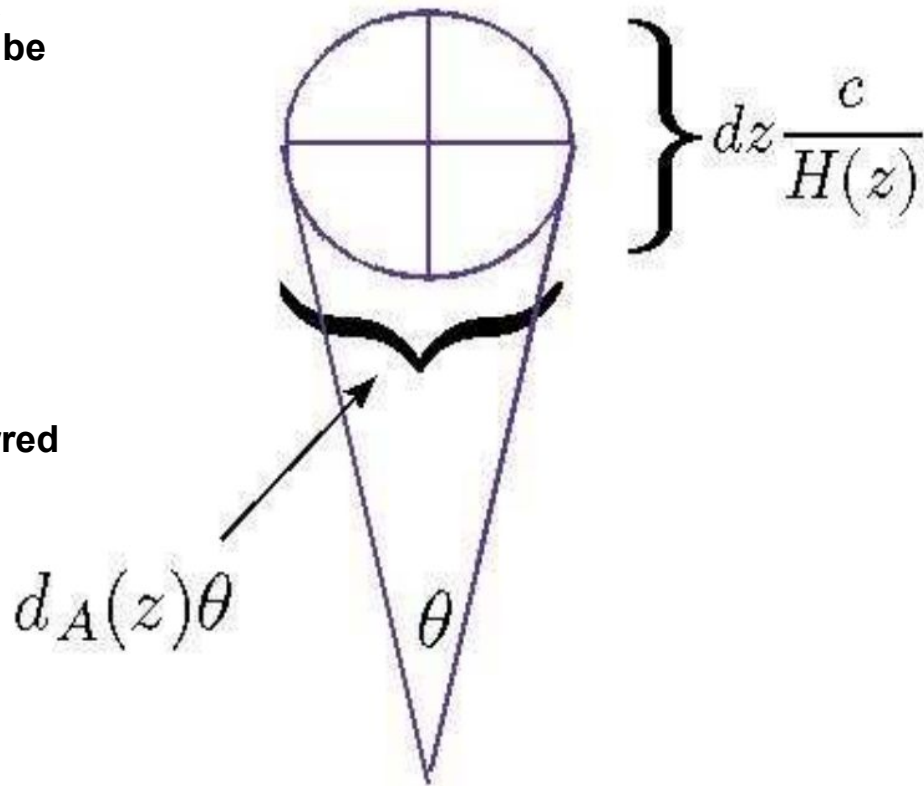
BARYONIC ACOUSTIC OSCILLATIONS

- **For a flat LCDM universe, at late time ($z \ll z_{eq}$):**

Angular diameter distance:

$$d_{\mathrm{A}}(z) = \frac{c}{H_0} \frac{1}{(1+z)} \int_0^z \frac{dz}{\left[\Omega_{\mathrm{m},0}(1+z)^3 + \Omega_{\Lambda,0}\right]^{1/2}}$$

Hubble parameter:

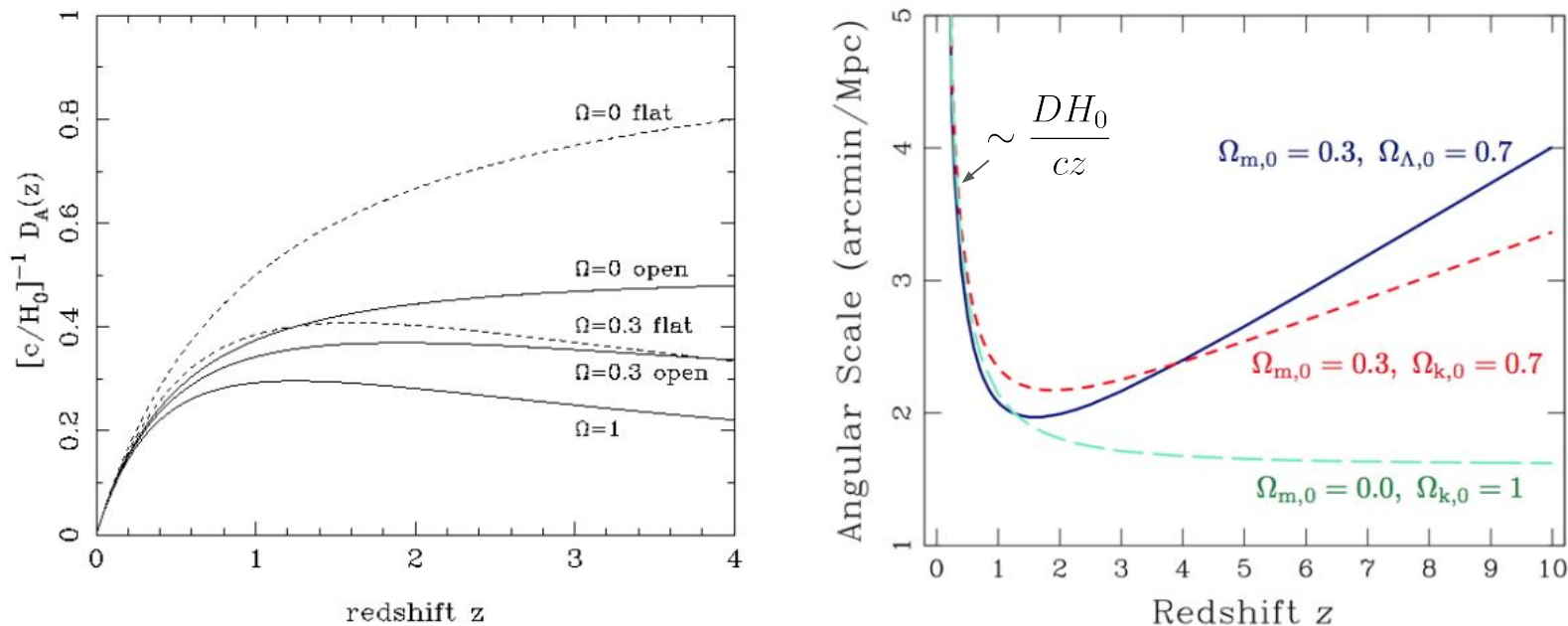$$H(z) = H_0 \sqrt{\Omega_{m,0}(1+z)^3 + \Omega_{\Lambda,0}}$$

$$\left.\right\} dz \frac{c}{H(z)}$$

$$d_A(z)\theta$$

$$\theta$$

Figure 5.4: *Left:* Plot of the angular diameter distance, d_A, (in units of c/H_0) as a function of redshift z in different cosmologies (in this figure $\Omega \equiv \Omega_{m,0}$). *Right:* Angle subtended on the sky by an object of proper size $D = 1\,\mathrm{Mpc}$ as a function of redshift for three different cosmologies, as indicated.
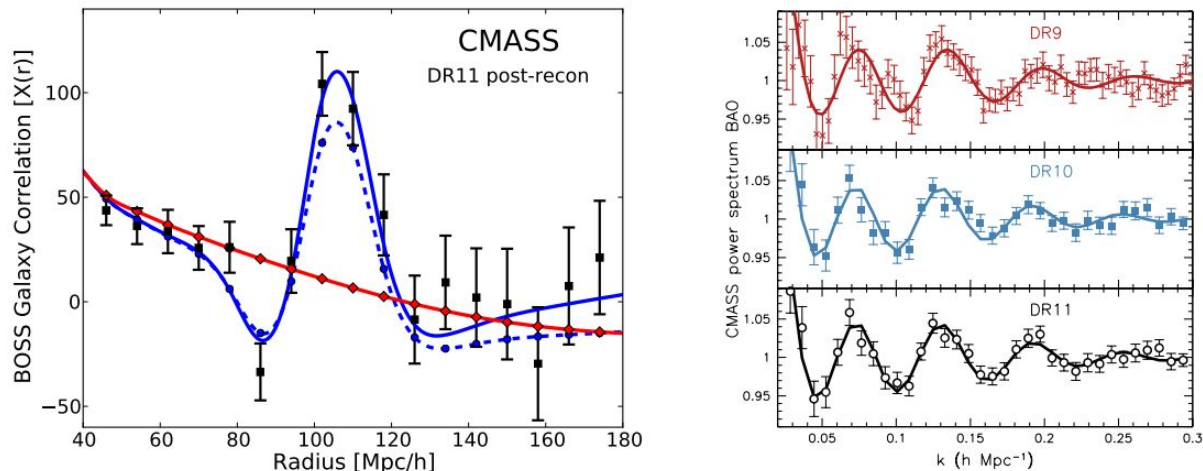
Figure 14.8: *Left:* Baryonic acoustic peak in the two-point correlation function of $\sim 10^6$ galaxies at redshifts $0.4 < z < 0.7$ as determined by the Baryon Oscillation Spectroscopic Survey (BOSS) project. The blue solid line is the best-fit BAO model, while the red line shows the fit by a model which does not include the BAO. *Right:* The BAO feature of the left panel is shown here in the power spectrum of the galaxy distribution: a spike in real space becomes a series of ripples in k-space. The results for three successive data releases of the BOSS project are shown separately. The data and the best fits have been normalised by dividing by the smooth model shown by the red continuous line in the left panel. (Figures reproduced from Anderson et al. 2014).

The inset for each color-coded section of the map includes an image of a typical galaxy or quasar from that section, and also the signal of the pattern that the eBOSS team measures there. As we look out in distance, we look back in time. So, the location of these signals reveals the expansion rate of the Universe at different times in cosmic history.
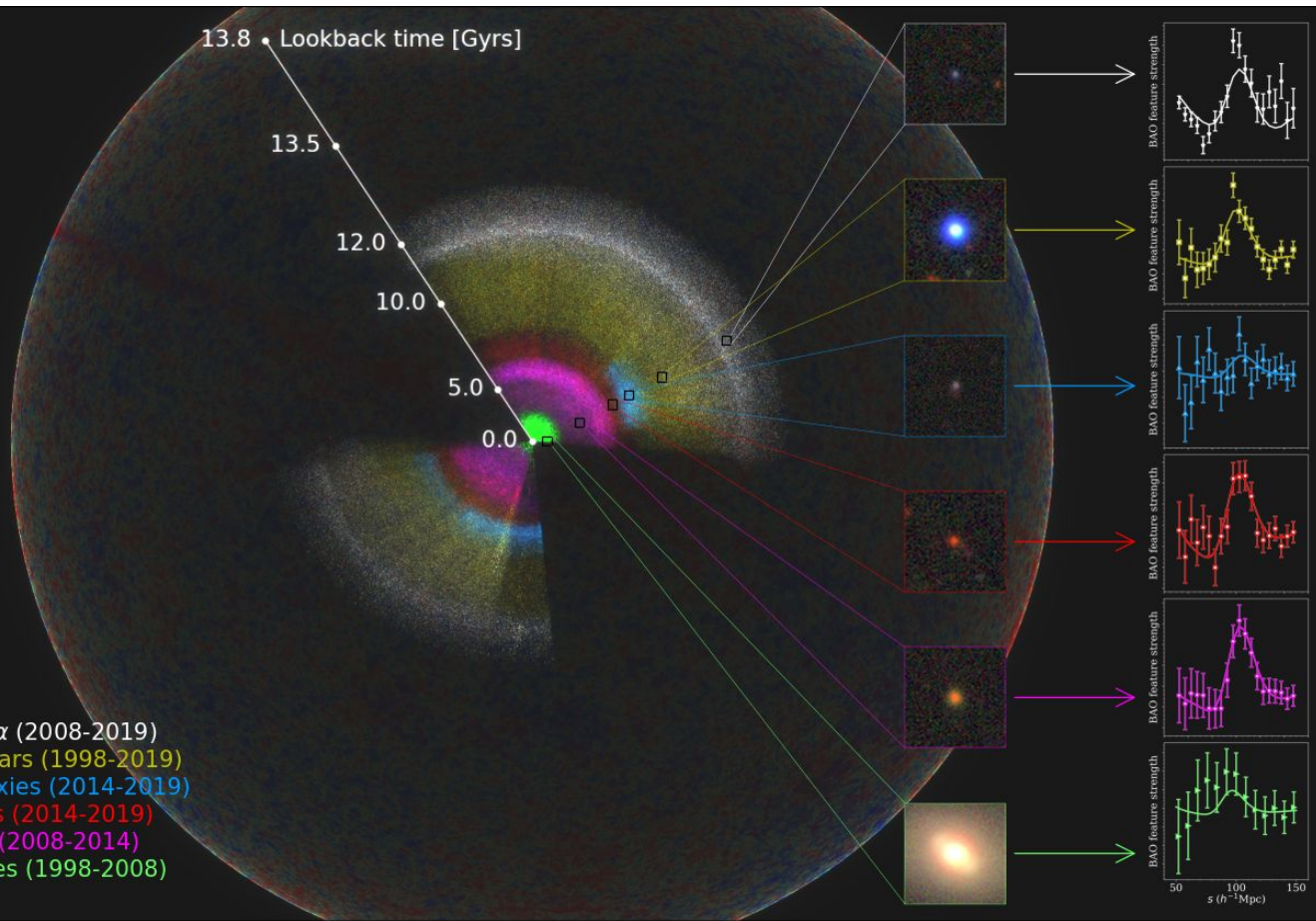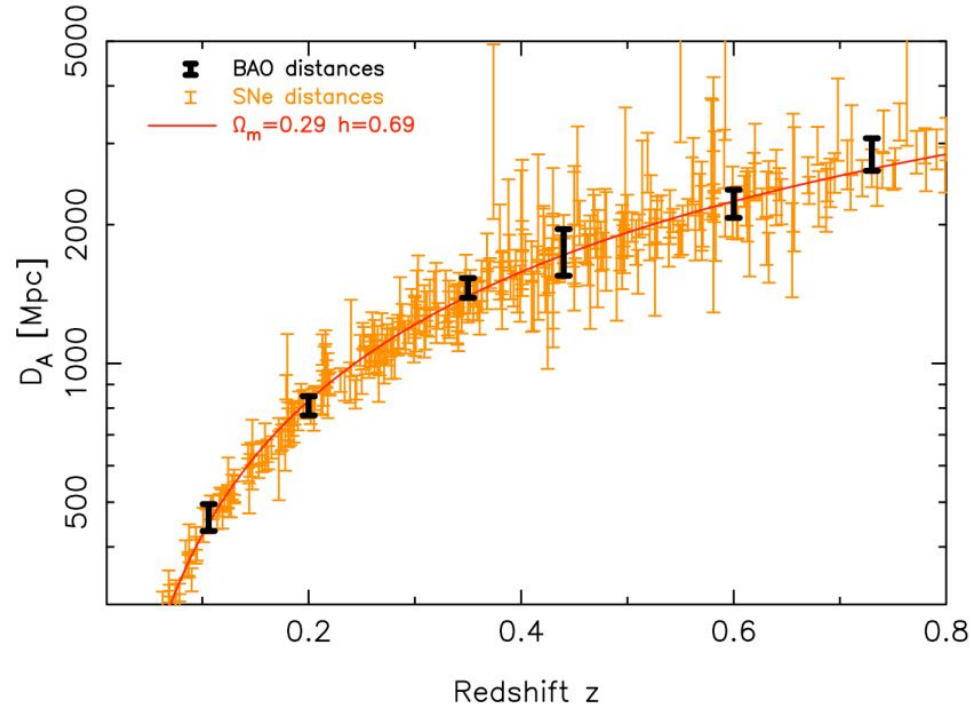
Figure 14.12: Comparison between the SN and BAO mapping of the cosmic distance scale. For the purpose of this figure, the SN d_{L} measurements have been converted to d_{A}, assuming $d_{\mathrm{A}}(z) = d_{\mathrm{L}}(z)/(1+z)^2$ (Figure reproduced from Blake et al. 2011).
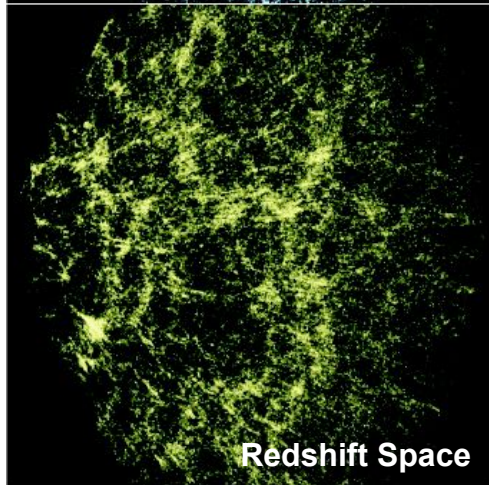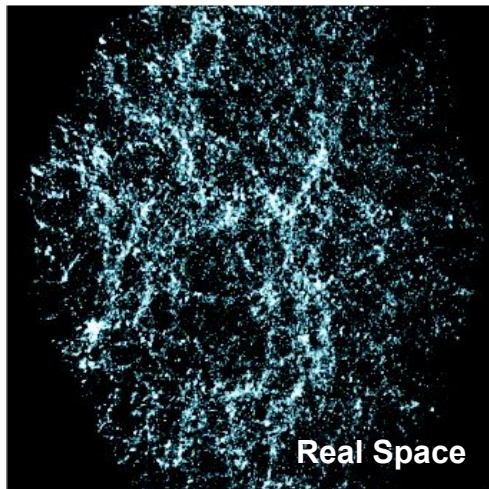
REDSHIFT SPACE DISTORTIONS

Due to peculiar velocities (along the line of sight), the redshift distances available from a galaxy redshift survey deviate from the true, proper distances. This results in **redshift space distortions** in the clustering measurements.

$$v = v_{\mathrm{exp}} + v_{\mathrm{pec}} = H_0 d(z) + v_{\mathrm{pec}}$$

$$z_{\mathrm{obs}} = z_{\mathrm{exp}} + \frac{v_{\mathrm{pec}}}{c}(1 + z_{\mathrm{exp}})$$

L.o.s. Proper Distance measured in redshift space:

$$s = \frac{v}{H_0} = d(z) + \frac{v_{\mathrm{pec}}}{H_0}$$

Real Space

Redshift Space

REDSHIFT SPACE DISTORTIONS

Real Space

- **Kaiser effect:**

On large scales, peculiar velocities reflect the (linear) infall motions towards overdensities, causing a circle in real space to appear "squashed" in redshift space.

Redshift Space

- **Finger-of-God effect:**

On small scales, peculiar velocities are due to the nonlinear virialized motion of galaxies inside their host haloes, causing a circle in real space to appear "stretched" in redshift space.
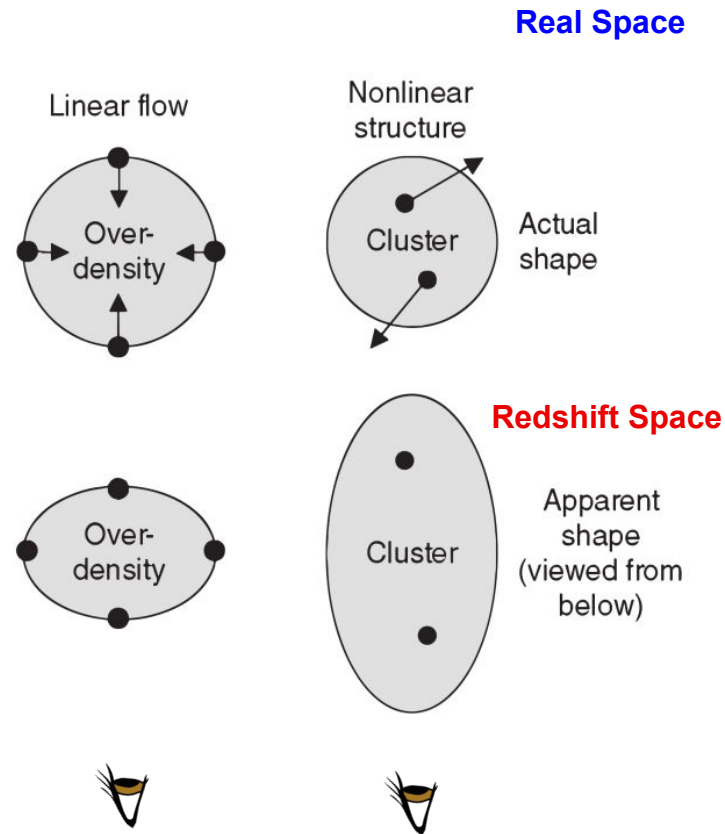
Only radial distances are modified by the Doppler effects of peculiar velocities. The complication is that the peculiar velocities arise from the clustering itself. Thus, the apparent clustering pattern in redshift space differs systematically from that in real space and the spatial correlation function of galaxies, which is isotropic in real space is no longer isotropic in redshift space.

We can decompose the distance between two galaxies in their perpendicular and parallel component along the l.o.s.:

$$\pi \equiv \frac{|s \cdot l|}{|l|} \qquad \sigma \equiv \sqrt{s \cdot s - \pi^2}$$

And compute $\xi(\pi, \sigma)$
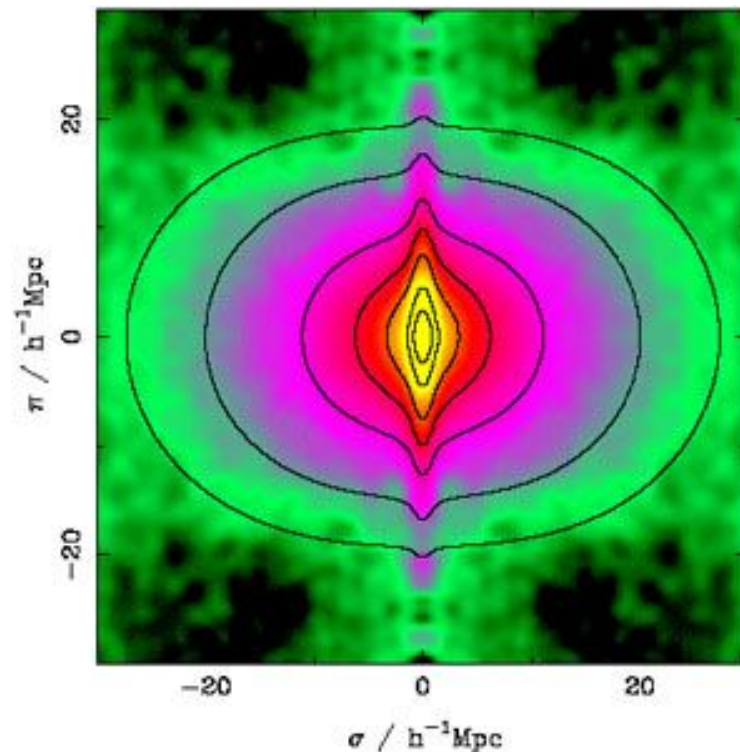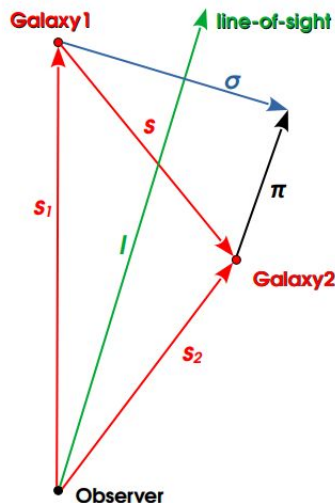
The two-point correlation function obtained from the 2dFGRS by Hawkins et al. (2003). Note the anisotropies due to Finger-of-God and Kaiser effect

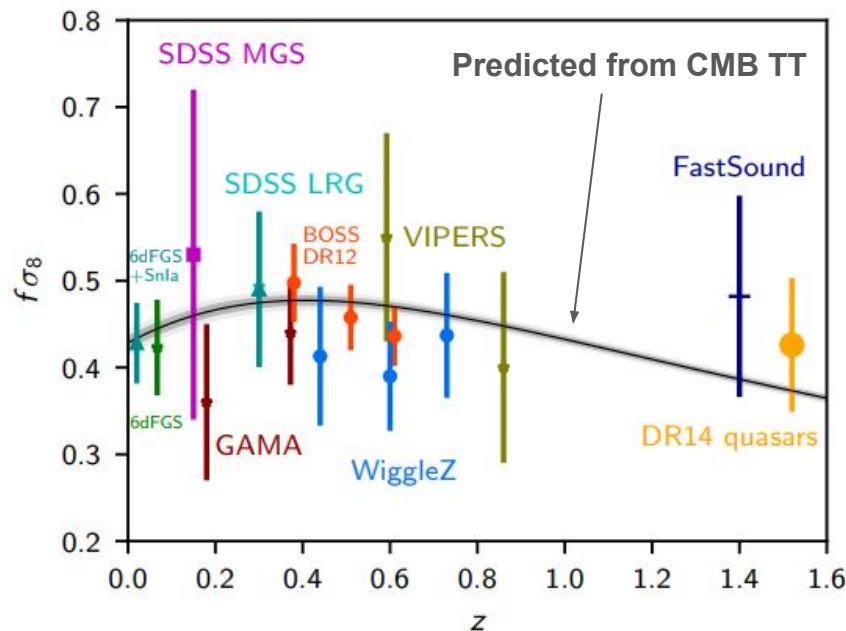**It can be shown that (in linear theory):**

$$\delta_s(\vec{k}) = (1 + \beta\mu^2)\delta_r(\vec{k})$$

$$P_s(k) = (1 + \beta\mu^2)^2 P_r(\vec{k})$$

Where μ is the cosine of the angle between the velocity vector and the line of sight and β is a function of the linear growth rate, *f*, and tracer bias, *b*:
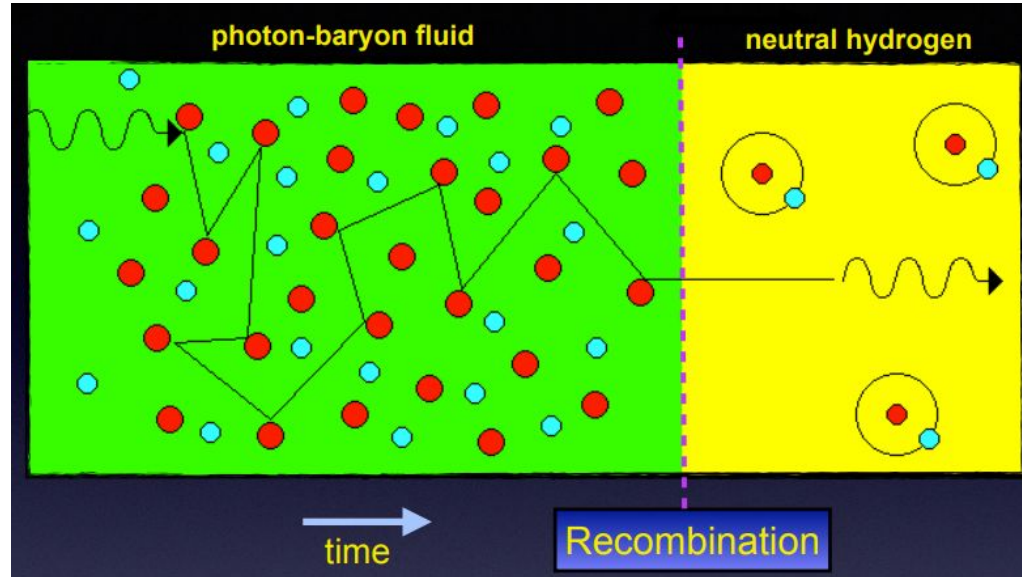
$$\beta = \frac{f(\Omega_m)}{b}$$

Thus we can use RSD to constrain the growth of structure over cosmic time.

STATISTICAL PROPERTIES OF THE LARGE SCALE STRUCTURES:
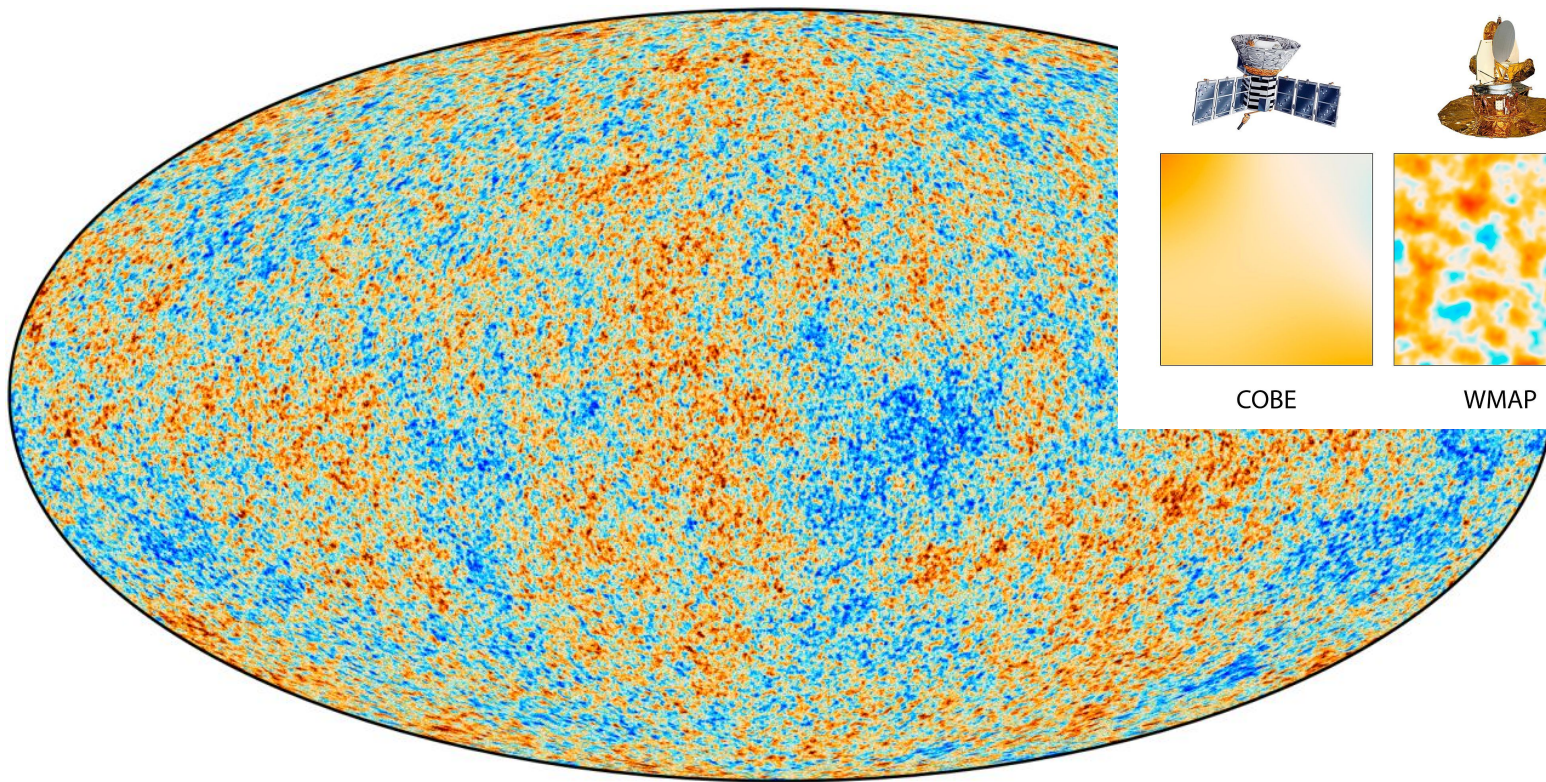# COSMIC MICROWAVE BACKGROUND ANISOTROPIES

For a review: https://www.annualreviews.org/content/journals/10.1146/annurev.astro.40.060401.093926
https://ned.ipac.caltech.edu/level5/March05/Scott/Scott_contents.html
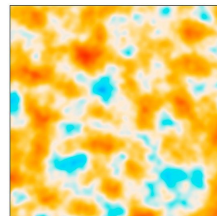https://arxiv.org/pdf/astro-ph/0110414.pdf

CMB radiation comes to us from last scattering surface (LSS). Since recombination is not instantaneous, in general $z_{LSS} \neq z_{rec}$. Here, the redshift of recombination, is defined as the redshift at which the ionization fraction drops below some value (typically 0.1). Rather $z_{LSS} = z_{dec} \simeq 1100$, where the latter is the redshift of decoupling, defined as the epoch at which the Thomson scattering rate is equal to the Hubble expansion rate
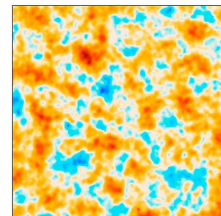
COBE   WMAP   Planck

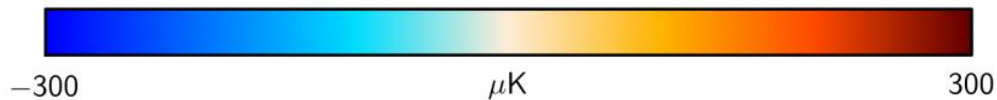-300 μK 300

hotter

direction of motion

colder

Our peculiar motion is made up of:

- Motion of Earth around Sun (~30 km/s)
- Motion of Sun around MW center (~220 km/s)
- Motion of MW towards Virgo cluster (~300 km/s)

Total vector sum of 369 km/s
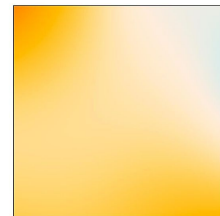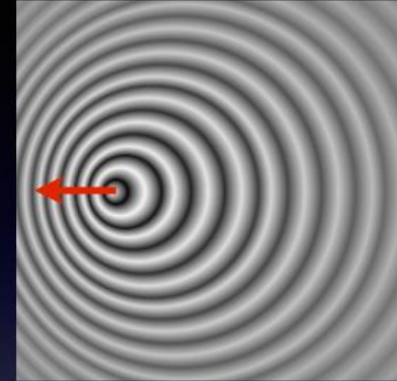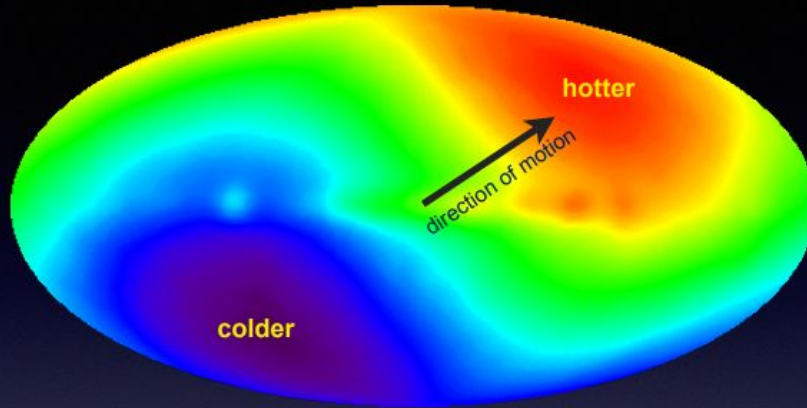
Origin of CMB dipole is Doppler effect due to our peculiar motion

Photons coming from the direction in which we are moving are blueshifted (as if that direction is moving towards us). Photons of a shorter wavelength correspond to photons of a higher temperature (i.e., Wien's law)

Define the CMB anisotropy distribution

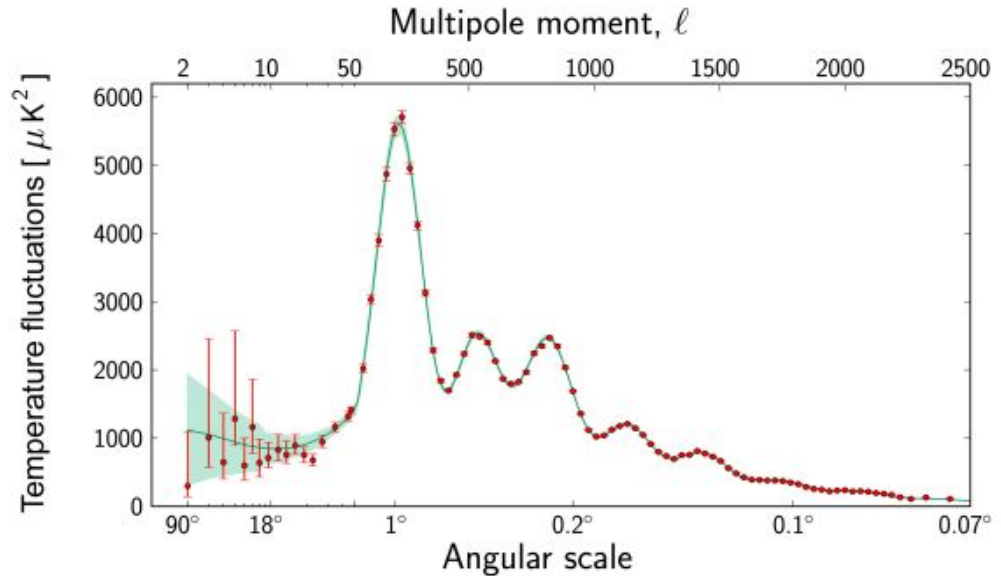$$\Theta(\hat{n}) \equiv \frac{\Delta T}{T}(\hat{n}) = \frac{T(\hat{n}) - \bar{T}}{\bar{T}}$$

Here $\hat{n} = (\vartheta, \phi)$ is direction on the sky, and $\bar{T}$ is the average CMB temperature.

We expand this in Spherical Harmonics:

$$\Theta(\hat{n}) = \sum_{l,m} a_{lm} Y_{lm}(\vartheta, \phi)$$

and define the power spectrum as

$$\mathcal{C}_l = \langle |a_{lm}|^2 \rangle$$

An important angular scale is that corresponding to the comoving Hubble radius at decoupling, $r_H = c/H(z_{dec})$:
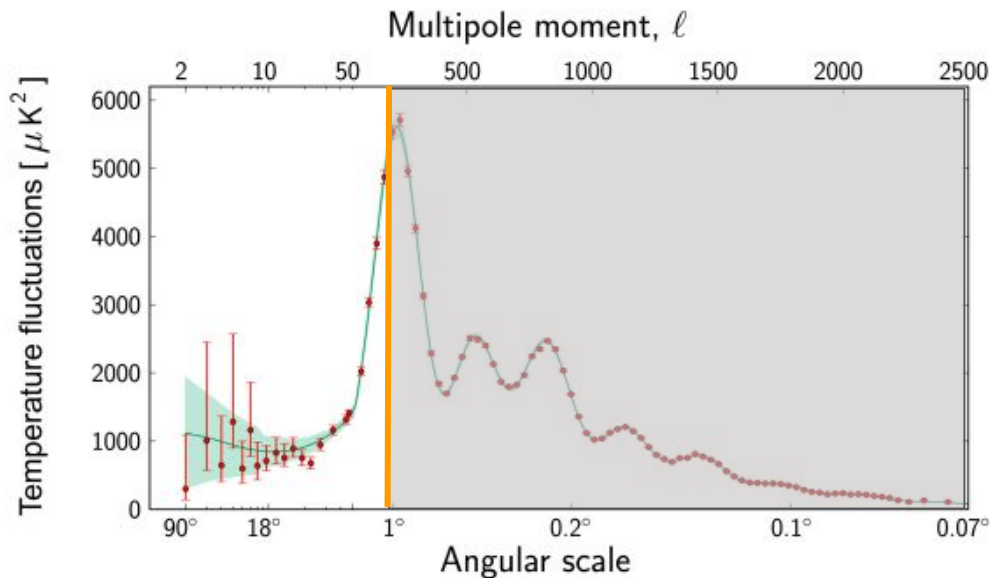
$$\theta_H = \frac{r_H}{d_A(z_{dec})(1+z_{dec})} \simeq 0.87°$$

Which corresponds to $\ell \simeq 200$; CMB anisotropies with $\ell < 200$ correspond to super-horizon scale perturbations. On these super-horizon scales, only two effects can contribute to non-zero $\Delta T/T$ fluctuations:

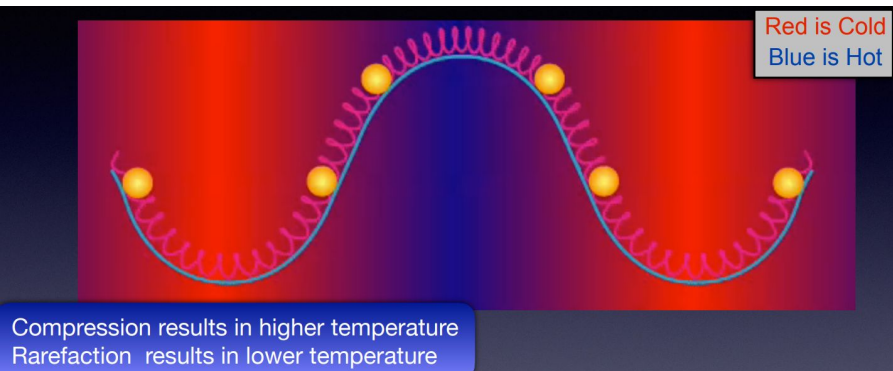i) fluctuations of the photon density at decoupling
ii) fluctuations in the gravitational potential (photons lose energy when climbing out of a potential well)

The combination of these two effects is known as the Sachs-Wolfe effect

The relation between ℓ and the associated angular scale ϑ is:

$$\theta \sim \frac{\pi}{\ell}\text{rad} \sim \frac{180°}{\ell}$$

Red is Cold
Blue is Hot

Compression results in higher temperature
Rarefaction results in lower temperature

On sub-horizon scales the rich structure observed in the temperature anisotropy spectrum is mainly a consequence of the acoustic oscillations of the tightly-coupled baryon-photon fluid in the pre-recombination era. Perturbations in the gravitational potential, dominated by the CDM component, drive the oscillations in the plasma, with photon pressure, due to Thomson scattering of photons off free electrons, providing most of the restoring force.
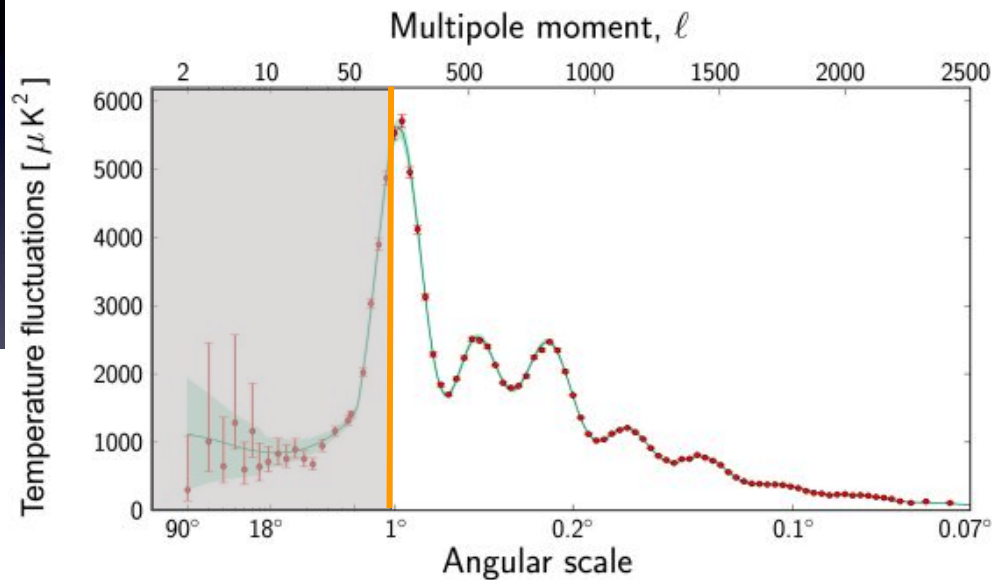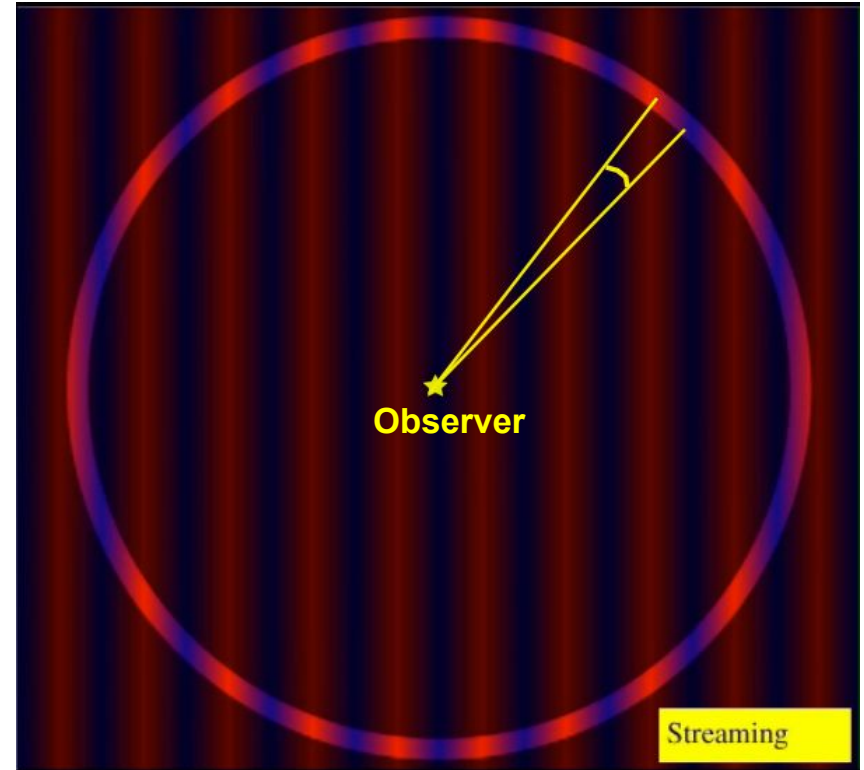

After recombination, photons can travel freely toward us, and the phases of the oscillations is imprinted in the CMB spectrum as a series of harmonic peaks. The last-scattering surface is a snapshot view of oscillation phases of all different modes.
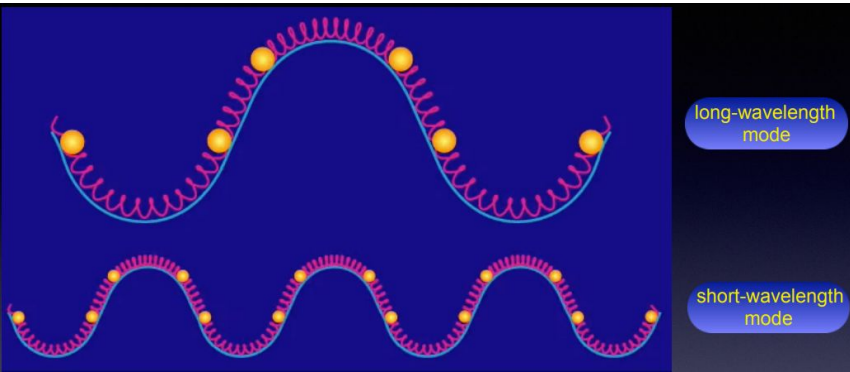
Oscillations

Observer

Streaming
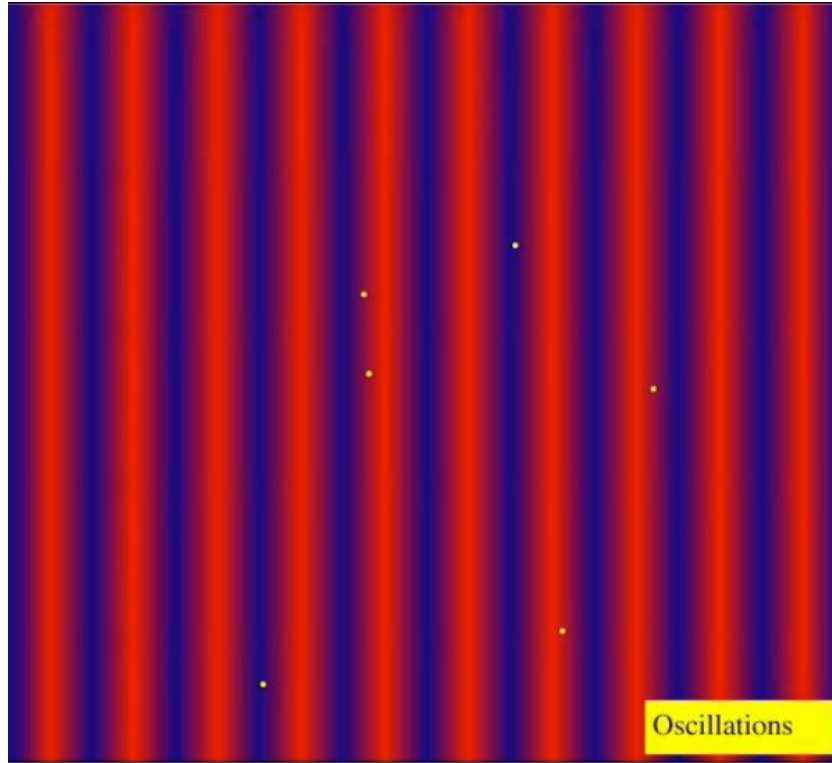
If we consider a single perturbation mode

The observer sees this mode as angular temperature fluctuation on the sky, with a characteristic angular scale set by the wavelength of the mode

Since sound speed of photon-baryon fluid is the same for all modes, those with a smaller wavelengths oscillate faster.
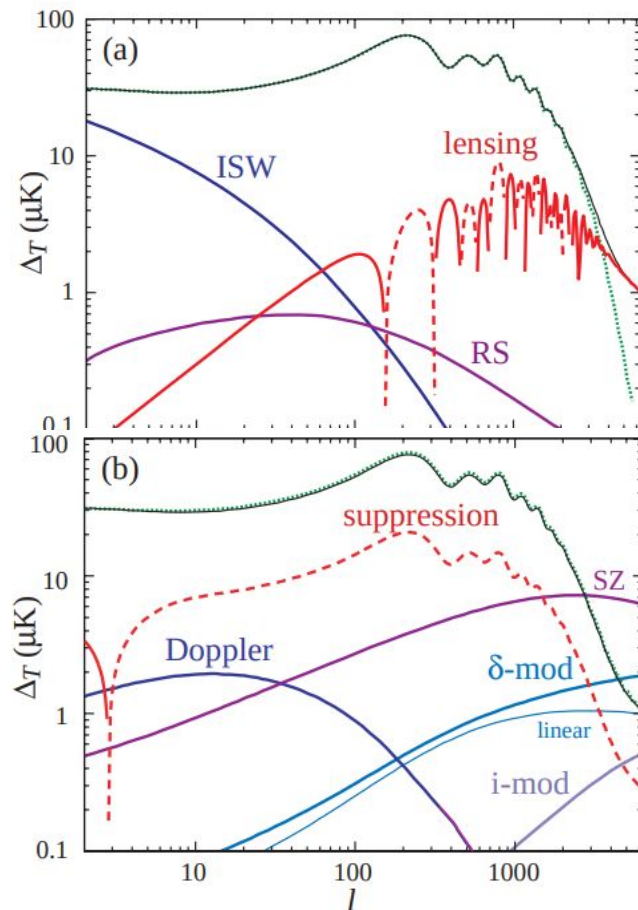
The **first peak** corresponds to the mode that is caught in its first compression by recombination. The **second peak** corresponds to the mode that went through a full cycle of compression and rarefaction by recombination. The even peaks are generally of smaller amplitude because the rebound has to fight against baryon inertia.
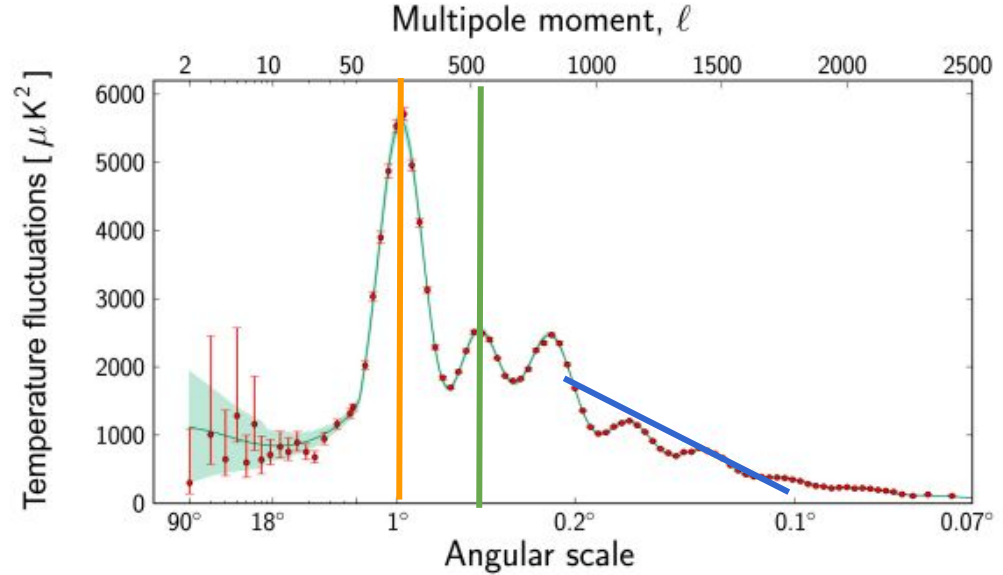
Since the recombination process is not instantaneous, the last scattering surface has a finite thickness. This leads to a smearing of the anisotropies on scales smaller than the width ($\Delta z \approx 80$) of the recombination process, $\ell > 1000$ (**diffusion damping**)
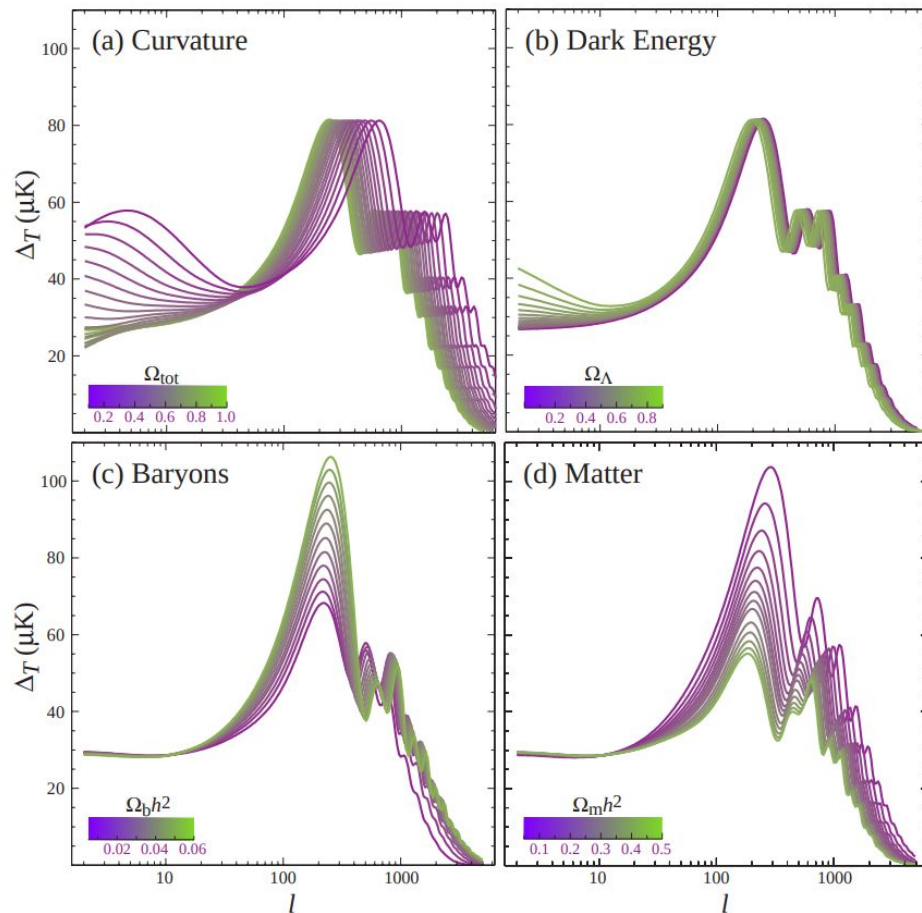
At angular scales smaller than few arc-minutes CMB temperature fluctuations are no longer dominated by primary effects at the surface of last scattering, but rather by the so-called **secondary anisotropies which arise from the interaction of the CMB photons with the matter along the line of sight**. The secondary anisotropies can be divided in two major families depending on the physical process which generate them. The **first family arises from the interaction of the photons with gravitational potential wells**, and it includes gravitational lensing and the late ISW effect. As for former, the gravitational deflection of CMB photons by intertwining non-linear structures causes a smoothing of the acoustic peaks up to 10% level at $\ell > 2000$, and generate small-scale power that dominates the primary anisotropies for $\ell > 4000$, where the diffusion damping is highly effective. Moreover, CMB lensing introduces non-Gaussianity in the four-point correlation function with a very specific and predictable shape, from which it is possible to reconstruct the power spectrum of the lensing potential. The **second family incorporates the effects of scattering of CMB photons with free electrons**, such as reionization effects and the Sunyaev and Zeldovich effect (see previous lectures).


Credit: Hu & Dodelson 2002

Credit: Hu & Dodelson 2002

The *position* of the acoustic peaks are **determined by the physical size of the sound horizon at decoupling**, and the **angular diameter distance of the last scattering surface**. Thus, the position of the peaks depends on the geometry of the space and on the value of Ω_b. Furthermore, the value of Ω_b **controls also the relative amplitude between even and odd peaks and the depth of the valleys**. In addition, the heights of the acoustic peaks can be affected by the strength of the initial perturbations (A_s and n_s), and by Ω_m through the time evolution of the gravitational potential induced by the self-gravity of the acoustic perturbations.

CMB POLARIZATION POWER SPECTRUM

Thomson scattering of a radiation field with a quadrupole anisotropy produces linear polarization. The relevant epoch for the generation of polarization in the CMB is around recombination since at early times scattering is too efficient to allow a significant quadrupole to grow, while after recombination scatterings are very rare (until the universe reionizes).
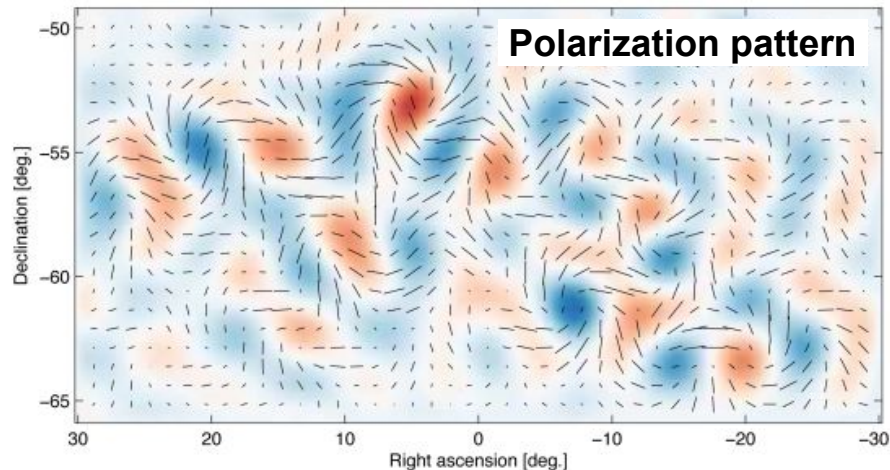
From acoustic density perturbations

Polarization pattern
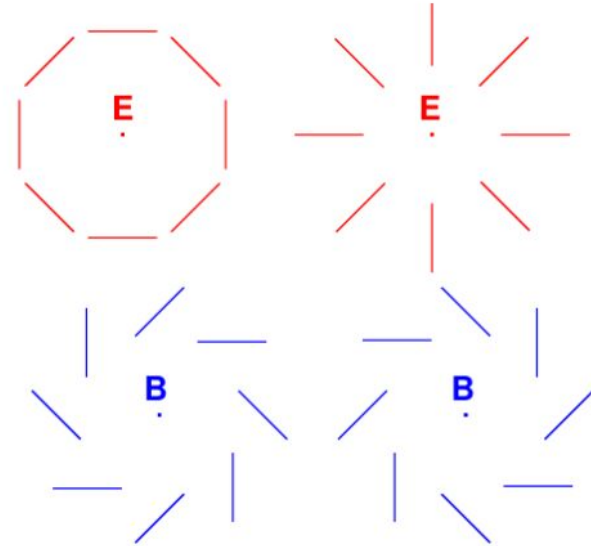
From primordial gravitational waves or lensing of CMB photons

The CMB polarization signal is expected to have a r.m.s. of ~ 5µK, peaking at multipoles l ≃ 1000 (the angle subtended by the photon mean free path at last scattering). The amplitude of the polarization signal is much smaller than the temperature power spectrum.

B-mode polarization can be induced by tensor perturbation, generated by the primordial gravitational waves predicted in the inflationary scenario, or by gravitational lensing due to the intertwining structures along the line of sight. **A measurement of the gravitational waves power probes directly the energy scale of inflation.**
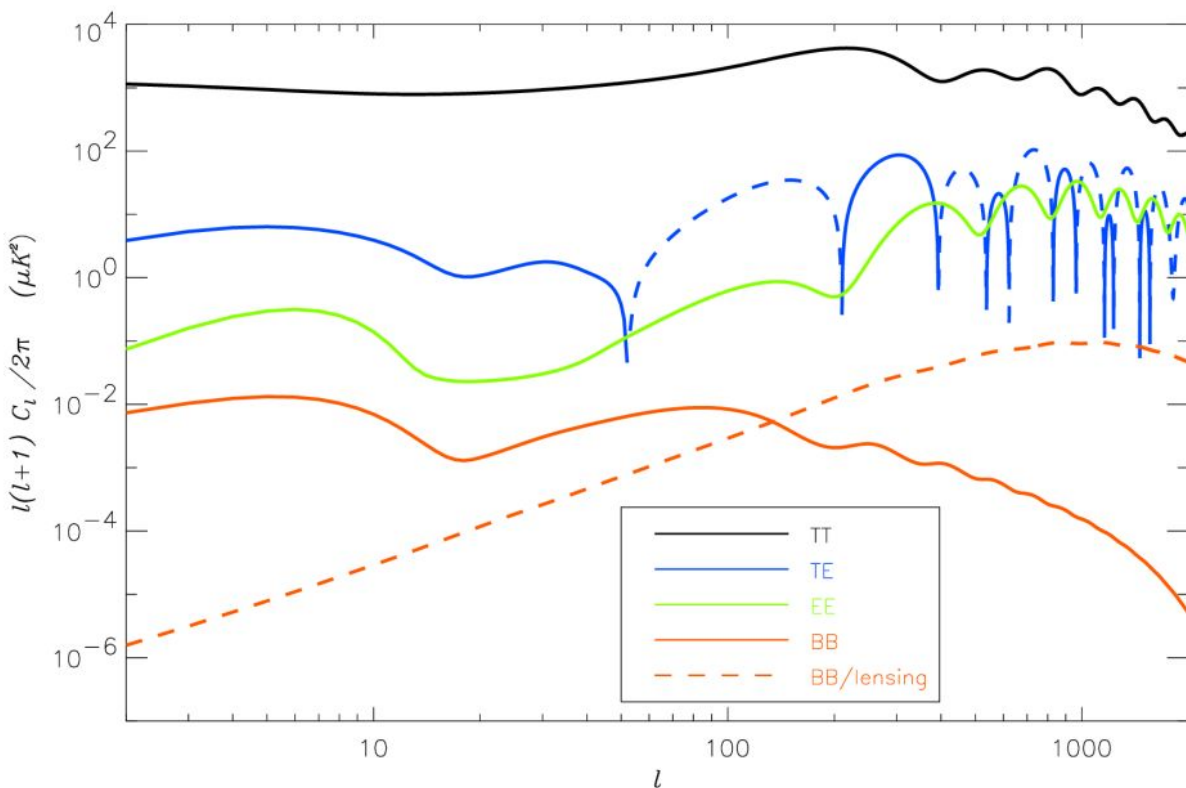
The "bump" at low multipoles (l< 20) in the polarization spectra is due to the re-scattering of CMB photons at reionization. The position of this peak is set by the size of the horizon at reionisation, while its amplitude is determined by the duration of the ionization process.

# STATISTICAL PROPERTIES OF THE LARGE SCALE STRUCTURES:
COSMIC SHEAR

For a review: https://arxiv.org/pdf/1201.2434.pdf (Sec 5)

https://arxiv.org/pdf/1612.06535.pdf

https://arxiv.org/pdf/0805.0139.pdf

https://arxiv.org/pdf/astro-ph/9912508.pdf

Gravitational lensing: Light's path is deflected by the gravitational potential wells of cosmic structures crossed along its journey toward us.

This leads to:

- **Change of the apparent positions of the sources**
- **Distorsion (shear) of source images**
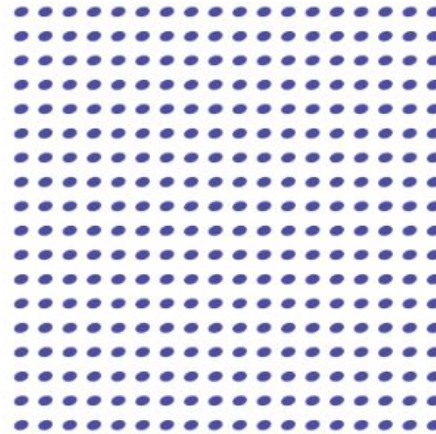- **Magnification of the source images**
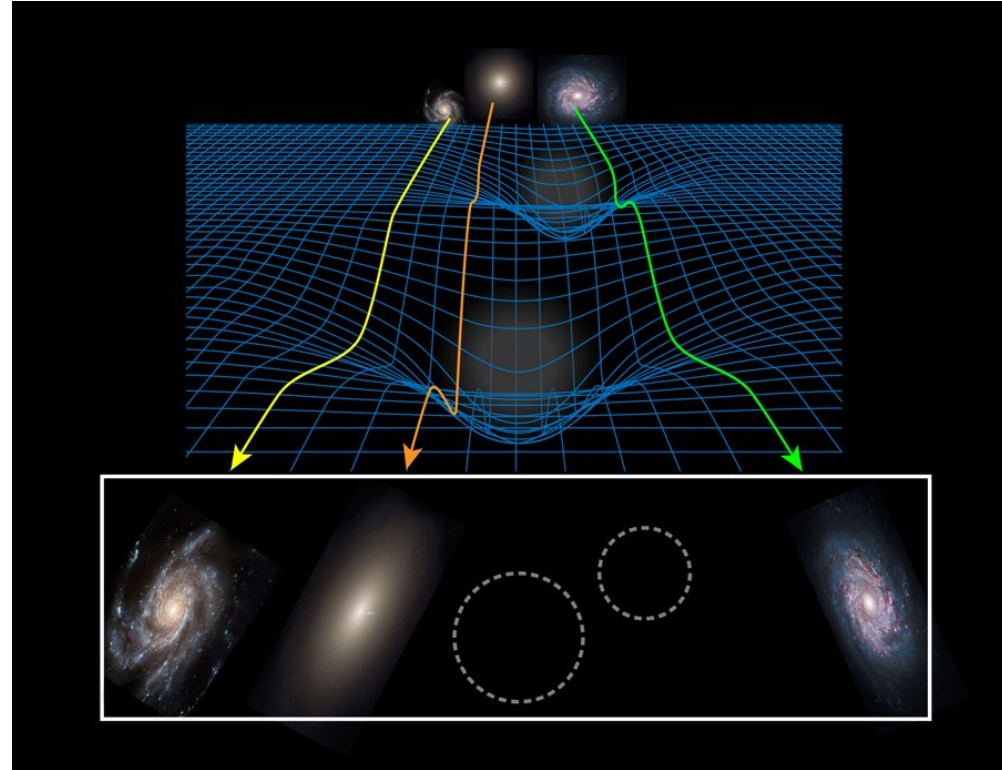
Strong lensing:

- **Multiple images of the same source**
- **Strong distortions and magnification**

Weak lensing:

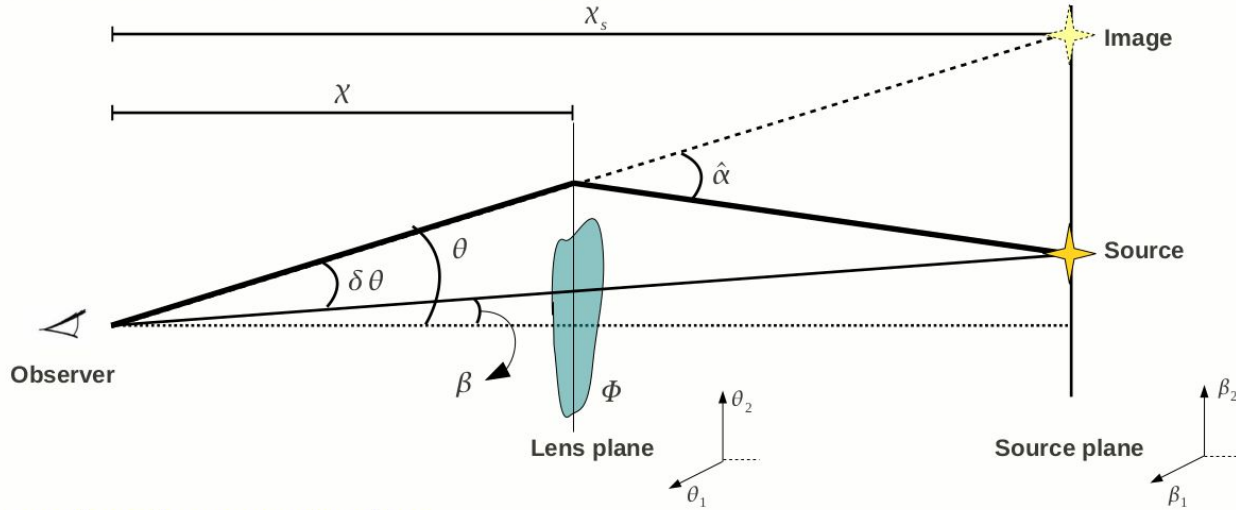- **Shape distorted, stretched or magnified**
- **Detectable only statistically**

Unlensed sources
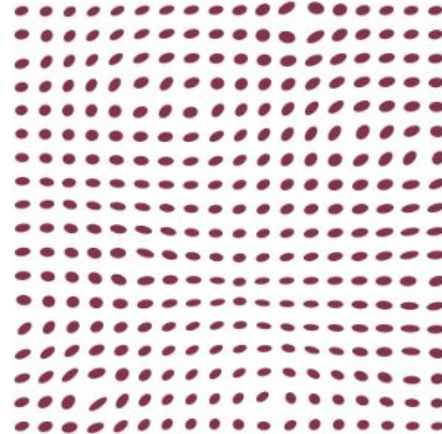
Weak lensing

- **Deflection of light ray by a gravitational potential fluctuation Φ:**

- **Using small angles approximation:**

$$\vec{\beta}\,\mathcal{D}(\chi_s) = \vec{\theta}\,\mathcal{D}(\chi_s) - \vec{\hat{\alpha}}\,\mathcal{D}(\chi_s - \chi)$$

- **Lens equation:**

$$\vec{\beta} = \vec{\theta} - \delta\vec{\theta} \qquad \text{with:} \quad \delta\vec{\theta} = \frac{\mathcal{D}(\chi_s - \chi)}{\mathcal{D}(\chi_s)}\vec{\hat{\alpha}} \qquad \textbf{(Scaled deflection angle)}$$

- **Perturbed metric:**

$$ds^2 = \left(1 + \frac{2\Phi}{c^2}\right) c^2 dt^2 - a^2(t) \left[\boxed{\left(1 - \frac{2\Phi}{c^2}\right)} (d\chi^2 + \mathcal{D}^2(\chi) d\Omega^2) \right]$$

Weak field approximation

n **refractive index**

- **Deflection angle:**

$$\vec{\hat{\alpha}} = \frac{2}{c^2} \int \nabla_\perp \Phi(\chi) d\chi$$
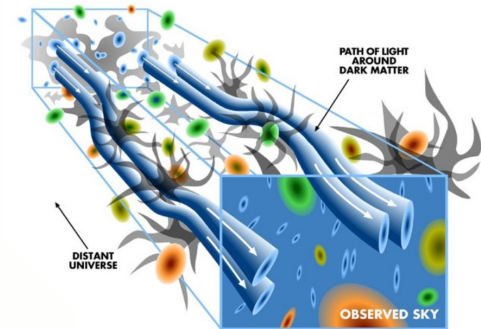
Thin lens approximation

Born approximation

- **Deflection angle of light ray arising from all the potential gradients between obs and source:**

$$\delta\vec{\theta} = \vec{\theta} - \vec{\beta} = \frac{2}{c^2} \int_0^{\chi_s} d\chi \frac{\mathcal{D}(\chi_s - \chi)}{\mathcal{D}(\chi_s)} \nabla_\perp \Phi(\chi)$$
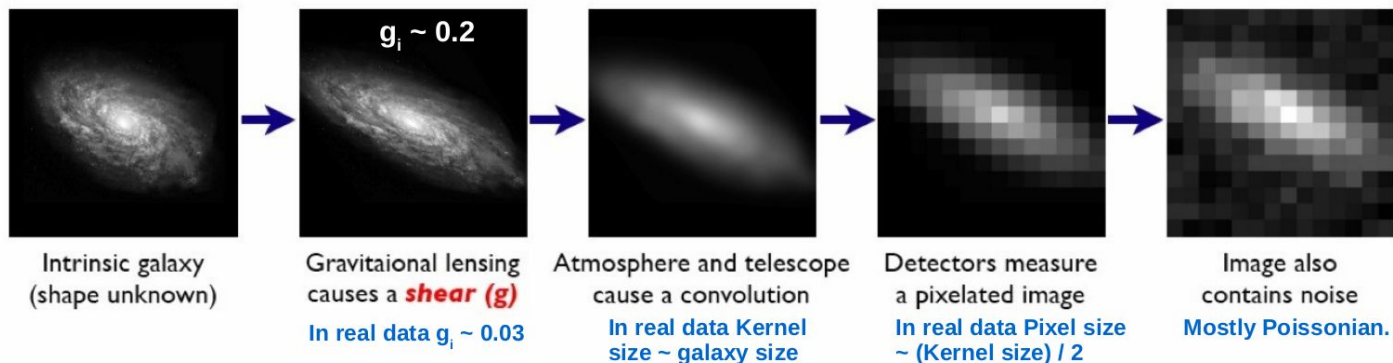
- **Deflection potential:**

$$\psi(\vec{\theta}, \chi_s) = \frac{2}{c^2} \int_0^{\chi_s} d\chi' \frac{\mathcal{D}(\chi_s - \chi)}{\mathcal{D}(\chi_s)\mathcal{D}(\chi)} \Phi(\mathcal{D}(\chi)\vec{\theta}, \chi)$$
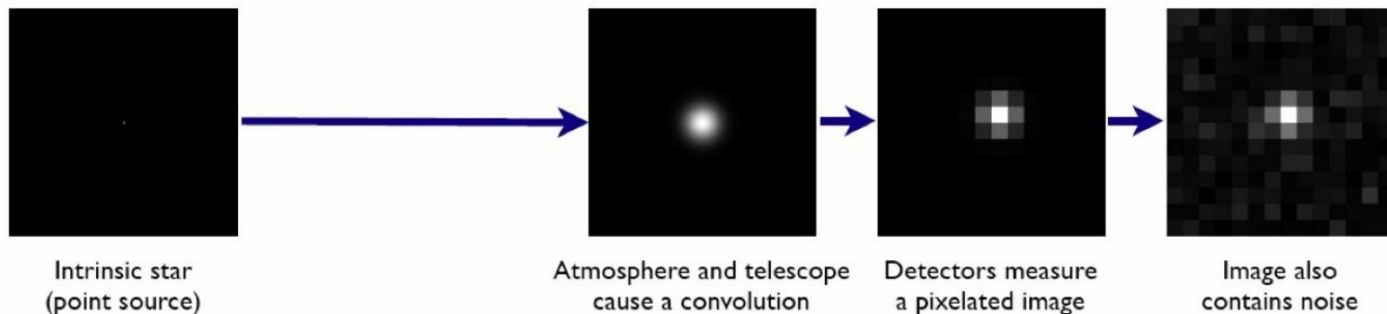

PATH OF LIGHT AROUND DARK MATTER

DISTANT UNIVERSE

OBSERVED SKY

The "forward" process of the source image:

Galaxies: Intrinsic galaxy shapes to measured image:

$g_i \sim 0.2$

| Intrinsic galaxy (shape unknown) | Gravitaional lensing causes a **shear (g)** | Atmosphere and telescope cause a convolution | Detectors measure a pixelated image | Image also contains noise |

In real data $g_i \sim 0.03$ In real data Kernel size ~ galaxy size   In real data Pixel size ~ (Kernel size) / 2   Mostly Poissonian.

Stars: Point sources to star images:

| Intrinsic star (point source) | Atmosphere and telescope cause a convolution | Detectors measure a pixelated image | Image also contains noise |

The "forward" process of the source image:

Galaxies: Intrinsic galaxy shapes to measured image:

$g_i \sim 0.2$

Intrinsic galaxy
(shape unknown)

Gravitaional lensing
causes a *shear (g)*

In real data $g_i \sim 0.0$

Atmosphere and telescope
cause a convolution

a pixelated image

contains noise

Stars: Point sources to star image

True, pointlike stars

Earth's atmosphere and telescope optics

Blurred images of stars

Atmosphere

Optics

10% ellipticity

The shape and size of images are affected by the PSF, which results from the telescope optics, bed focusing, etc. and for ground-based images, from atmospheric turbulence.

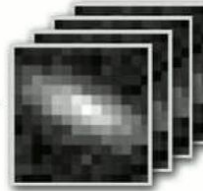The PSF correction is the most difficult, yet most important step in the measurement of lensing signal.

Intrinsic star
(point source)

Atmosphere and telescope
cause a convolution

Detectors measure
a pixelated image

Image also
contains noise
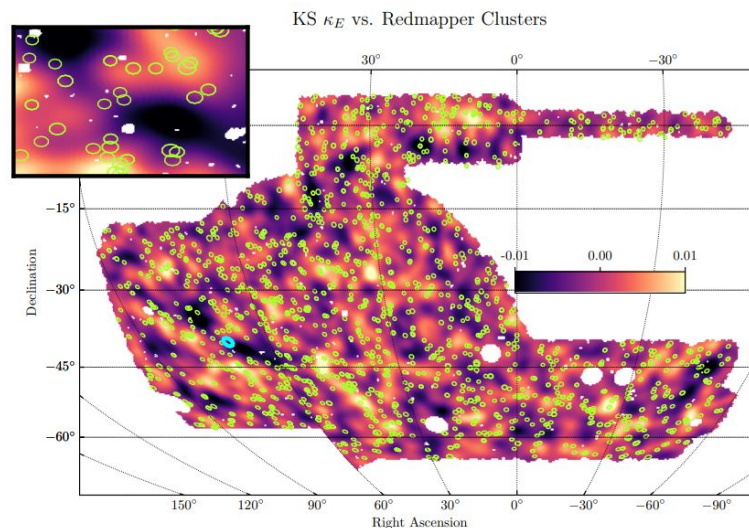
Cosmic Shear:

- **Map the matter distribution directly (no assumption about the relation between DM and baryonic matter)**
- **Lensing measurements are sensitive to the geometry and provide measures of the growth of LSS → powerful probe of DE and modified gravity theories**
- **It helps in breaking parameter degeneracies when combined with other cosmological probes**

First detection of cosmic shear in 2000 by four independent groups (Bacon et al. 2000; Kaiser et al. 2000; van Waerbeke et al.; Wittman et al. 2000) using ~10^5 galaxies, 1 deg^2. Current results from >10^8 galaxies over a few 10^3 deg^2.

Weak lensing mass map with redMaPPer clusters derived from DES Y3 shear catalogue of 100,204,026 galaxies in 4143 deg^2 .
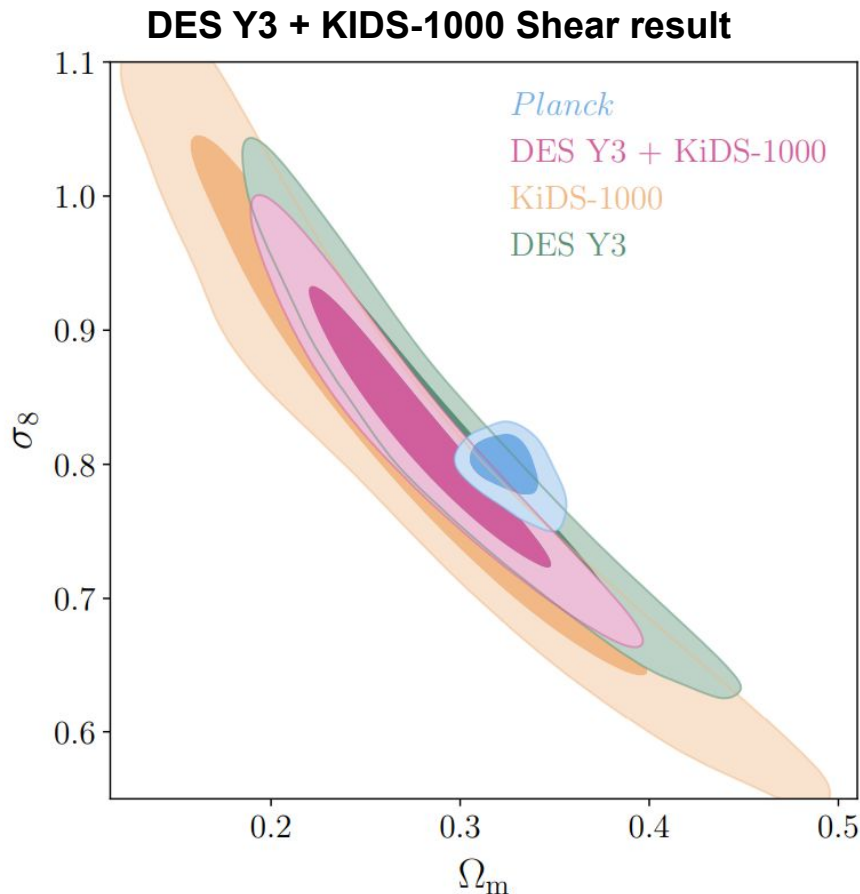

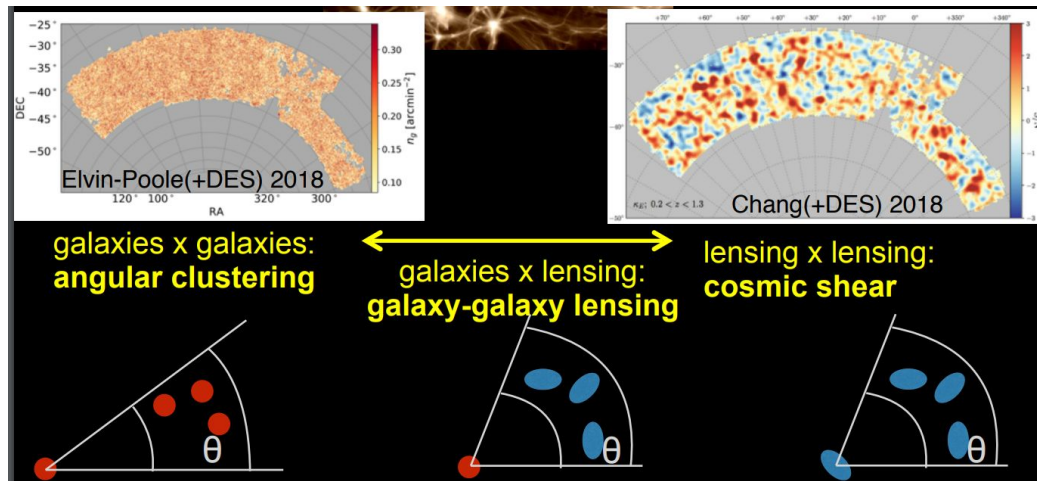KS κ_E vs. Redmapper Clusters

Cosmic Shear:

- **Map the matter distribution directly (no assumption about the relation between DM and baryonic matter)**
- **Lensing measurements are sensitive to the geometry and provide measures of the growth of LSS → powerful probe of DE and modified gravity theories**
- **It helps in breaking parameter degeneracies when combined with other cosmological probes**

First detection of cosmic shear in 2000 by four independent groups (Bacon et al. 2000; Kaiser et al. 2000; van Waerbeke et al.; Wittman et al. 2000) using ~10^5 galaxies, 1 deg^2.
Current results from >10^8 galaxies over a few 10^3 deg^2.

DES Y3 + KIDS-1000 Shear result

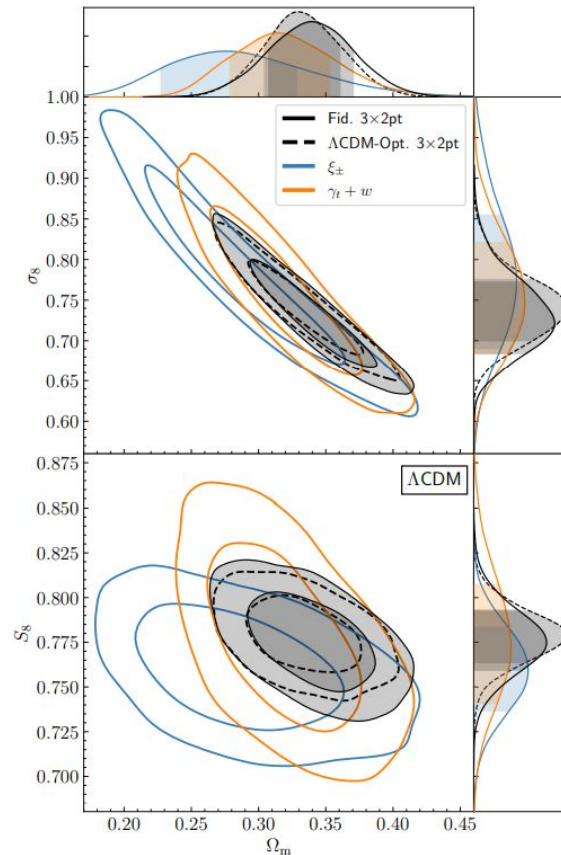https://arxiv.org/pdf/2305.17173.pdf

MULTI-PROBE COSMOLOGY: 3x2pt

- **The combination of galaxy clustering, cosmic shear, and galaxy–galaxy lensing measurements – the so called 3x2pt analysis – has proven to provide powerful constraints on the structure formation in the late universe, while self calibrating many astrophysical (e.g. galaxy bias) or systematic parameters (e.g. intrinsic alignments and photo-z errors) in the model.**

Elvin-Poole(+DES) 2018

Chang(+DES) 2018

galaxies x galaxies:
angular clustering

galaxies x lensing:
galaxy-galaxy lensing

lensing x lensing:
cosmic shear

DES Y3 3x2pt analysis

CMB LENSING POWER SPECTRUM

CMB lensing effect leaves subtle imprints in the temperature and polarization anisotropies, which can be used to reconstruct a map of the lensing potential whose gradient determines the lensing deflections. For example, in propagating through a large overdense clump of matter on the line of sight, angular structures in the CMB get magnified appearing bigger on the sky. **Essentially, by looking how the typical size of hot and cold spots in the CMB temperature map vary across the sky, we can reconstruct the lensing deflections and hence the integrated distribution of dark matter.**

The lensing map provides a new cosmological observable, similar to maps of cosmic shear estimated from the shapes of galaxies. Its power spectrum (see below) provides access to cosmological parameters from the CMB alone that **affect the late-time expansion and geometry of the Universe, and the growth of structure** — parameters that have only degenerate effects in the primary CMB anisotropies.

The lensing map reconstructed from the Planck 2018 data
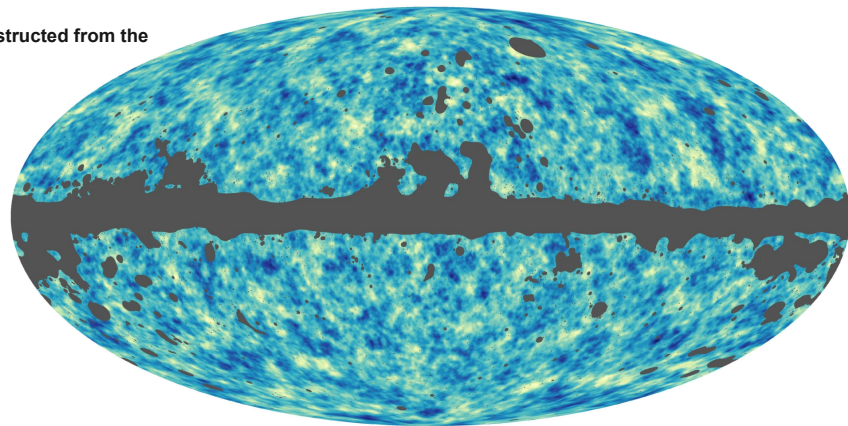
Power spectrum of the CMB lensing potential estimated from the 4-point function (trispectrum) of the Planck 2018 temperature and polarization maps (pink boxes), compared with the theoretical expectation for the LCDM model with parameters determined from the Planck measurements of the CMB power spectra.
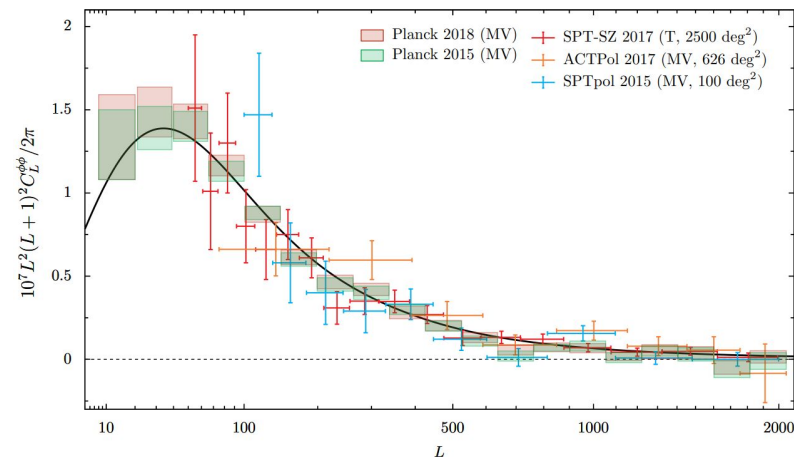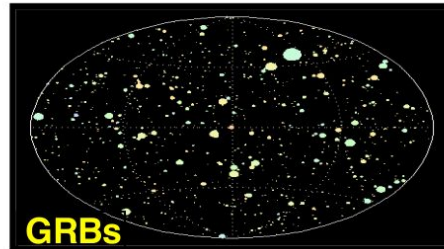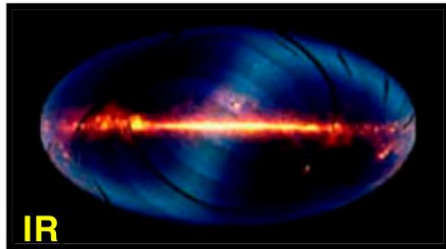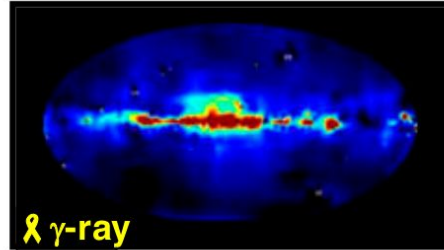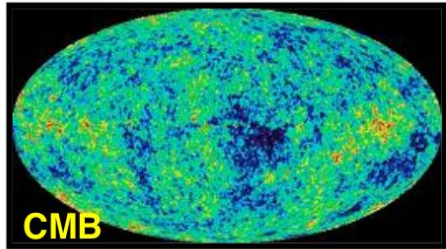
COSMOLOGY WITH GRAVITATIONAL WAVES

For a review: http://arXiv.org/abs/0903.0338v1

MULTI-MESSENGER COSMOLOGY
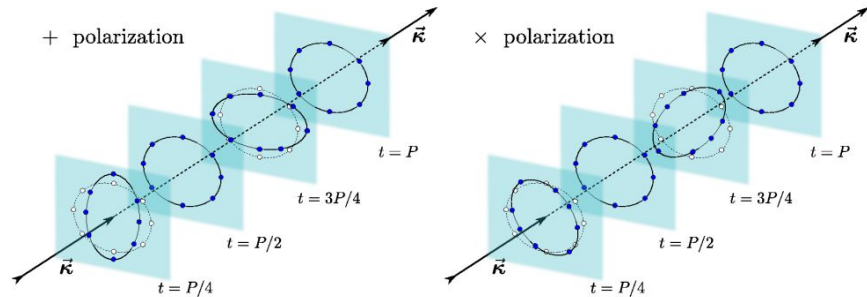

Radio

x-ray

CMB

γ-ray

IR

GRBs
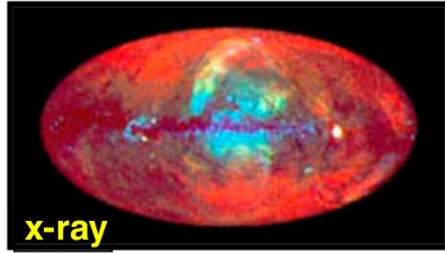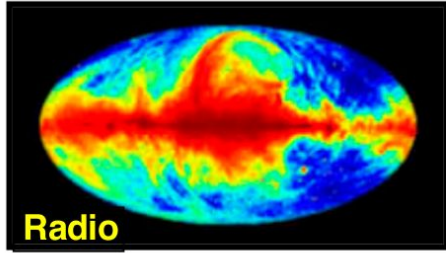
Most of what we know about the Universe is through photons.

Lots of ongoing efforts to obtain information about the universe using non-EM cosmic messengers.
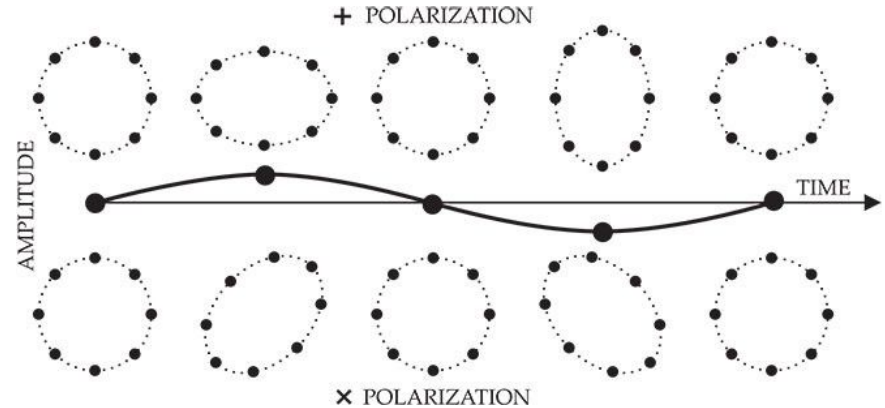
General Relativity predicts that space-time perturbations propagate through empty space at the speed of light.
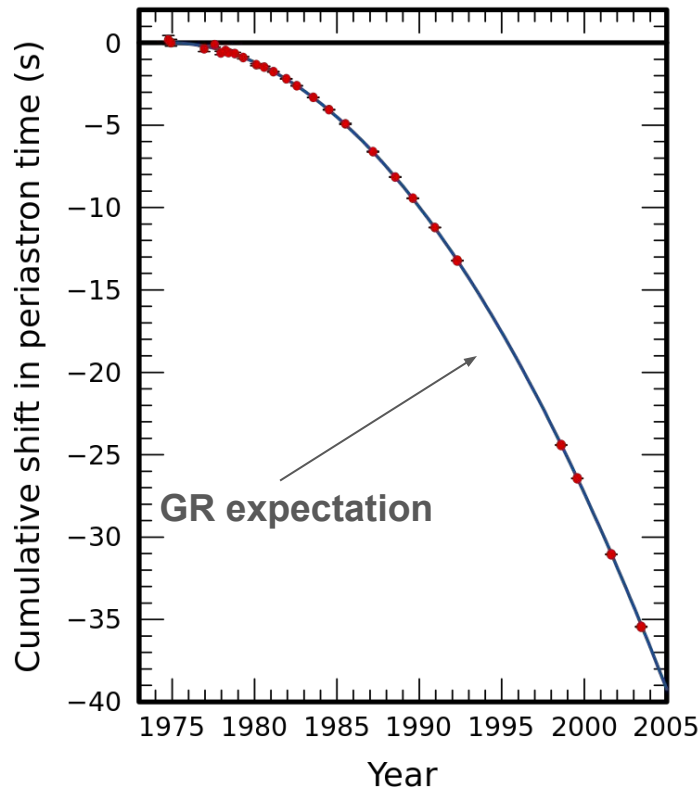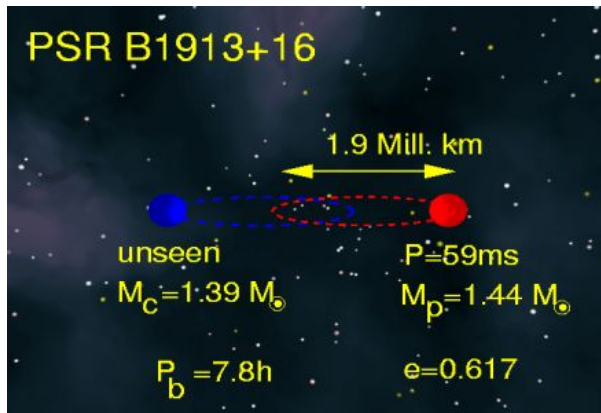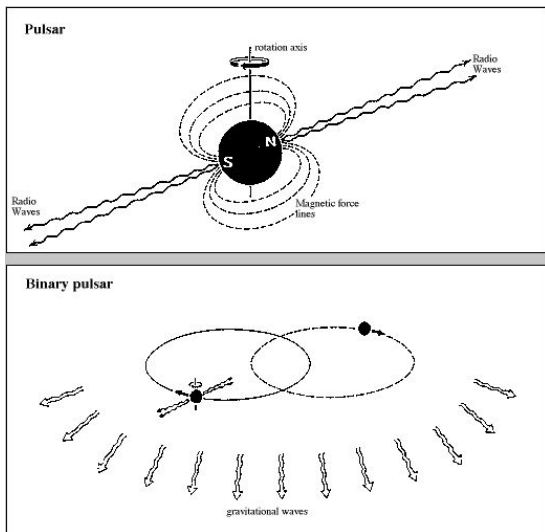
$$\left(-\frac{\partial^2}{\partial t^2} + \nabla^2\right)\bar{h}^{\alpha\beta} = 0.$$

Two possible polarizations:
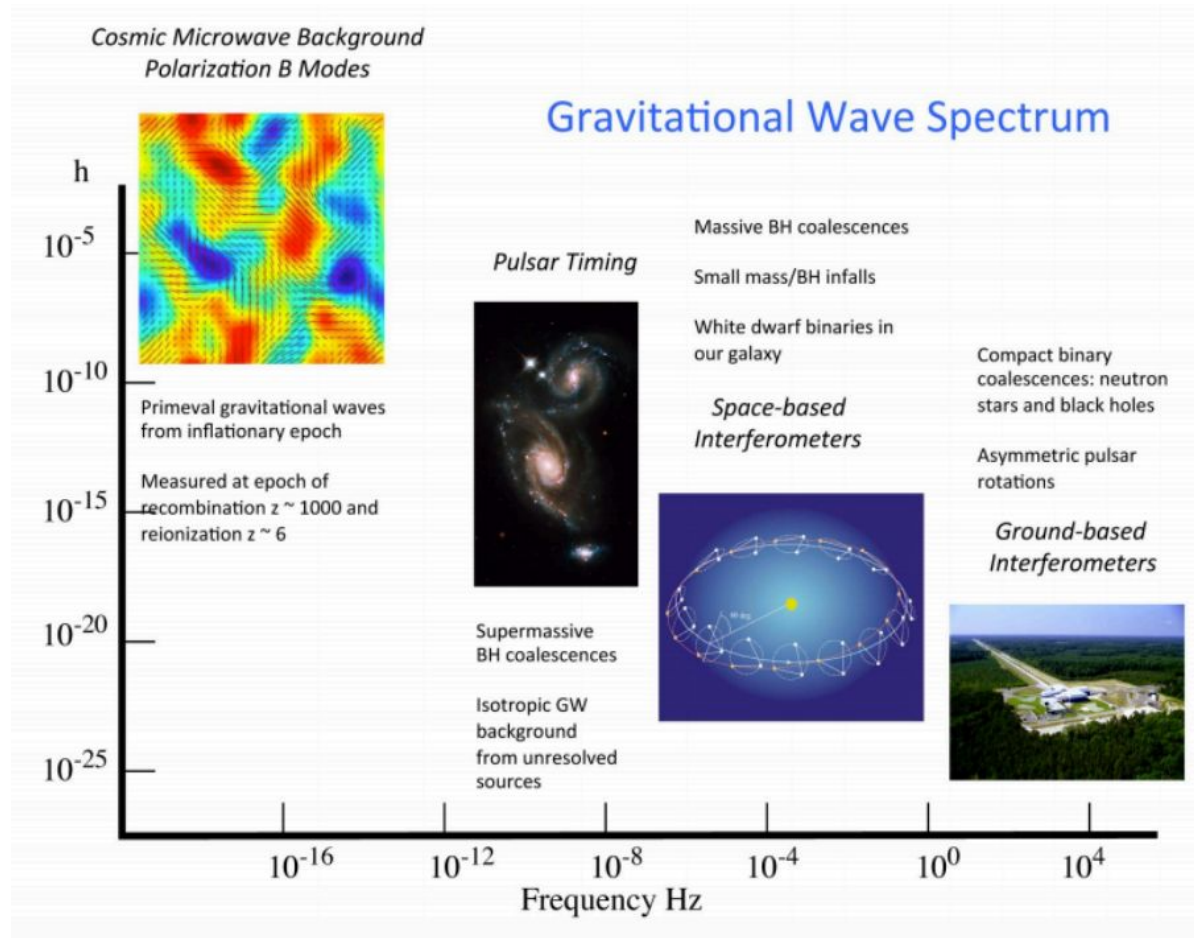
PSR B1913+16: First indirect evidence from orbital period decay of binary system composed of a neutron star and pulsar, a rapidly rotating, highly magnetized neutron star (1993 Nobel prize J. Taylor, R. Hulse): the orbital decay match the energy loss predicted from GR due to gravitational wave radiation.

PSR B1913+16

1.9 Mill. km

unseen
$M_c = 1.39 M_\odot$

P=59ms
$M_p = 1.44 M_\odot$

$P_b = 7.8h$

e=0.617

GR expectation

Cumulative shift in periastron time (s)

Year
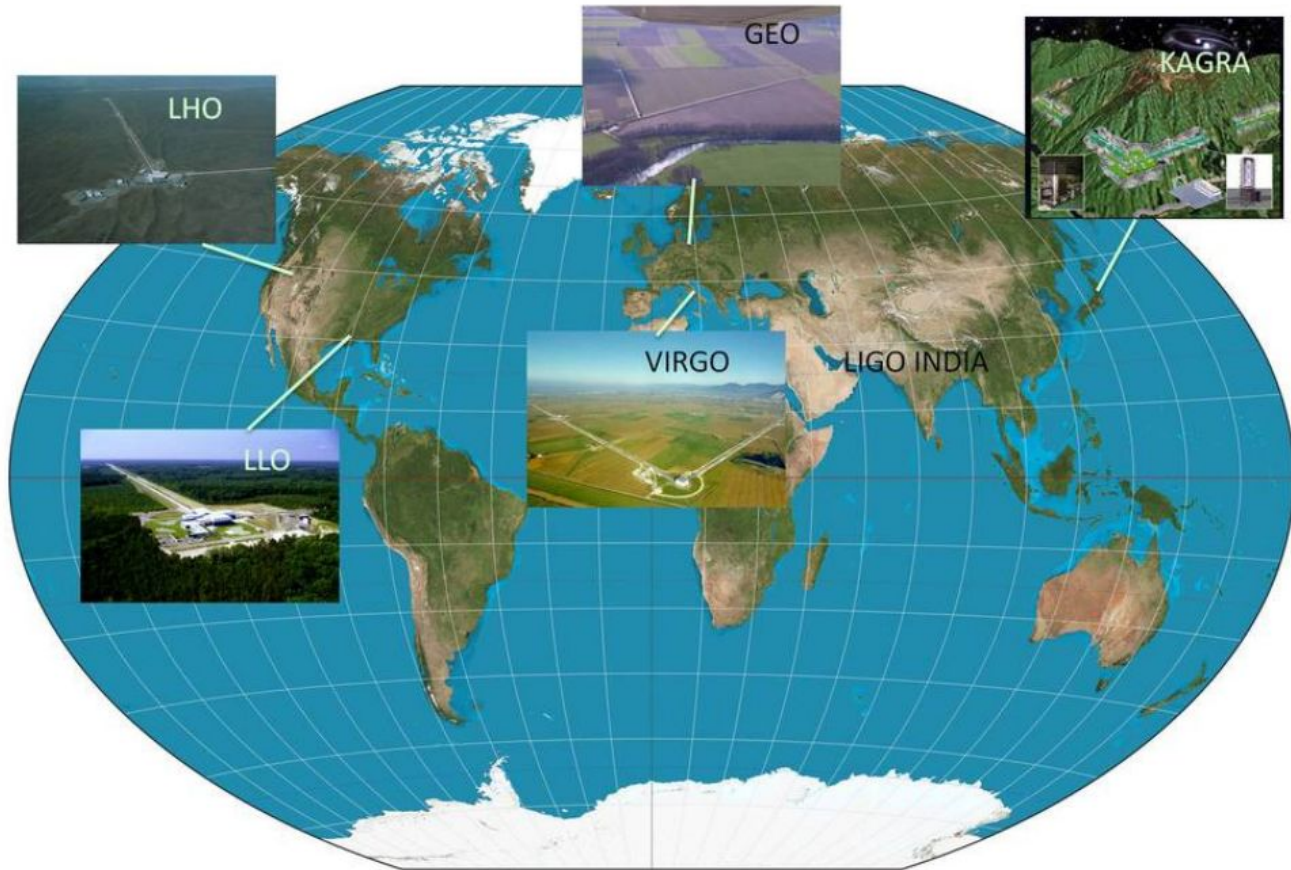
Gravitational Wave Spectrum

LIGO & VIRGO Detectors

LIGO observatory contains 2 (H2) km and 4 km (H1) interferometers at Hanford, WA and a 4 km interferometer at Livingston, LA (L1) separated by 3000 km (10ms)

Hanford
4 km

Livingston
4 km

VIRGO
3 km Cascina,
Italy

Laser

Power recycling mirror

Photo-detector

Beam splitter

Arm 1

Near mirror

Arm 2

Far mirror
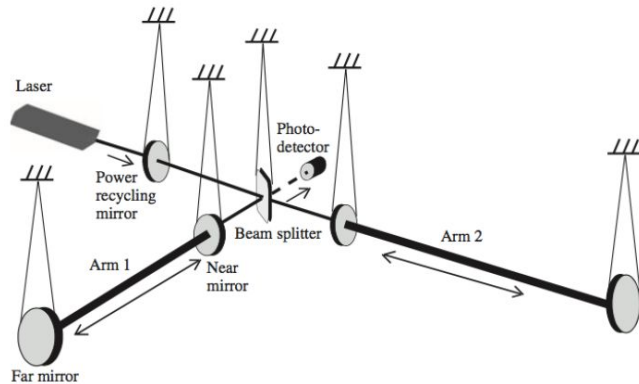
For a binary system the wave's frequency sweep and amplitude (strain) depend on $\mathscr{M} = (m_1 m_2)^{3/5}/(m_1 + m_2)^{1/5}$, and luminosity distance:

Dimensionless strain, h= Δl/l, is the main observable measured; the typical relative deformation:

$$\frac{d\Omega}{dt} \propto \left(\frac{G\mathscr{M}}{c^3}\right)^{5/3}$$

$$h = \frac{\Delta l}{l} \sim 10^{-21}$$

$$h \propto \frac{1}{D_L}\left(\frac{G\mathscr{M}}{c^3}\right)^{5/3}\Omega^{2/3}$$

E.g. for the Laser Interferometer Gravitational-Wave Observatory (LIGO):

l~4km → Δl~10⁻¹⁶cm

GW150914: First LIGO detection of Binary BH
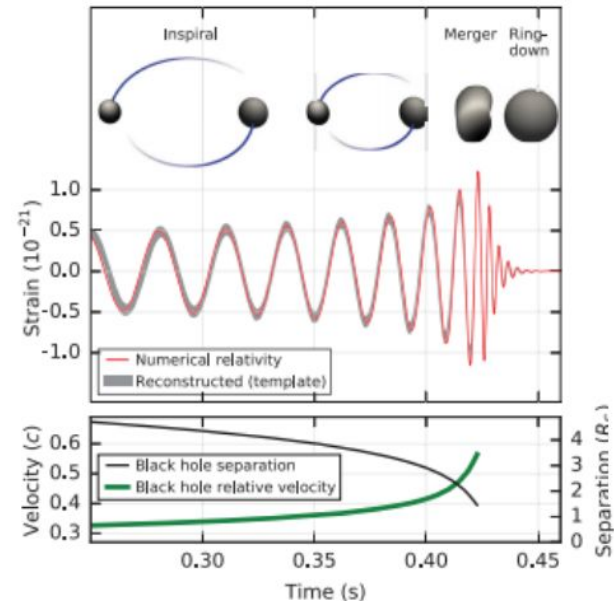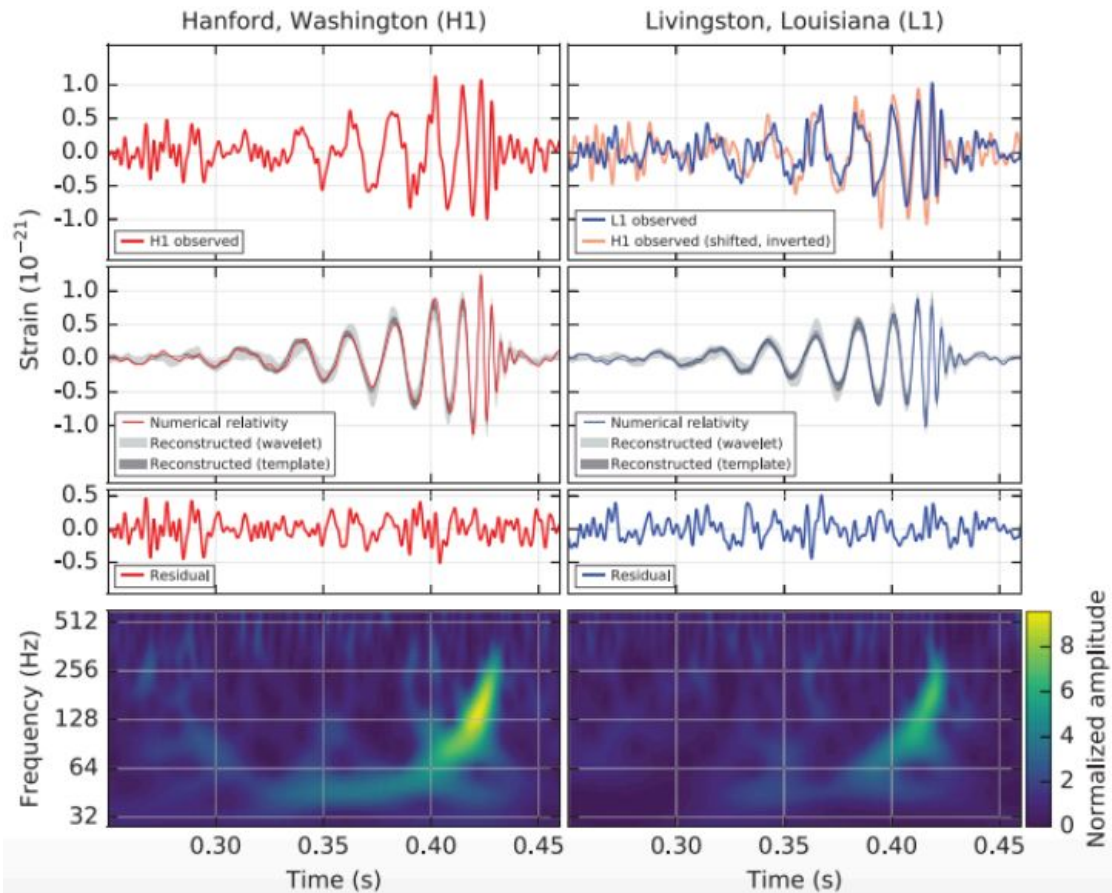
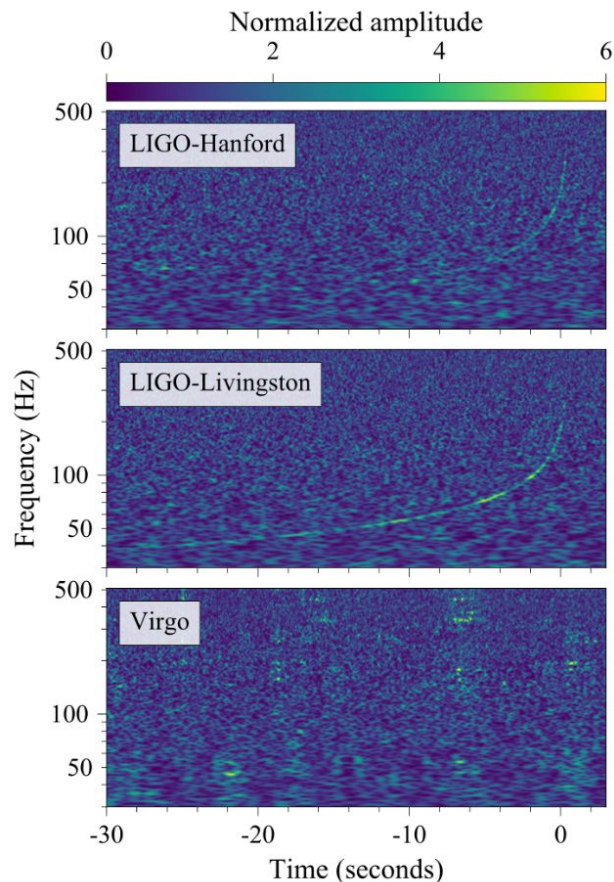|	
Primary black hole mass	$36^{+5}_{-4} M_\odot$
Secondary black hole mass	$29^{+4}_{-4} M_\odot$
Final black hole mass	$62^{+4}_{-4} M_\odot$
Final black hole spin	$0.67^{+0.05}_{-0.07}$
Luminosity distance	410^{+160}_{-180} Mpc
Source redshift z	$0.09^{+0.03}_{-0.04}$

Summary of Ligo-Virgo-KAGRA Binary mergers
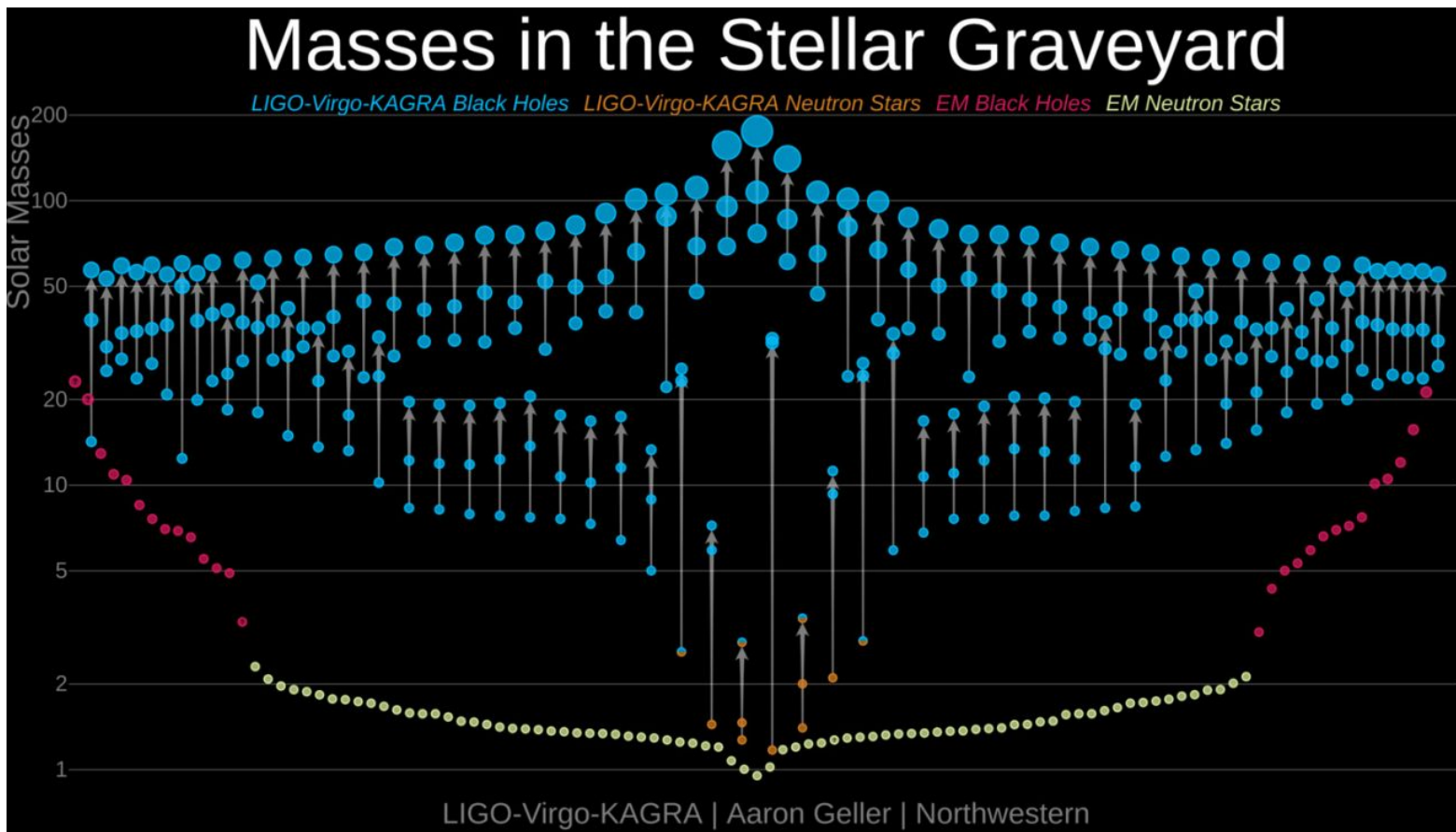
GW 170817: First Binary Neutron star merger

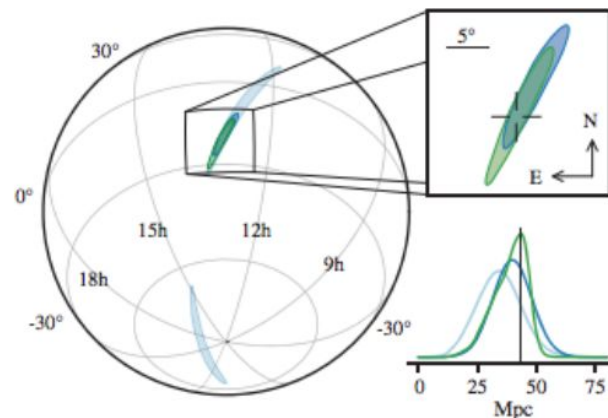**Triangulation of the GW signal:**

FIG. 3. Sky location reconstructed for GW170817 by a rapid localization algorithm from a Hanford-Livingston (190 deg², light blue contours) and Hanford-Livingston-Virgo (31 deg², dark blue contours) analysis. A higher latency Hanford-Livingston-Virgo analysis improved the localization (28 deg², green contours). In the top-right inset panel, the reticle marks the position of the apparent host galaxy NGC 4993. The bottom-right panel shows the *a posteriori* luminosity distance distribution from the three gravitational-wave localization analyses. The distance of NGC 4993, assuming the redshift from the NASA/IPAC Extragalactic Database [89] and standard cosmological parameters [90], is shown with a vertical line.

- GW are "self-calibrating" sources (Schutz 1986)
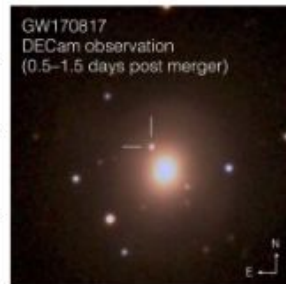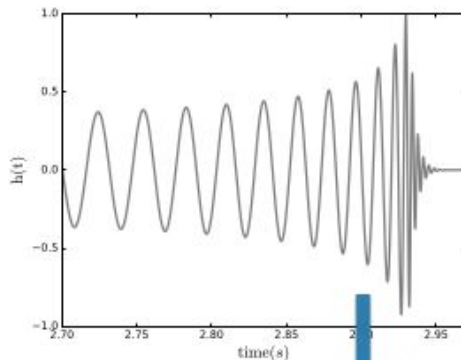
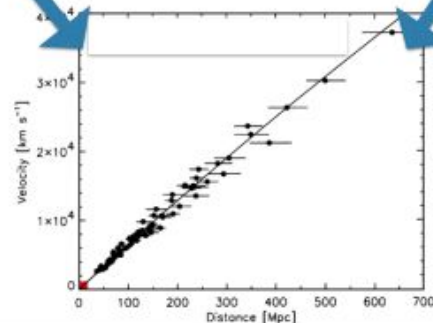$$h \sim D_L^{-1}$$

  - Direct measurement of luminosity distance

  - "Standard sirens"

- In general, no redshift from GWs (Krolak & Schutz 1987)

$$m_{obs} = m_{src}(1 + z)$$

- From GW alone
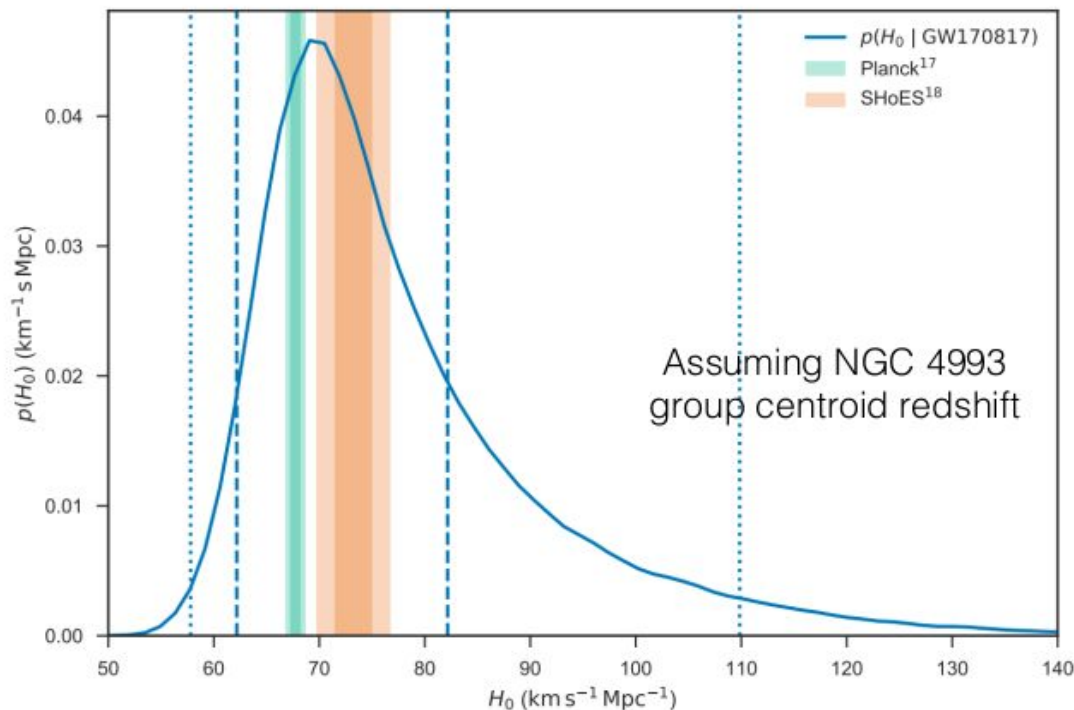
$$D_L = 44^{+3}_{-7}\,\mathrm{Mpc}$$

- NGC 4993

$$z = 0.0098$$

$$H_0 = 70^{+12}_{-8}\,\mathrm{km\,s^{-1}\,Mpc^{-1}}$$

Assuming NGC 4993 group centroid redshift

arxiv:1710.05835

Cosmological GW background: signature of the Early Universe Inflation, preheating, reheating ($10^{-18} - 10^{8}$ Hz); Phase transitions (a narrow band feature peaking at 10^{-12} Hz + broadband component in the band $10^{-5} - 1$ Hz). Cosmic strings ($10^{-10} - 10^{10}$ Hz); Alternative cosmologies

Astrophysical GW background: Such a GW background may result from the superposition of a large number of unresolved sources since the beginning of stellar activity. Its detection would constrain the physics of compact objects, the IMF, the star formation history. It would probe the Universe at z ~ 0.02–10. However, from the point of view of detecting the cosmological background produced in the primordial Universe, the astrophysical background is a 'noise', which could possibly mask the relic cosmological signal

THE GRAVITATIONAL WAVE SPECTRUM
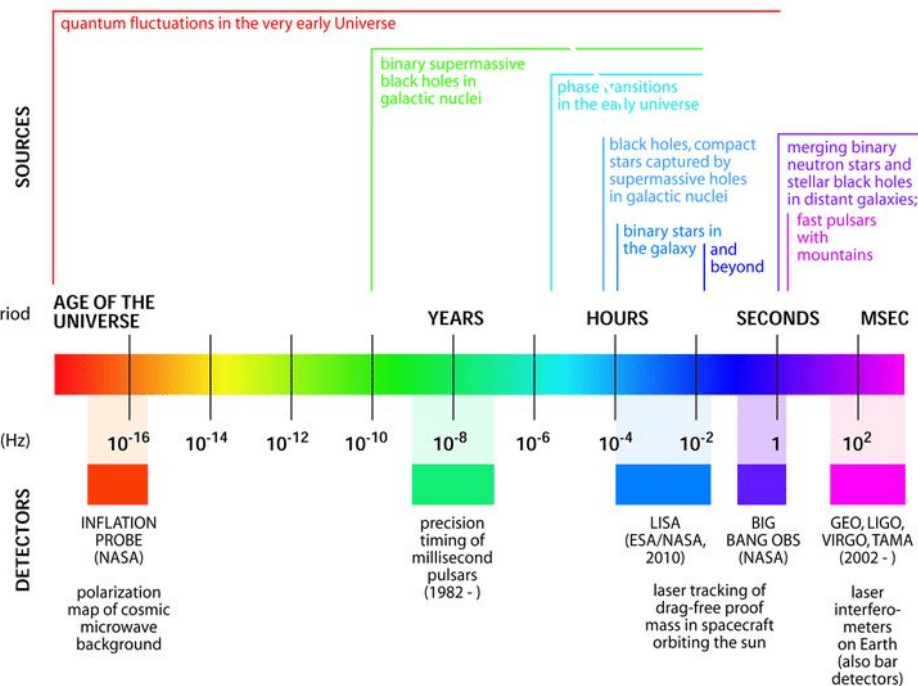
PULSAR TIMING ARRAY
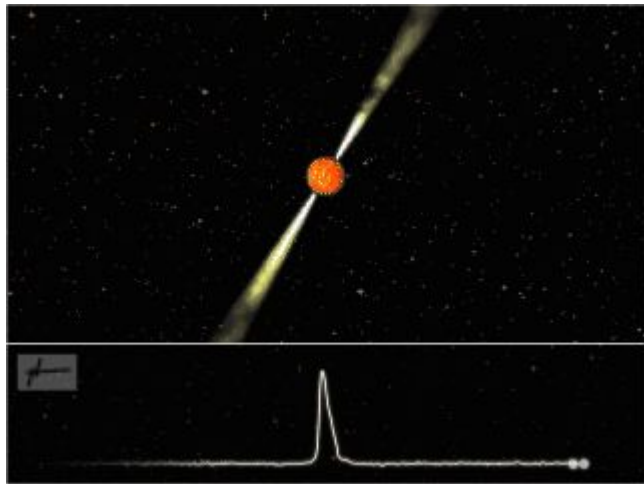
Highly magnetized rotating neutron stars, ultra-precise stellar clocks:

• **Beamed radio pulses emitted from magnetic poles**
• **Periods of 10^{-3}-1 s.**

Array of pulsars across the Milky Way can be used GW detector of galactic dimensions:
• **Look for tiny distortions in pulse travel times caused by nanohertz GWs.**
• **Signal builds up over time; monitor PTA over years and decades.**

TIMING: Performing repeated observations of the Times of Arrival (ToAs) at the telescope of the pulsations from a given pulsar and searching the ToAs for systematic trends on many different timescales, from minutes to decades

The key quantities are the RESIDUALS:
i-th residual r_i is the difference in spin phase Φ between the observed phase of arrival of the i-th pulse and the phase of arrival of that pulse as predicted by the model:

$$r_i = \phi_{\text{observed,i}} - \phi_{\text{model,i}}$$

E.g.: Expected residual for due to GW emitted by a double SMBH with a total mass of 5.4 · 10^{10} M $_{sun}$ and an orbital period of order ~yr (Jenet+2004)
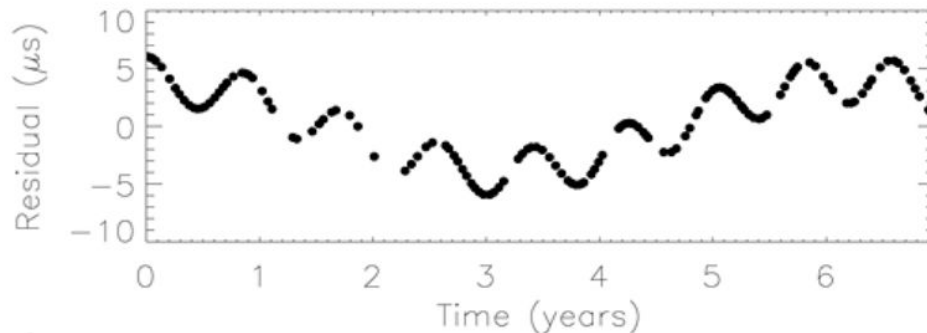
**Pulsar Timing Array:** Using a number of pulsars distributed across the sky it is possible to separate the timing noise contribution from each pulsar from the signature of the GW background, which manifests as a local (at Earth) distortion in the times of arrival of the pulses which is common to the signal from all pulsars.

➢ **Clock errors**
  All pulsars have the same TOA variations: **Monopole** signature

➢ **Solar-System ephemeris errors**
  Dipole signature

➢ **Gravitational waves background**
  Quadrupole signature

$$\zeta(\theta_{ab}) = \frac{3}{2}\left(\frac{1-\cos\vartheta_{ab}}{2}\right)\log\left(\frac{1-\cos\vartheta_{ab}}{2}\right) - \frac{1}{4}\left(\frac{1-\cos\vartheta_{ab}}{2}\right) + \frac{1}{2} + \frac{1}{2}\delta_{ab}$$

Pulsar **a**   Pulsar **b**

ϑ_{ab}

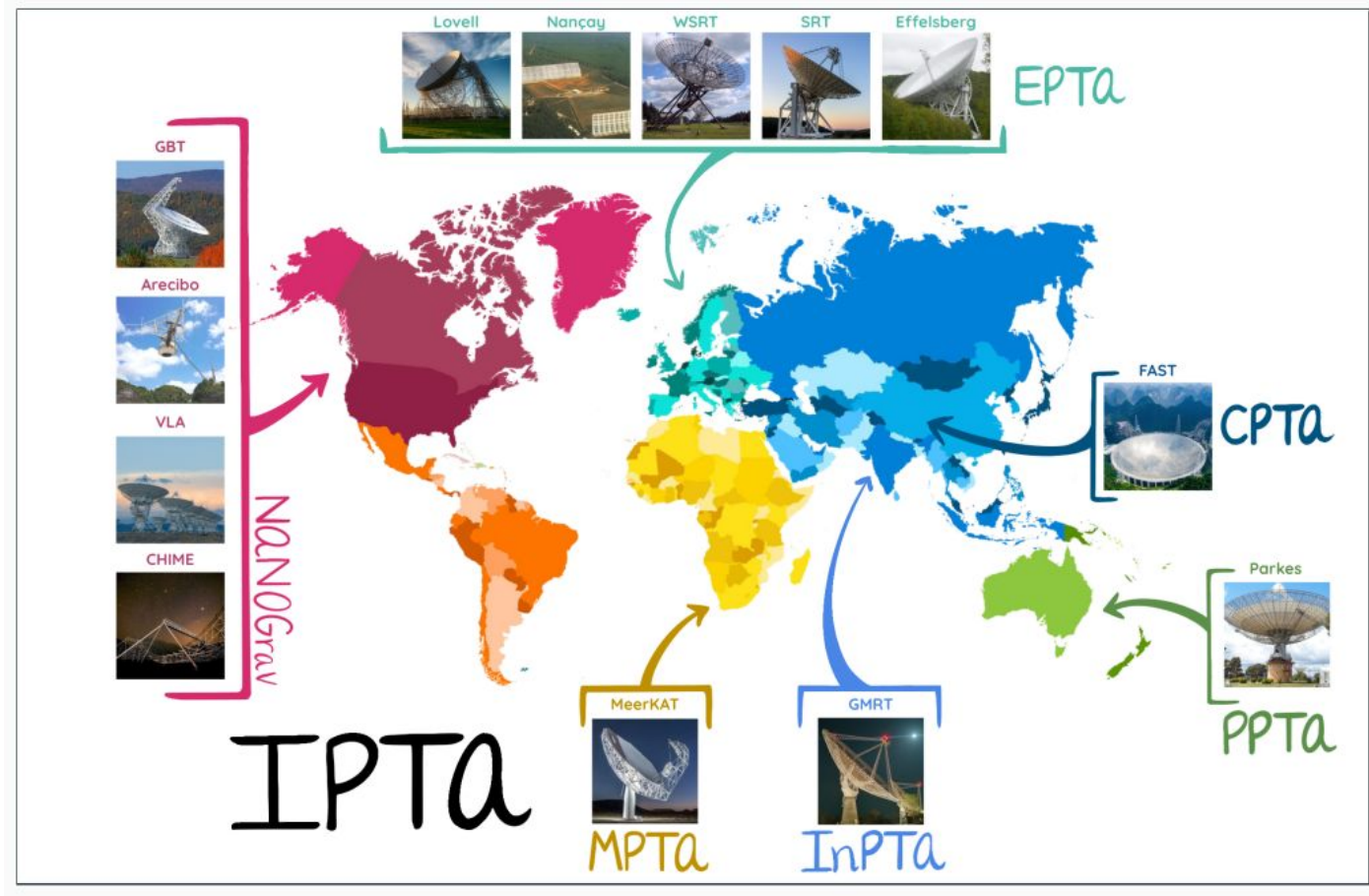[slide adapted from Manchester 11]
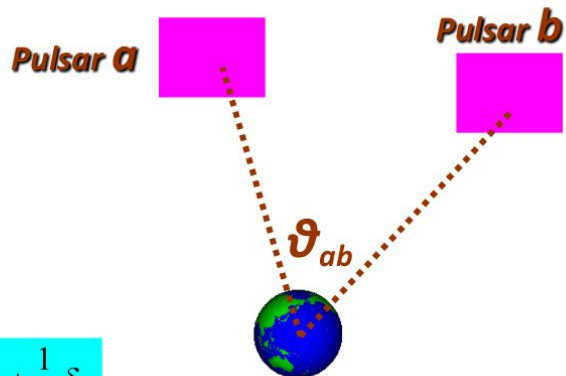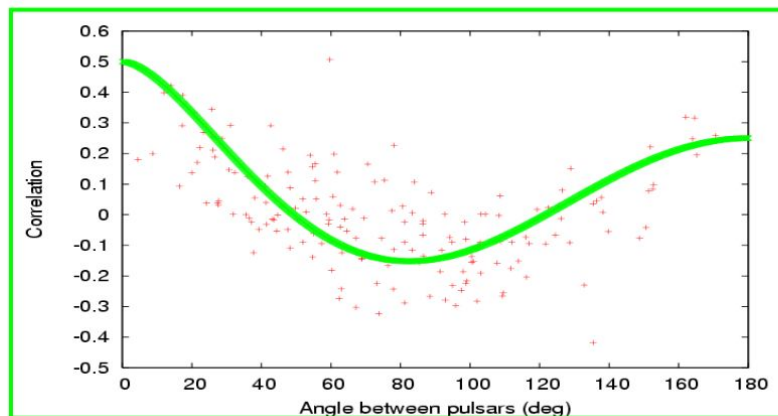
Hellings & Downs [1983]: correlation that an isotropic, stationary and stochastic GWB leaves on the timing residuals of pairs of pulsars a and b separated by angle ϑ_{ab} in sky

Evidence (2 - 4.6 σ) for quadrupole correlation signal from different collaborations.

The signal can be interpreted as:

1. **Cosmic population of in-spiralling SMBHB (realistic)**
2. **New Physics (speculative)**

2306.16213: NANOGrav
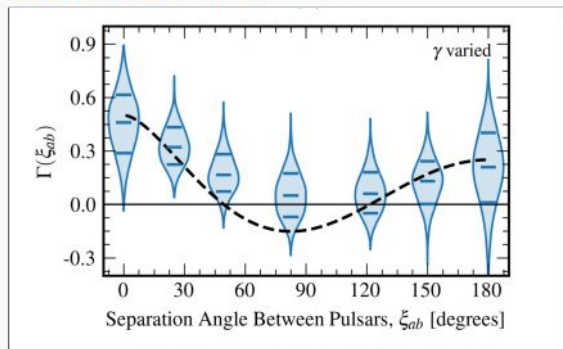
68 pulsars, 16 yr of data, HD at $\sim 3 \cdots 4\,\sigma$

2306.16214: EPTA+InPTA

25 pulsars, 25 yr of data, HD at $\sim 3\,\sigma$

2306.16215: PPTA
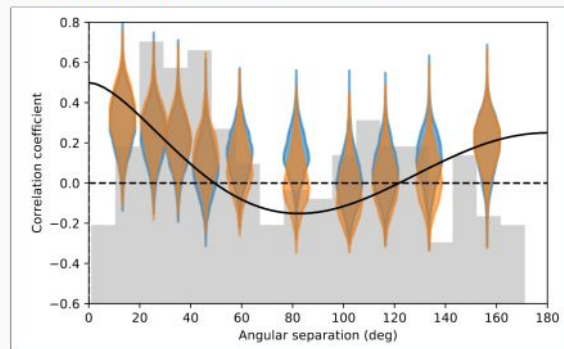
32 pulsars, 18 yr of data, HD at $\sim 2\,\sigma$

2306.16216: CPTA
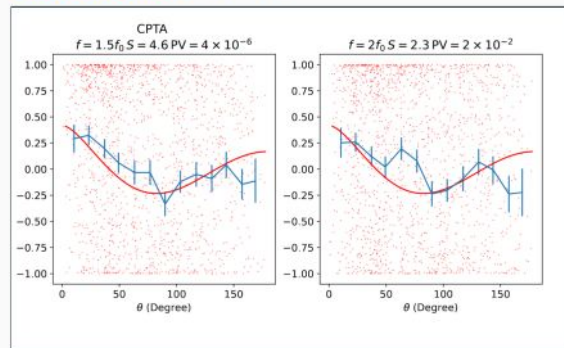
57 pulsars, 3.5 yr of data, HD at $\sim 4.6\,\sigma$

GW background due to Supermassive Black-Hole Binaries (SMBHBs):

It's well known that current paradigm is that [e.g. Ferrarese & Merrit 2000]
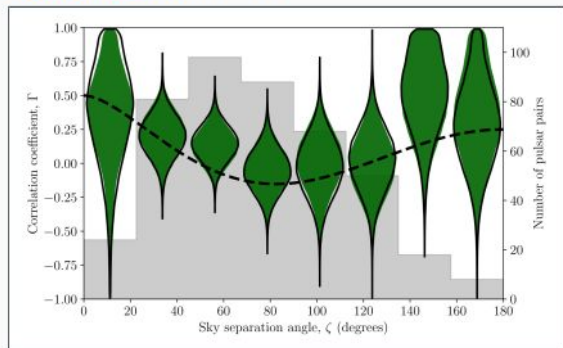- mergers are an essential part in galaxy formation and evolution
- nuclei of most (all?) large galaxies host Massive BH(s) i.e. mass $M \gtrsim 10^6 \, M_\odot$

When reaching orbital separation a of less than about 1 pc, GW emission at frequency f become the dominant term in energy loss, making the MBH binary to shrink faster and faster

$$f \sim 3 \text{ nHz} \left[\frac{M}{10^9 \, M_\odot} \right]^{1/2} \left[\frac{a}{0{,}01 \text{ pc}} \right]^{-3/2}$$

[© CSIRO]

Expected Strain Spectrum of GWB from SMBHB population:

$$P_{\mathrm{GWB}}(f) \simeq A^2 f^{-\gamma} \qquad A \simeq 10^{-15}, \gamma = 13/3$$

## Observed Strain Spectrum of GWB:

2306.16213: NANOGrav
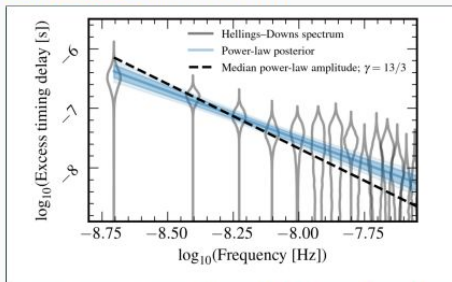
68 pulsars, 16 yr of data, HD at $\sim 3 \cdots 4\sigma$

2306.16214: EPTA+InPTA
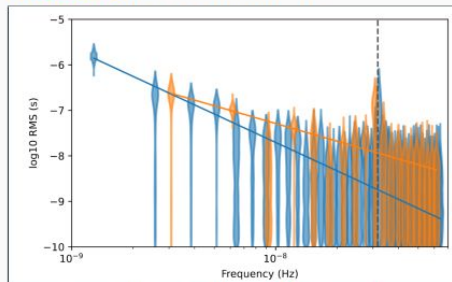
25 pulsars, 25 yr of data, HD at $\sim 3\sigma$

2306.16215: PPTA
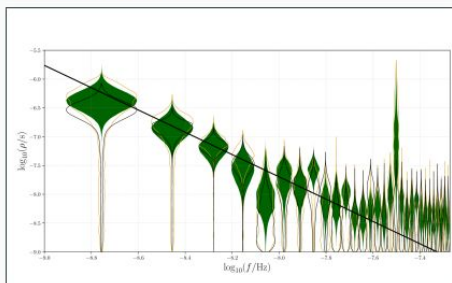
32 pulsars, 18 yr of data, HD at $\sim 2\sigma$

2306.16216: CPTA
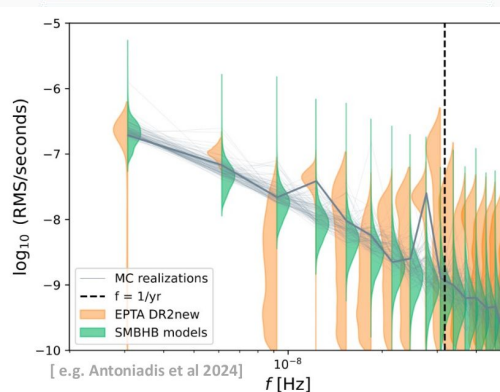
[e.g. Antoniadis et al 2024]
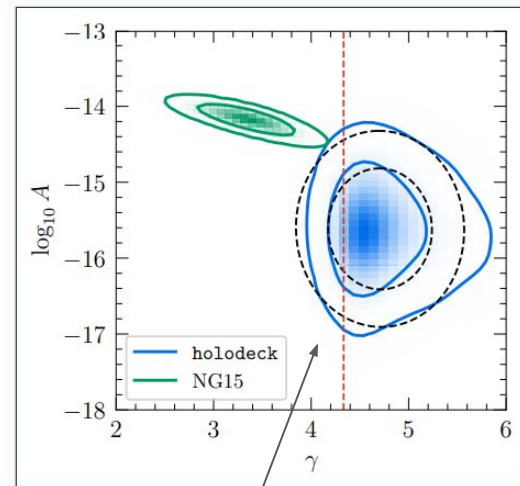
Simplest models of binary evolution (holodeck) struggle to explain the data (NG15), but many sources of systematic can hamper the interpretation of the results

Many Beyond-Standard-Model models predict GWB from the Big Bang:

Inflation
- Nonminimal blue-tilted models
- Interplay with CMB observables
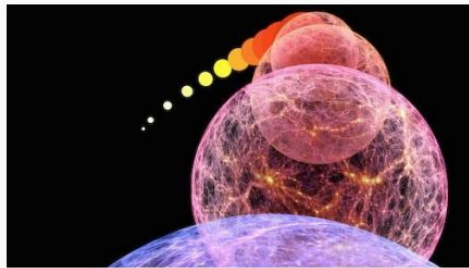
Phase transition
- Modified QCD transition, dark sector
- Complementary to laboratory searches
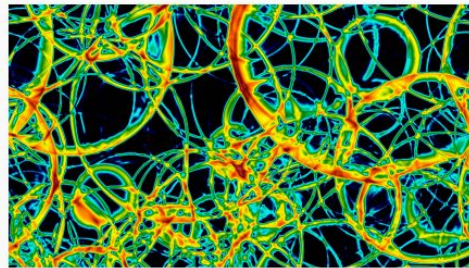
Cosmic defects
- Cosmic strings, domain walls
- Access to grand unified theories

Scalar perturbations
- Associated with primordial black holes
- PBH dark matter, supermassive BHs
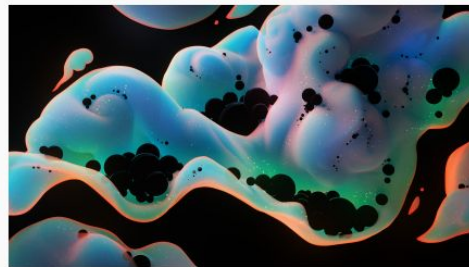
STATISTICAL PROPERTIES OF THE LARGE SCALE STRUCTURES:

LYMAN-α FOREST

For a review: https://arxiv.org/pdf/1512.00086.pdf

Absorption spectra of distant luminous quasars (QSOs) provide a means to probe the properties of the intergalactic medium at high redshift through the analysis of the so called Ly-α forest.
The UV light of a distant quasar – in the wavelengths blue-wards of the Ly-α emission line, λ < 1216Å – traversing the IGM towards the observer could be absorbed by intervening bunches of neutral hydrogen atoms once the photons are redshifted – due to cosmic expansion – to the proper transition frequency. **The Ly-α forest, that is the series of absorption features observed in QSOs spectra at wavelengths corresponding to 1216 (1 + z_a) Å, where z_a is the redshift of the absorbers, can be used to map the distribution of the IGM, which is a biased tracer of the underlying DM distribution.**
Therefore, the clustering statistics of the flux can be used to constrain the shape and amplitude of the matter power spectrum and measure the structure growth at redshifts 2<z<6, **a redshift inaccessible to other LSS probes such as cosmic shear or clusters.**
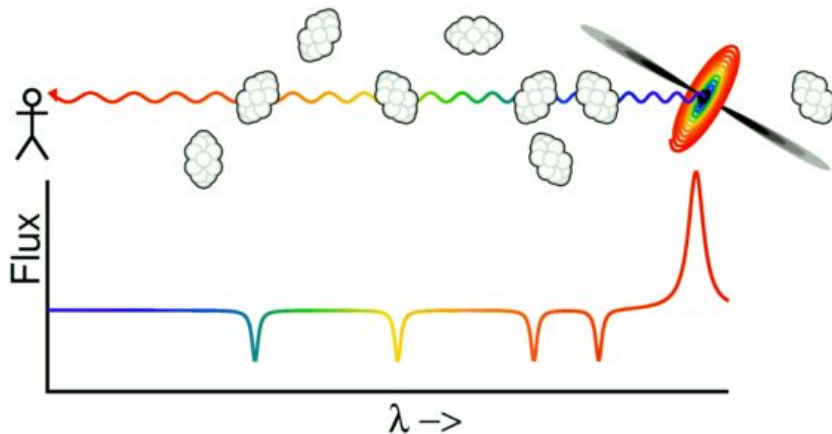
Ly-α optical depth:

$$\tau_{\mathrm{Ly}\alpha}(z) = 1.3\,\Delta_b \left(\frac{x_{\mathrm{HI}}}{10^{-5}}\right)\left(\frac{1+z}{4}\right)^{3/2}\left(\frac{dv/dx}{H(z)/(1+z)}\right)^{-1}$$

$\propto$ **Baryon density**

Fraction of neutral hydrogen

The "trees" in the forest are the highly photoionized sheets, filaments, and halos that result from cosmic structure formation
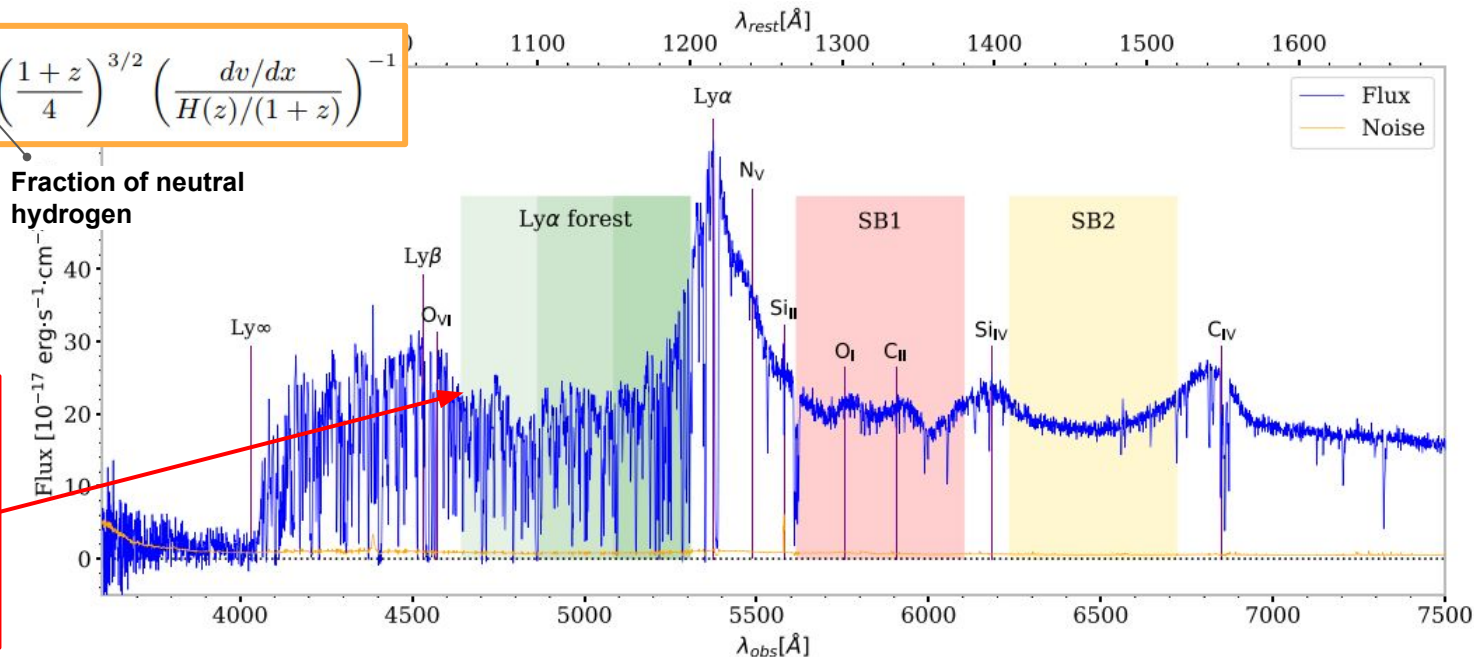
Figure 1. A particularly high-signal spectrum of a quasar located at a redshift $z = 3.42$ measured by DESI with an exposure time of 2300 s. This quasar was observed on 2021 April 12, in the SV3 programme, on DESI tile 221 (TARGETID $= 39627746095137037$, RA $= 217.263°$, Dec. $= -1.755°$). The quasar flux is represented in blue and its noise in orange. The Ly α forest is shown in green. The side-band regions 1 and 2 pictured in red and yellow are used to estimate the forest contamination by metals.

Above k ≈ 0.02 s/km sensitive to the "warmness" of the dark matter

The fluctuations of the Ly α forest flux, δ_f = F(x)/<F(x)> -1, along the line of sight L, can be used to measure the one-dimensional (1D) Ly-α forest power spectrum:

$$P_F(k) \equiv \frac{|\tilde{\delta}_f(k)|^2}{L}$$

Cosmological inference from the Lyα forest spectra is complicated by there being **no reliable analytic model for the mildly nonlinear densities probed by the forest**. All analyses require a comparison with large cosmological simulations.

The flux power spectrum measurements of the XQ-100 data sample
https://arxiv.org/pdf/1702.01761.pdf

STATISTICAL PROPERTIES OF THE LARGE SCALE STRUCTURES:
21cm COSMOLOGY

For a review: https://iopscience.iop.org/article/10.1088/1742-6596/956/1/012003/pdf
https://arxiv.org/pdf/2203.17039

21-CM RADIATION

21-cm radiation originates from the hyperfine transition (spin-flip) of the hydrogen atom:

- **Strongly forbidden line, $t_{1/2} \sim 10^7$ yr**
- **HI very abundant**
- **Spectrally isolated**
- **Small obscuration**
- **Earth's atmosphere is transparent to radio frequencies**

HI

$\lambda = 21\,cm$

the radio sky is *easy* to look at!
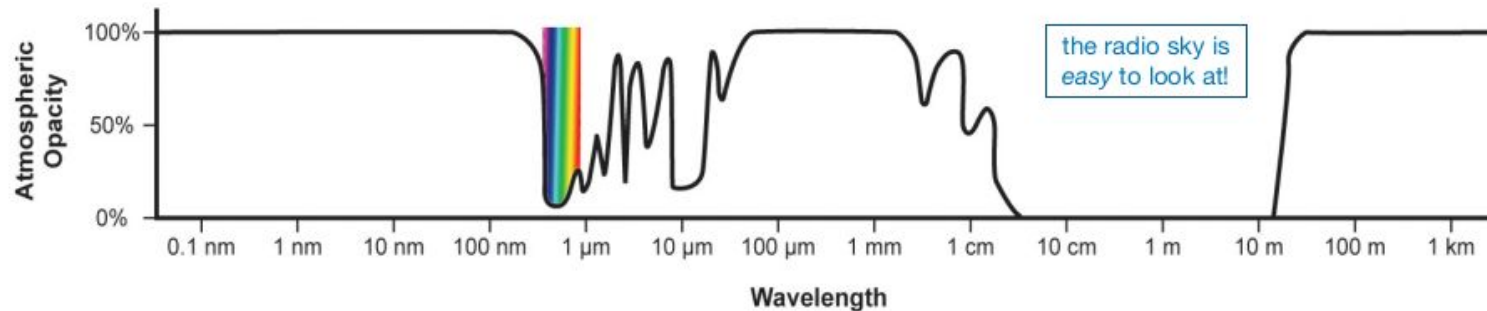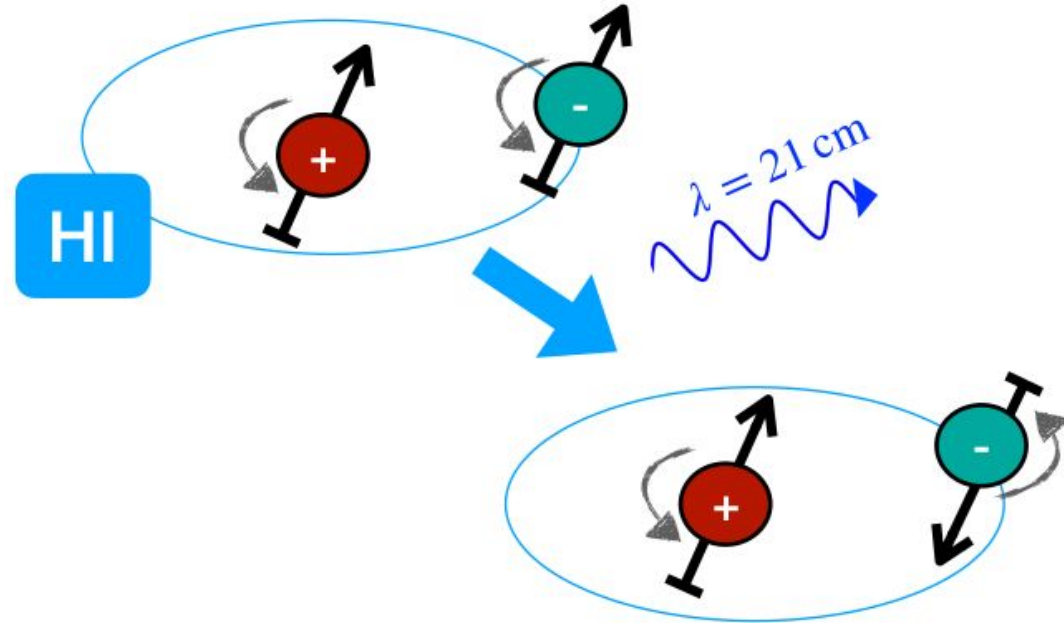
Intensity mapping is an observational technique for surveying the large-scale structure of the universe by using the integrated radio emission from **unresolved** HI gas clouds.

The frequency of the emission line is redshifted by the expansion of the Universe, thus the signal can be used to reconstruct the matter density field over cosmic time (tomography).

Intensity mapping surveys can be carried out much faster than conventional optical redshift surveys; it is possible to map-out significantly larger volumes of the Universe.

GALAXY FIELD
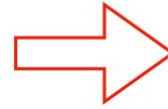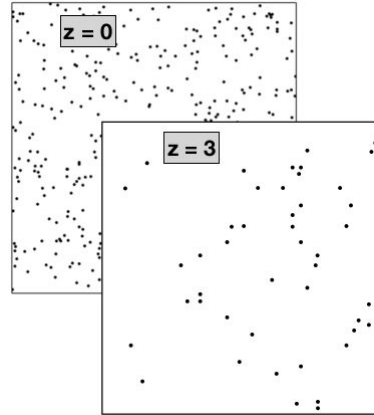
HI INTENSITY FIELD

$$\nu = \frac{\nu_{21}}{1+z}$$
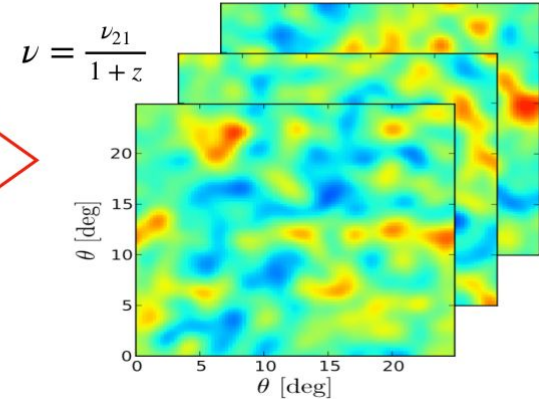
It can be used to probe the cosmological "dark ages" from recombination (when stable hydrogen atoms first formed) to reionization:

- **It can provide a picture of how the universe was re-ionized: neutral hydrogen which has been ionized by radiation from stars or quasars will appear as holes in the 21 cm background.**

- **By mapping the intensity of redshifted 21 cm radiation – λ = 21cm×(1+z) – it can measure the matter power spectrum in the period after recombination (BAO, RSD, etc, etc).**

Recombination

Dark Ages

Reionization

Large-scale Structure

1100
200
30
13
7
1
0

CMB

Line-Intensity Mapping (Atomic and Molecular)

Galaxy Surveys

Astrophysical Bursts (GWs, FRBs, GRBs...)

z
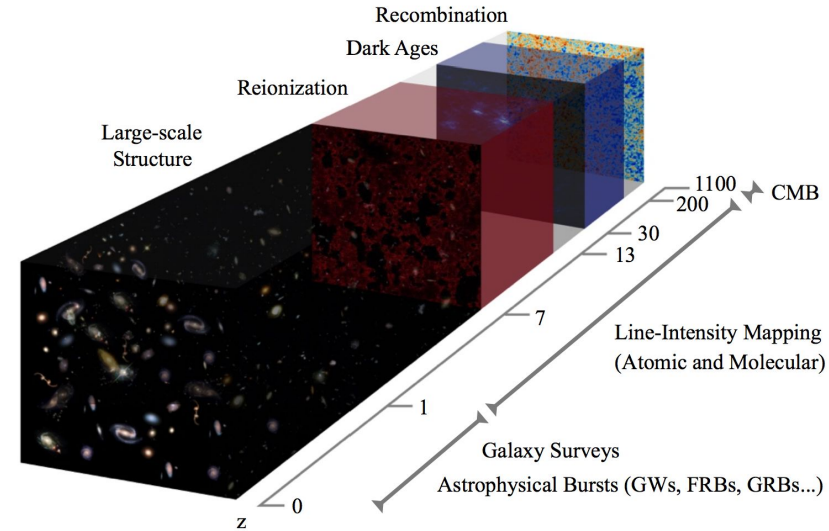
✅ 1. Large areas

✅ 2. Deep and accurate redshifts (distances)

✅ 3. Better coverage of the Universe epochs

CHALLENGES:

The IM signal is weak compared to the contaminants

- **Receiver Noise:** amplitude comparable to signal -> isotropic, 1/f noise can be removed, manageable in power spectrum space
- **Instrumental errors:** calibration uncertainties, sidelobes, pointing errors, polarization leakage
- **Radio Frequency Interference:** contaminates in spatial and frequency space -> go to the desert, stay away from satellites
- **Foreground contaminations:** Galactic emission and extra-Galactic point sources
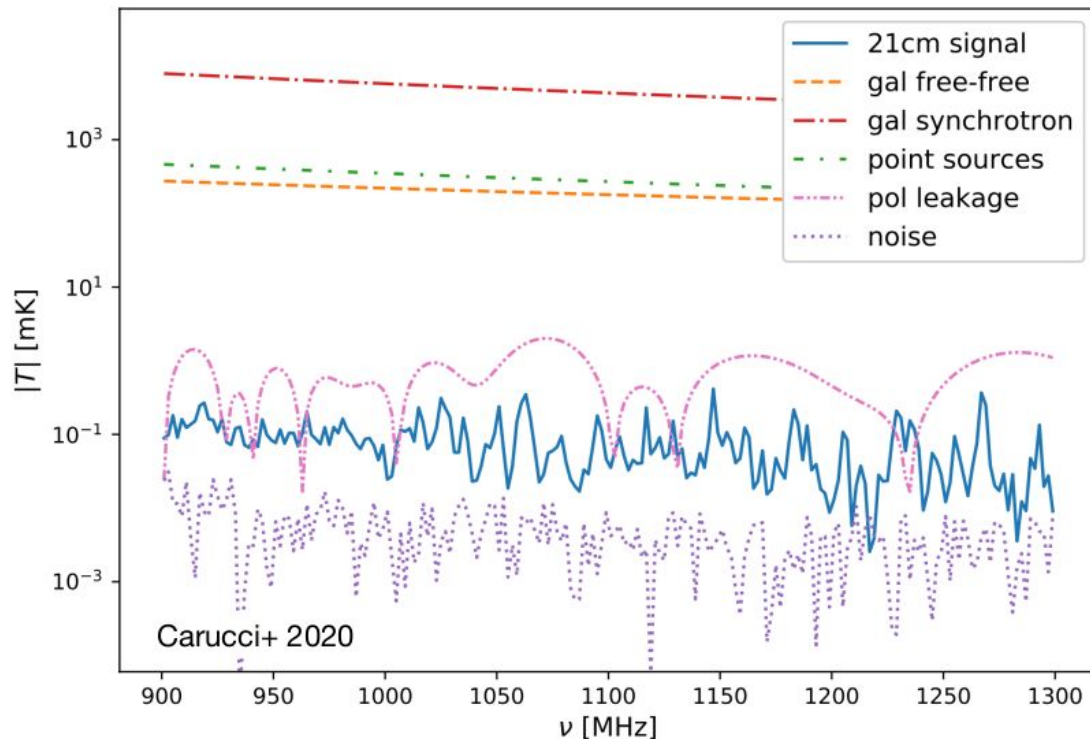
TIME DELAY COSMOGRAPHY

For a review: **https://link.springer.com/article/10.1007/s00159-022-00145-y**
See also: https://arxiv.org/pdf/2505.22738

Multiply imaged time-variable sources can be used to measure absolute distances as a function of redshifts and thus determine cosmological parameters, chiefly the Hubble Constant H_0.
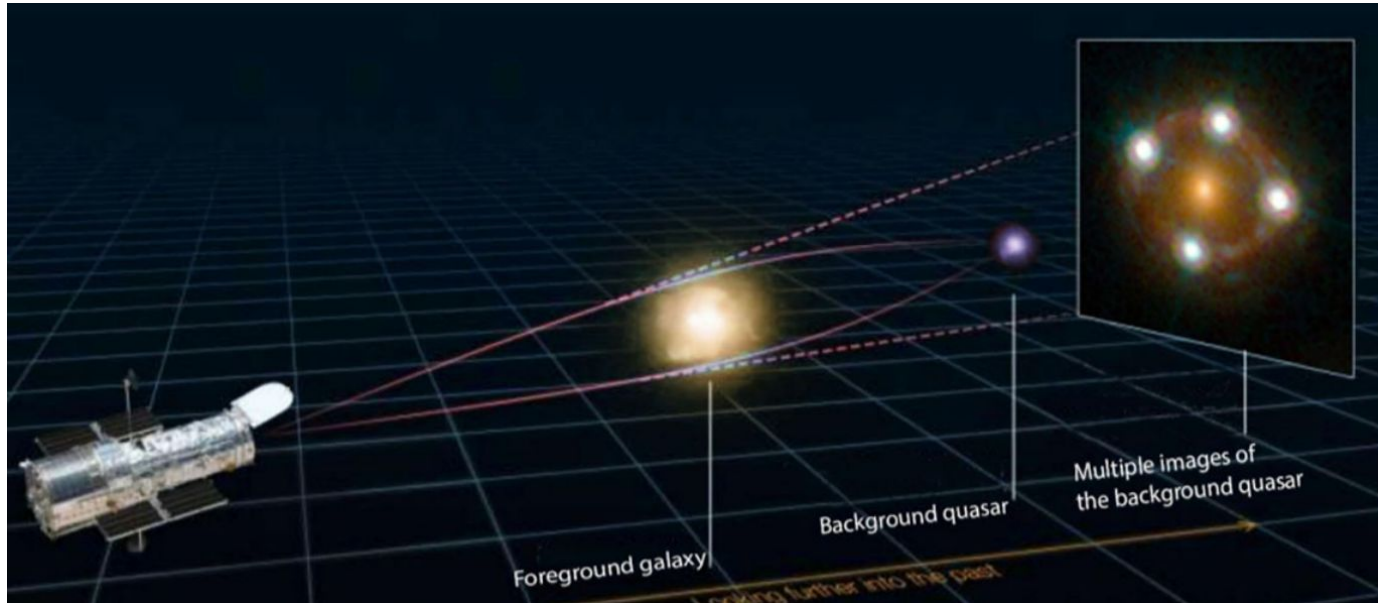
When a distant variable source (e.g., a supernova or a quasar) is multiply imaged by a foreground mass distribution (e.g., a galaxy or cluster of galaxies), the multiple images appear offset in time to the observer. The delay(s) between the leading image and trailing one(s) arise from the combination of two effects. The first one is the difference in length of the optical paths. The second is a general relativistic effect, called the Shapiro (1964) delay, owing to the difference in gravitational potential experienced by the photons along the paths.

The time delay between image A and image B is given by:

$$\Delta\tau_{AB} = \frac{D_{\Delta t}}{c}\Delta\Phi_{AB}$$

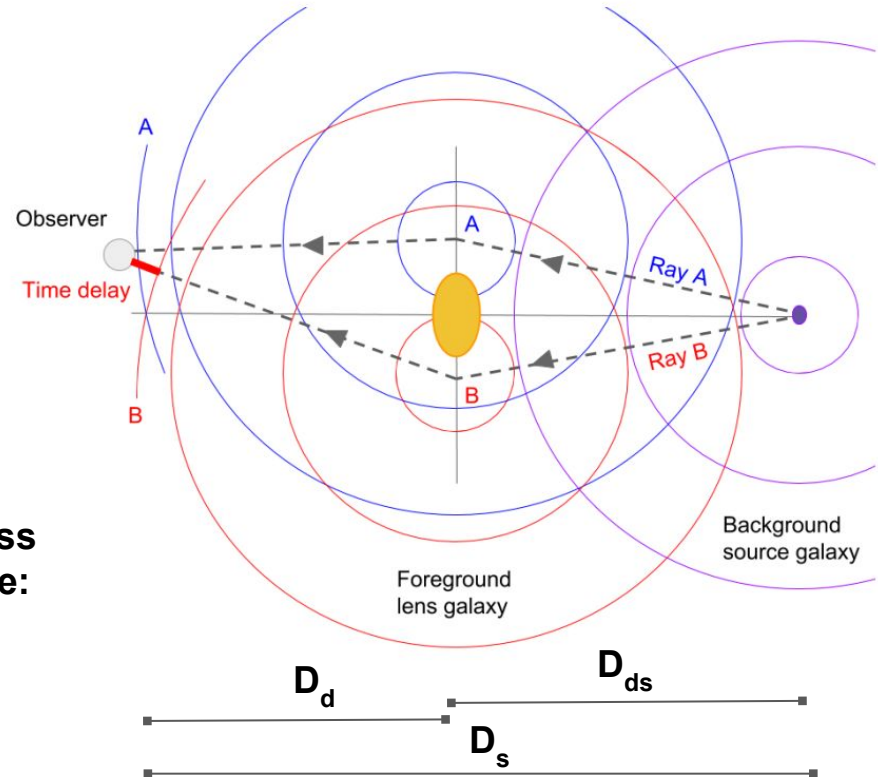$$D_{\Delta t} \equiv (1+z_d)\frac{D_d D_s}{D_{ds}}$$

$\Delta\phi$ **: Fermat potential difference between two image position. It can be predicted given a model for the mass distribution of the lens, along with the deflection angle:**
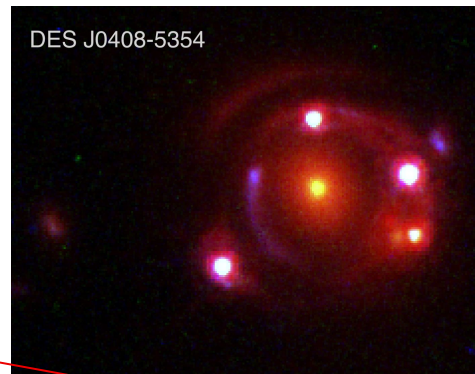
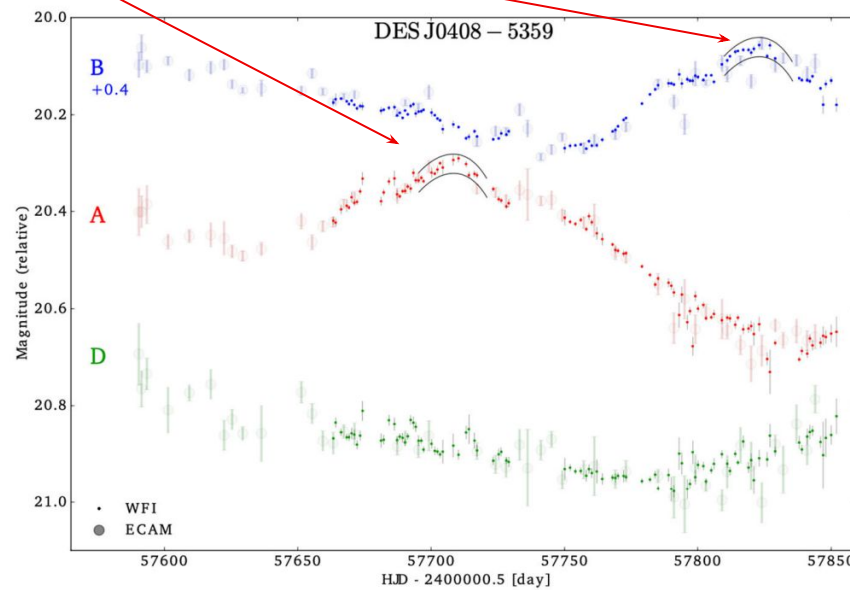$$\phi = \frac{1}{2}(\theta-\beta)^2 - \psi(\theta)$$

TIME DELAY COSMOGRAPHY

Steps:

- **Measure the time-delay between two images**
  - The basic idea is to detect variations in the brightness of the quasar images in a lens system and use these variations to determine the time delay between the multiple images, given that the intrinsic brightness variations of the quasar manifest in each of the multiple images.
- **Measure and model the potential**
- **Infer the time delay distance $D_{\Delta t}$**
- **Convert it into cosmological parameters**

H0 measurements of 6 lensed quasars from the H0LiCOW program

DES J0408-5354

$H_0 \in [0, 150] \quad \Omega_m \in [0.05, 0.5]$

$H_0 : 71.0^{+2.9}_{-3.3}$
$H_0 : 78.2^{+3.4}_{-3.4}$
$H_0 : 71.7^{+4.8}_{-4.5}$
$H_0 : 68.9^{+5.4}_{-5.1}$
$H_0 : 71.6^{+3.8}_{-4.9}$
$H_0 : 81.1^{+8.0}_{-7.1}$

$H_0 : 73.3^{+1.7}_{-1.8}$

All
B1608 (Suyu+2010, Jee+2019)
RXJ1131 (Suyu+2014, Chen+2019)
HE0435 (Wong+2017, Chen+2019)
J1206 (Birrer+2019)
WFI2033 (Rusu+2019)
PG1115 (Chen+2019)

probability density

$H_0 \; [\mathrm{km\,s^{-1}\,Mpc^{-1}}]$

DES J0408 − 5359

B
+0.4

A

D

Magnitude (relative)

WFI
ECAM

HJD - 2400000.5 [day]
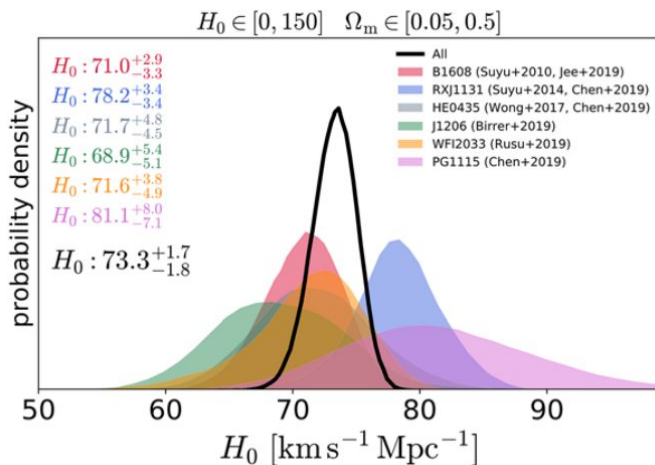
COSMIC CHRONOMETERS

For a review: https://arxiv.org/pdf/2201.07241.pdf

STANDARD CLOCKS AND CHRONOMETERS

Given how the age of the Universe scales as a function of redshift:

$$t(z) = \frac{1}{H_0} \int_0^z \frac{dz'}{E(z')(1+z')}$$

$$E(z) = \frac{H(z)}{H_0} = \sqrt{\Omega_m(1+z)^3 + \Omega_\Lambda}$$

finding the oldest objects at each redshift it is possible to use them to constrain the Hubble parameter. In other words, we can use **standard clocks** – i.e. objects whose absolute age is known – to constrain cosmology.

Or we can consider:

$$H(z) = -\frac{1}{1+z}\frac{dz}{dt}$$

By measuring the differential age of the Universe (how much the Universe has aged between two redshifts) it is possible to obtain a direct determination of the expansion rate H(z). The main difference here is that instead of looking for some standard clocks, we will be looking for **standard chronometers**, a homogeneous population of objects with a synchronized formation, i.e. whose clocks started "ticking" at the same time and that are therefore optimal tracers of the differential age evolution of the Universe

The pillars of the cosmic chronometers method are:

• Selection of a population of optimal cosmic chronometers, i.e. a population of objects able to trace homogeneously how much the Universe has aged between two redshifts.

• Robust measurement of the differential age dt (the advances in spectroscopic surveys makes the measurement of dz remarkably accurate when a spectroscopic redshift is available – typically $\delta z/(1 + z) \lesssim 10^{-3}$).

→ The most elementary objects in the Universe that we can date and that can be found from the local Universe up to high redshifts are galaxies. To apply the cosmic chronometer method, the idea is therefore to find at each redshift the oldest population of galaxies available. Massive passively evolving galaxies are among the best candidates: having formed most of their mass (>90%) at very high redshifts (z> 2-3), in a very quick episode of star formation, and having mostly exhausted their gas reservoir are expected to evolve passively as a function of cosmic time.

When observed at cosmic times considerably later than their formation epoch, the age evolution of ETGs stars serves a clock that is synchronized with the evolution of cosmic time.

To minimize the dependence of the age estimate on evolutionary stellar population synthesis (EPS) models, one can study a direct observable of galaxy spectra, the 4000 ˚A break (D4000).

$$D_n 4000 = A(SFH, Z/Z_\odot) \cdot age + B,$$

$$H(z) = -\frac{1}{1+z} A(SFH, Z/Z_\odot) \frac{dz}{dD_n 4000}$$
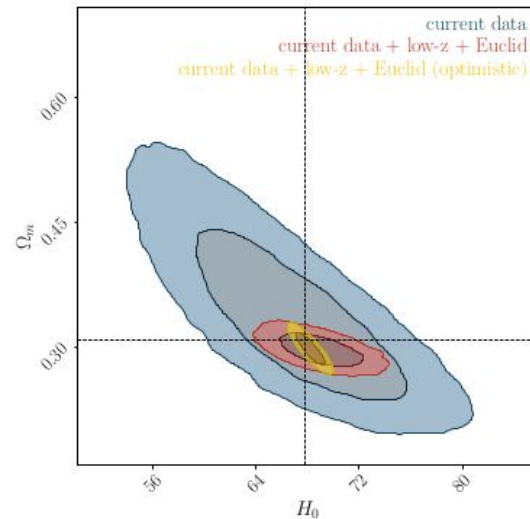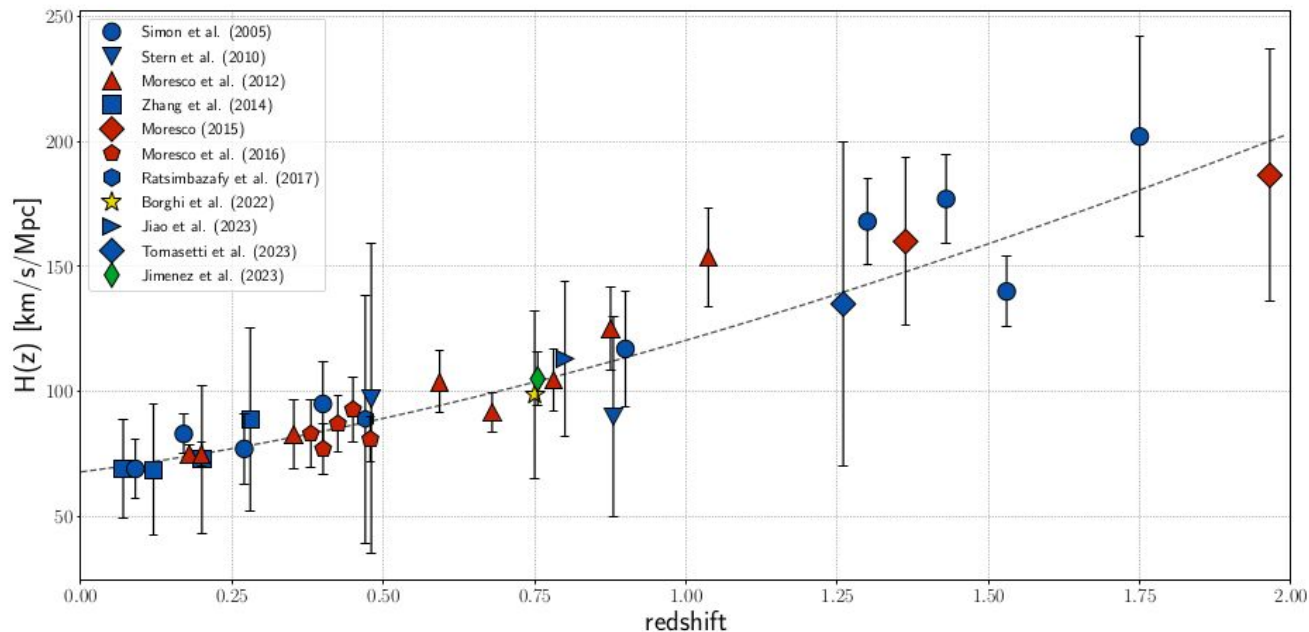

https://arxiv.org/pdf/1601.01701
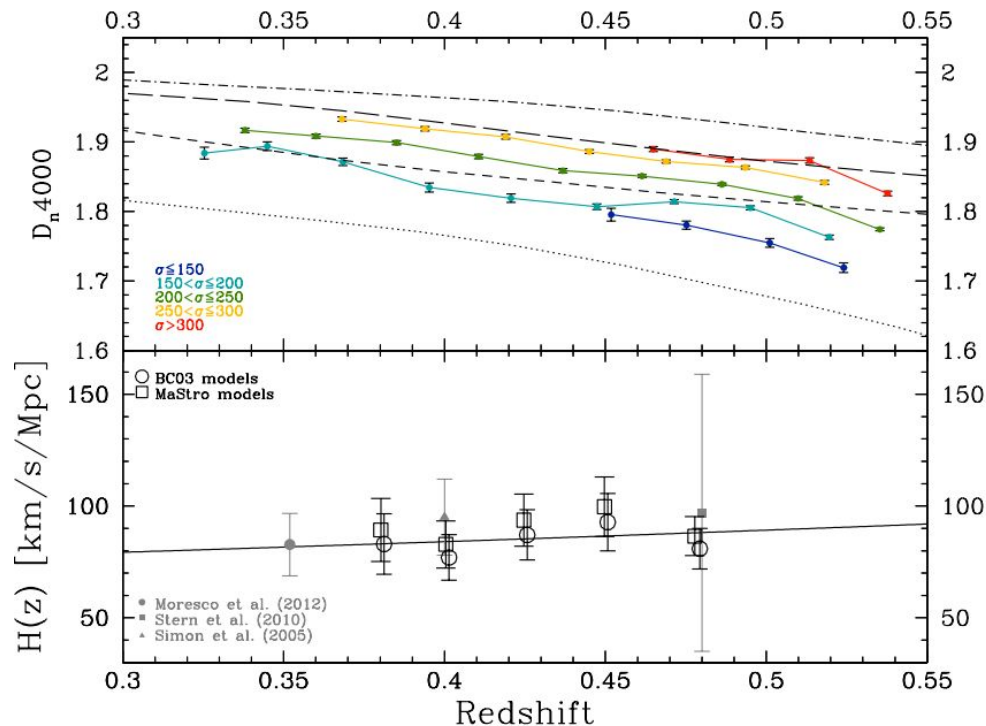
Figure 5: Hubble parameter measurements obtained with the CC method. Different colors refer to different methods adopted to estimate dt, as presented in Tab. 1. The dashed line shows the flat ΛCDM cosmological model from Planck Collaboration et al. (2020a) as a pure illustrative reference.

STANDARD CLOCKS AND CHRONOMETERS

Advantages

- **Model-independent**: No assumption on the underlying cosmological model.

- Complementary to other probes like **BAO**, **SNe Ia**, and **CMB**.

- Useful at **intermediate redshifts (z ~ 0.1–2)**, where other probes are sparse.

Challenges

- Requires accurate age-dating of galaxies (affected by metallicity, star formation history).

- Systematics in stellar population modeling must be controlled.